The impact of siderophores and iron acquisition on *Klebsiella pneumoniae* pathogenesis

by

Victoria Iome Holden

A dissertation submitted in partial fulfillment
of the requirements for the degree of
Doctor of Philosophy
(Microbiology and Immunology)
in the University of Michigan
2016

Doctoral Committee:

Assistant Professor Michael A. Bachman, Chair
Professor Marc B. Hershenson
Professor Harry L.T. Mobley
Professor Bethany B. Moore

DEDICATION

To my grandmother, Edith Holden

ACKNOWLEDGMENTS

I owe my mentor, Mike Bachman, my utmost appreciation for his patience and mentorship during my thesis work in his lab. I am undoubtedly a better scientist, public speaker, writer, and person thanks to his guidance and support. I also greatly appreciate the lab members that have been part of our group along the way, particularly Paul Breen and Rebekah Martin, for their helpful comments about both science and life. I am so thankful to have been a member of this lab.

To my family, I am eternally grateful for their love and support. From day one, my parents have never questioned my goals but have helped me remember to be kind to myself through this process. My brother, Vincent, has made me laugh more times than I can count, and that is an immeasurably valuable support to have.

My boyfriend and partner, Aaron Stein, has taught me more about work-life balance in the last 2 years than I thought could be possible. It is a wonderful thing to have a partner who understands the desire to work hard and achieve your goals while also reminding you to slow down and enjoy the process [1].

Everyone needs a friend who believes in you without question, and I could not imagine a better person for this role in my life than Carla Pretto. From day one of my first rotation, Carla has been whispering in my ear that I will achieve great things, and at some point I began to believe her. Thank you for your

relentless love, support, and belief in me. I can only hope to serve this role half as well for someone else in my future.

Many thanks to my best friends in graduate school, Kaitlin Flynn and Kathryn Iverson, for their willingness to help with science, share with me in hardship, and grab a beer (or three) after work. I will sorely miss being in such close proximity to these two amazing women, but I look forward to seeing the great accomplishments they will achieve.

To my support group outside of Michigan, thank you for putting up with my often one-track science mind. Julie Simmons, Laura Rust, and Valerie Schell have stood by me and supported me since college, and I am so thankful to have friendships that can span distance and time.

Over the years, I have persuaded a few wonderful people into mentorship roles for me. My committee, Harry Mobley, Beth Moore, and Marc Hershenson, have provided great guidance during my thesis. Additionally, I owe many thanks to Mary O'Riordan and Michelle Kahlenberg for their thoughtful mentorship and conversations over the years.

Finally, I have been blessed with a fun group of friends during my time at Michigan. At one point in time, I was a member of a sketch comedy group, and those were some of the best months of my life. Thank you to Zack Abbott and Elizabeth Cameron for thinking that I am funny. I often miss the friends who have graduated, including Alyx Schubert and Joe Zackular. To my friends who are still here, including Hayley Warsinske, Courtney Luterbach, Laura Mike, and Natalie Maricic, thank you for the laughter and conversation.

TABLE OF CONTENTS

LIST OF TABLES

LIST OF FIGURES

LIST OF ACRONYMS AND ABBREVIATIONS

2,3-DHBA	2,3-Dihydroxybenzoic acid
Aer	Aerobactin
ANOVA	Analysis of Variance
CR	Carbapenem-resistant
CRE	Carbepenem-resistant *Enterobacteriaceae*
DFO	Desferrioxamine
DMOG	Dimethyloxalylglycine
DUSP	Dual specificity phosphatases
Ent	Enterobactin
FAC	Ferric Ammonium Citrate
FeEnt	Ferric Enterobactin
GEO	Gene Expression Omnibus
HIF	Hypoxia Inducible Factor
HIF+/+	HIF+/+ wild-type mice
HIF-/-	HIF-/- knockout mice
IFN	Interferon
IL	Interleukin
K_d	Dissociation constant
kD	kilodalton

Lcn2	Lipocalin 2
LcnKO	Lipocalin 2 knockout mice
LPS	Lipopolysaccharide
MAPK	Mitogen-activated protein kinases
MLST	Multilocus Sequence Type
MWCO	Molecular Weight Cutoff Column
ODD	Oxygen Dependent Domain
ODD-Luc	ODD-Luciferase reporter mice
Pch	Pyochelin
PDTC	Pyridine-2,6-bis(thiocarboxylic acid)
PLA	Pyogenic liver abcess
ROS	Reactive Oxygen Species
Sal	Salmochelin
ST	Sequence type
TPM	Transcripts per kilobase million
UPR	Unfolded Protein Response
UPEC	Uropathogenic *Escherichia coli*
UTI	Urinary Tract Infection
VEGF	Vascular Endothelial Growth Factor
WT	Wild-type
Ybt	Yersiniabactin

ABSTRACT

Klebsiella pneumoniae is a Gram-negative bacterium that can cause a wide range of infections, including pneumonia, urinary tract infection, wound infection, and sepsis. *K. pneumoniae* is the most common species of carbapenem-resistant *Enterobacteriaceae*, of which isolates are resistant to all or nearly all antibiotics. To acquire iron required for replication, *K. pneumoniae* secretes siderophores, small molecules with high affinity for iron. In addition, recent research has identified novel, non-iron acquisition functions for siderophores. This thesis describes the inflammatory properties of siderophores and how siderophore secretion by *K. pneumoniae* impacts bacterial infection. *In vitro*, respiratory epithelial cells treated with siderophores and the host protein Lcn2 induced secretion of pro-inflammatory cytokines including IL-8, IL-6, and CCL20. Additionally, siderophores stabilized the master transcription factor HIF-1α. *In vivo* studies identified a role for siderophores in the induction of the host immune response, including IL-6, KC, and MIP-2 secretion, during pneumonia. Siderophores were also shown to promote bacterial dissemination to the spleen, which required HIF-1α from alveolar epithelial cells. Finally, clinical isolates of *K. pneumoniae* can be divided into two clades based on their genomic contents, including a deletion of the siderophore exporter, *entS*. Transcriptional analysis (RNASeq) under iron-limited growth conditions identified novel iron acquisition

mechanisms potentially utilized by the isolates that contain the deletion in *entS*. Combined, these results demonstrate novel roles for siderophores in the induction of inflammation and bacterial dissemination during infection, and identify novel potential iron acquisition pathways that may be active in carbapenem-resistant *K. pneumoniae*. Iron acquisition in non-siderophore dependent manners may allow bacteria to acquire iron in a manner that does not perturb the host immune response. By understanding the host response to siderophores, novel therapies can be designed to combat infection with siderophore-secreting bacteria.

CHAPTER I

INTRODUCTION

Summary

Siderophores are low molecular weight, high affinity iron-chelating molecules that are essential virulence factors in many Gram-negative bacterial pathogens. Whereas the chemical structure of siderophores is extremely variable, the function of siderophores has been narrowly defined as the chelation and delivery of iron to bacteria for proliferation. The discovery of the host protein Lipocalin 2, capable of specifically sequestering the siderophore Enterobactin but not its glycosylated-derivative Salmochelin, indicated that diversity in structure could be an immune evasion mechanism that provides functional redundancy during infection. However, there is growing evidence that siderophores are specialized in their iron-acquisition functions, can perturb iron homeostasis in their hosts, and even bind non-iron metals to promote bacterial fitness. The combination of siderophores produced by a pathogen can enable inter-bacterial competition, modulate host cellular pathways, and determine the bacterial “replicative niche” during infection. This chapter will review both classical and novel functions of siderophores to address the concept that siderophores are non-redundant virulence factors used to enhance bacterial pathogenesis. Additionally, this

chapter will define the central hypothesis that will be addressed in this work, as well as outline the results discussed in the following chapters.

1.1 Introduction

Iron is required for many processes necessary for life, including DNA replication and electron transfer, due to its ability to assume multiple oxidative states [2-4]. Each oxidation state of iron poses challenges to the cell: ferrous iron (Fe^{2+}) is highly toxic in its free form due to its participation in the Fenton reaction, whereas ferric iron (Fe^{3+}) is insoluble at physiological pH and not readily bioavailable [5-7]. Therefore, free iron levels are exceedingly low, and the majority of iron in the human body is bound by storage, transport, and metabolic proteins. Because bacteria require iron for replication during colonization and infection, pathogens must compete to acquire iron that is tightly regulated by the host. To outcompete tight iron binding by host molecules such as transferrin and lactoferrin, Gram-negative bacteria, Gram-positive bacteria, and some fungi secrete small iron-sequestering molecules called siderophores [5, 6, 8].

Siderophores were first discovered in the 1950s with the identification of mycobactin as a growth factor for *Mycobacterium johnei* [9, 10]. Since then, over 500 distinct siderophores have been identified [11], indicating the importance of siderophores and the evolutionary pressure on pathogens to acquire iron from host environments. Siderophores are small molecules, often between 500-1500 daltons in molecular weight with high affinities for ferric iron [7, 11]. Many siderophores are important virulence factors, particularly in pathogens that

encode multiple siderophores due to acquisition of siderophore synthesis systems by horizontal gene transfer [12, 13]. In fact, strains capable of over-producing siderophores are considered to be hypervirulent [14], whereas strains unable to produce or secrete siderophores have decreased virulence and fitness during infection and colonization [15-18].

Though it is widely accepted that iron chelation by siderophores represents an important fitness advantage and virulence factor for many bacteria, the fact that so many unique siderophores are produced to perform one redundant function warrants further examination. If all siderophores chelate iron, what are the advantages of secreting more than one? The discovery of Lipocalin 2 (Lcn2; also siderocalin, neutrophil gelatinase-associated Lipocalin [NGAL], or 24p3), a molecule capable of specifically sequestering the prototypic catecholate siderophore Enterobactin (Ent) [19], supported the idea that structural diversity with functional redundancy may allow evasion of host immune factors. Specifically, many enteric pathogens can produce a glycosylated-derivative of Ent called Salmochelin (Sal) that Lcn2 cannot bind [20]. However, there is growing evidence that structural diversity allows specialization of function in scavenging iron and even other metals. These specialized roles of siderophores may impact virulence and alter the pathogenesis of bacterial infections.

This chapter will focus on the functional specialization of siderophores of Gram-negative pathogens and the impact of specialization on pathogenesis. First, the diverse capabilities of iron acquisition by siderophores, based on iron affinity, membrane permeability, and interactions with Lcn2 will be discussed.

Next, siderophore functions other than iron scavenging, including affinity for other metals, heavy metal detoxification, and the ability of siderophores to perturb host pathways will be explored. Finally, the effect of the diverse siderophore structure and function on bacterial competition, pathogenesis, and virulence will be examined. These examples indicate that siderophores are distinct and non-redundant virulence factors, consistent with their structural diversity and production in specific combinations by successful pathogens. This chapter will provide the foundational knowledge that is required to frame the hypotheses addressed within this thesis.

1.2 Specialization of siderophores for iron delivery

In order to successfully scavenge iron and deliver it to its bacteria of origin, siderophores must outcompete host proteins and the iron-acquisition mechanisms of other microorganisms occupying the same niche. Variation in siderophore structure leads to differences in iron affinity, pH optimum, membrane partitioning, and ability to evade Lcn2 within the host.

1.2.1 Structural families and ferric iron (Fe^{3+}) affinity

Bacterial siderophores can be divided into three major families based on the chemical groups involved in iron binding: catecholate, hydroxamate, and carboxylate [7, 8]. All families utilize negatively charged oxygen atoms to coordinate ferric iron, but each family has distinct characteristics that affect their affinity for iron. In addition to these three families, many mixed-type siderophores have been characterized, complicating the simple “three family” view of

siderophores. An overview of the siderophore structural families is depicted in Figure 1.1.

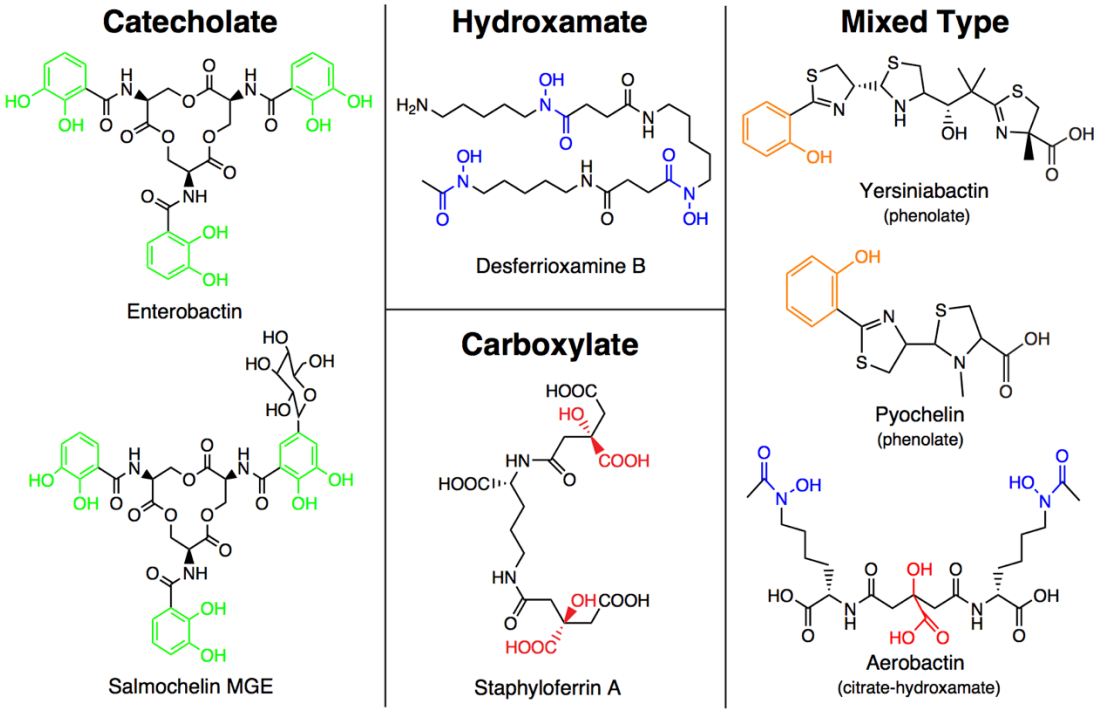

Figure 1.1: Siderophores can be divided into structural families.

Siderophores can be divided into three main structural families: catecholates, hydroxamates, and carboxylates. Binding moieties for prototypic siderophores are highlighted in green (catecholate), blue (hydroxamate), and red (carboxylate). "Mixed type" siderophores are siderophores that are considered to have elements of two or more siderophore families. Binding moieties for "mixed type" siderophores are highlighted in orange (phenolate) or a color stated above, representing its binding moiety. Salmochelin mono-glucosylated Ent (MGE) is shown as a representative of Salmochelins.

One well-studied family of siderophores is the catecholate siderophores, which include Ent, its glycosylated-derivative Sal, and bacillibactin [21-23]. Catecholate-based siderophores form 5-membered chelate rings and have the highest ferric iron affinity of any family [7, 11]. In particular, the Fe-Ent complex has a dissociation constant (K_d) of 10^{-49} M, and is capable of dissociating iron from host proteins, including the high affinity iron-binding protein transferrin (K_d=10^{-20} M) [7, 24-26]. The hydroxamate family of siderophores includes the fungal siderophores ferrichrome and (des)ferrioxamine (DFO; K_d=10^{-30} M), a *Streptomyces*-derived siderophore used clinically to chelate iron [27-31]. Hydroxamate siderophores also form five-membered chelate rings but have lower affinities for iron than catecholate siderophores [32].

Carboxylate siderophores include staphyloferrin and citrate [33, 34]. In general, at physiological pH, carboxylate siderophores are less successful at iron chelation than both the catecholate and hydroxamate families. Instead, carboxylate siderophores are more efficient chelating ferric iron at acidic pH where catecholate and hydroxamate siderophores remain protonated [32]. Thus, carboxylate siderophores may be useful to microbes living in acidic environments but are predicted to be outcompeted for iron scavenging by catechol-based siderophores in human serum and blood (pH 7.4) [32]. This is the case for phytosiderophores, which are plant-produced siderophores that utilize carboxylate oxygens to chelate iron in soil, where high affinity at pH 7 is less important than affinity at acidic pH [35].

Some siderophores, such as yersiniabactin and pyochelin, contain phenol groups and are considered to be in a phenolate family of siderophores [36, 37]. However, rather than considering phenolate siderophores as a structural family, most consider these siderophores to be “mixed-type” siderophores, with elements of two or more siderophore families [7]. Yersiniabactin (Ybt) has a moderate affinity for iron (K_d=$10^{-36.6}$ M) [38] and includes phenolate, thiazole, oxazoline, and carboxylate groups involved in iron binding [7]. Parabactin and carboxymycobactin are mixed type siderophores that include oxazoline rings [10]. Other siderophores included in this group are aerobactin (Aer, K_d=10^{-27} M, [7, 39]) that contains hydroxamate and carboxylate moieties, petrobactin that contains catechol and carboxylate moieties, and pyoverdin that is a complex mixed-type siderophore that expresses a yellow-green fluorescence [32, 39-41].

1.2.2 Lipocalin 2 binding and evasion

As the molecule with the highest known affinity for ferric iron, Ent can out-compete with host iron carriers for binding. To oppose the acquisition of iron by Ent, host epithelial cells and neutrophils secrete the protein Lcn2. Initially discovered as a neutrophil granule protein [42], it was later shown to bind to and sequester Ent with high specificity and affinity [15, 19, 43, 44]. The binding of Ent by Lcn2 has been shown to be pro-inflammatory, as indicated by the secretion of the neutrophil chemoattractant Interleukin (IL)-8 by cultured respiratory epithelial cells [45]. The affinity of Lcn2 for Ent is similar to that of its bacterial receptor FepA, allowing Lcn2 to effectively compete with bacteria for binding to Ent, thus limiting bacterial growth [20, 46]. Lcn2 is induced as a general response to both

Gram-positive and Gram-negative infections [43, 47]. Its protective effect was first illustrated in an *Escherichia coli* sepsis model, in which wild-type (WT) mice survived infection with an Ent-producing strain of *E. coli* but Lcn2-deficient mice did not. In contrast, Lcn2-deficient (LcnKO) mice were equally as sensitive as wild-type mice to infection with *Staphylococcus aureus*, bacteria that do not rely on Ent for iron acquisition [43]. Lcn2 is also protective against nasal colonization and pneumonia caused by *K. pneumoniae* and urinary tract infections (UTI) caused by *E. coli,* provided that the bacteria depend on Ent for iron acquisition [13, 15, 48-50]. In addition to Ent, Lcn2 can bind and sequester the catecholate siderophore bacillibactin from *Bacillus anthracis* and the mixed-type, oxazoline containing siderophores carboxymycobactin from *M. tuberculosis* and parabactin, demonstrating that Lcn2 is capable of binding siderophores from both Gram-positive and Gram-negative pathogens [51, 52].

Due to the strong bacteriostatic effects of Ent sequestration by Lcn2, bacteria have developed mechanisms to evade Lcn2 in their quest to obtain iron. One mechanism of evasion is to modify Ent through the addition of glucose groups to produce Sal [18, 20, 53]. Sal is structurally identical to Ent except for the covalent addition of one to three glucose groups at the ends of the catecholate arms. The *iroA* gene cluster, found in many pathogenic Gram-negative bacteria, encodes the glycosylation, export, import, and esterase activities required to produce and utilize this siderophore [18, 54]. Glycosylation of Ent prevents interaction between Sal and Lcn2 due to steric hindrance, which

leads to effective evasion of Lcn2, acquisition of iron required for bacterial replication, and the restoration of virulence in Lcn2-producing mice [15, 18, 20].

Another method bacteria employ to evade Lcn2 is to encode additional siderophores that Lcn2 cannot bind. Strains of *K. pneumoniae* that encode Ybt readily cause pneumonia, whereas strains that only encode Ent are opportunistic, causing severe pneumonia but only in LcnKO mice [13]. Similarly, *B. anthracis* commonly secretes petrobactin in addition to bacillibactin, a Lcn2 ligand. Only petrobactin, a Lcn2-evasive siderophore, is required for virulence in macrophages and murine models [51, 55-57]. Many successful pathogenic bacteria encode multiple siderophores, including- or sometimes exclusively-Lcn2-evasive siderophores [13, 58-61]. For example, *Yersinia pestis* secretes Ybt but not Ent [62].

Finally, an additional way to evade Lcn2 is to utilize xenosiderophores: Siderophores produced by another microorganism that the pathogen cannot make itself. This has been demonstrated both *in vitro* and *in vivo* with bacterial use of the fungal siderophore ferrichrome [43]. Addition of ferrichrome to *E. coli* H9049 enhances bacterial growth under iron-limiting conditions as well as in the presence of Lcn2. During infection models, WT mice infected with *E. coli* H9049 survived infection, but injection of ferrichrome caused susceptibility to infection [43]. In sites of polymicrobial colonization or infection, the ability to utilize xenosiderophores could provide a general fitness advantage in competition with other microorganisms for iron and specifically aid in the evasion of Lcn2. Together, the literature demonstrates the significance of the siderophore-Lcn2

interaction, which causes detrimental effects to bacterial growth and infection but can be subverted by siderophore modification or the encoding of additional Lcn2-evasive siderophores.

1.2.3 Membrane partitioning

In the host, there are both intracellular and extracellular sources of iron, separated by cellular membranes. Differences in structure between various siderophores suggest disparities in siderophore function and ability, including the ability to access cellular contents via membrane partitioning [8]. As reviewed above, the addition of hydrophilic glucosyl groups to Ent creates Sal, a Lcn2-evasive siderophore. Glycosylation, followed by linearization of Sal, also reduces the molecule's affinity for membranes, effectively decreasing the membrane partitioning constant [54]. In contrast, Ent's high affinity for membranes causes it to partition into phospholipid vesicles. When iron is present outside these vesicles, the ability of Ent to scavenge this iron decreases ~75%, whereas Sal retains its scavenging ability. Sal could therefore aid in the acquisition of extracellular iron in membrane-rich environments [18, 54].

Although Ent readily partitions into membranes and depletes cellular iron, it does not appear to deliver cell-associated iron back to bacteria. In contrast, Aer secreted by *E. coli* can readily deliver host cellular iron back to bacteria [63]. When *E. coli* were incubated with ^{59}Fe labeled transferrin or leukemia cells, but separated from both by a dialysis membrane, Ent delivered iron by scavenging it away from transferrin whereas Aer scavenged iron primarily from host cells [63]. The preferential scavenging of iron from tissues by Aer may explain why invasive

strains of bacteria are more likely to secrete Aer even though it has lower affinity for iron than other siderophores [63, 64]. Although these data indicate that Aer efficiently accesses cellular iron, it is not known if this corresponds to a high membrane partitioning constant. The differing ability of siderophores to chelate iron among physiologically relevant molecules, such as lipids, indicates distinct roles for siderophores depending on the niche in which the bacterium finds itself.

1.3 Non-iron delivery functions of siderophores

As detailed above, siderophores are highly potent iron binding molecules that are specialized in their ability to scavenge iron for bacterial replication under varying conditions. Recent literature suggests novel roles and characteristics of siderophores, including the ability to bind other metals, prevent oxidative burst during infection, and perturb host cell homeostasis (Figure 1.2).

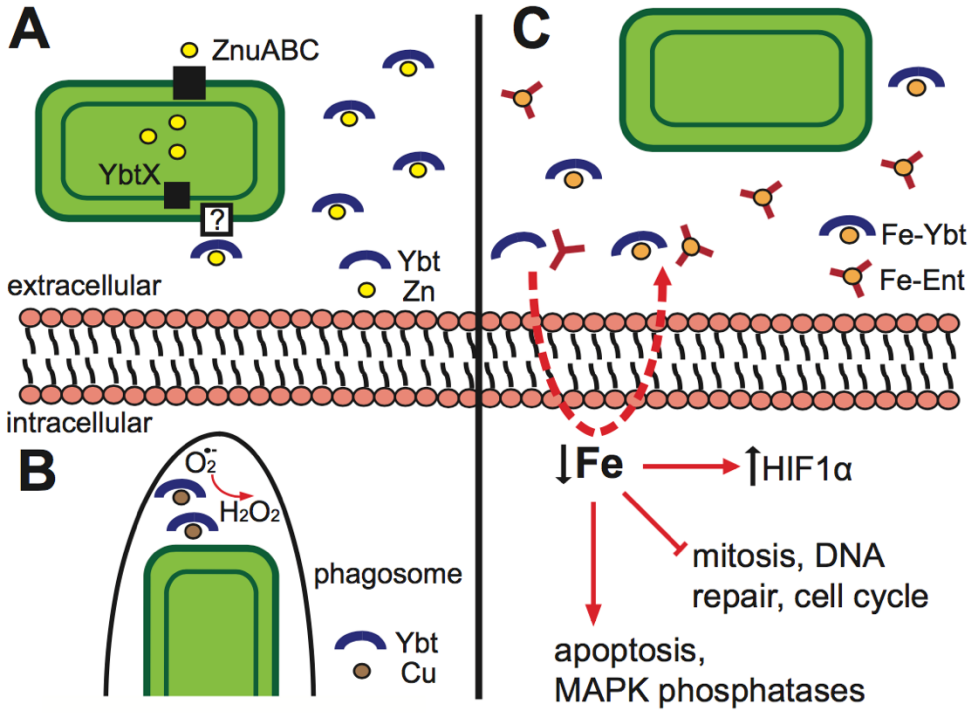

Figure 1.2: Novel characteristics and roles of siderophores.

A) Bacteria can secrete Ybt to sequester Zn^{2+}, which is taken up by the inner membrane receptor YbtX. This function can compensate for loss of the Zn^{2+} active transport system ZnuABC in septicemic plague. B) Cu^{2+}-Ybt can act as a superoxide dismutase mimic within phagosomes, protecting bacteria from harmful reactive oxygen species. C) Iron chelation by siderophores can modulate host pathways, including the stabilization of HIF-1α, the upregulation of apoptosis genes and MAPK phosphatases, and the downregulation of DNA repair, mitosis, and cell cycle genes.

1.3.1 Heavy metal sequestration and detoxification

Although they have extremely high affinity for ferric iron, siderophores are capable of binding additional metals as well [65, 66]. For example, DFO can bind Ga^{3+}, Al^{3+} and In^{3+}, albeit at a lower affinity than for Fe^{3+} [67]. Binding of non-iron metals by siderophores may benefit bacteria by preventing heavy metal toxicity [65]. For example, pyoverdin and pyochelin-mediated binding of metals including Al^{3+}, Co^{2+}, Cu^{2+}, Eu^{3+}, Ni^{2+}, Pb^{2+}, Tb^{3+}, and Zn^{2+} results in increased metal tolerance of *Pseudomonas aeruginosa*. This protection appears to be due to extracellular binding to metals by siderophores without subsequent internalization of the siderophore-metal complex [68-70]. Although the pyochelin (Pch) receptor FptA binds Pch complexes with non-iron metals with similar affinity as Fe-Pch, these metals are internalized at substantially reduced rates or not at all [69]. Ybt-mediated binding of Cu^{2+} results in increased copper resistance in Uropathogenic *E. coli* (UPEC) compared to rectal isolates, and Cu-Ybt complexes are present in urine from infected women at concentrations greater than Fe-Ybt [71]. These findings indicate that siderophores can sequester toxic metals, and bacteria can exclude these complexes from their cytoplasm at the step of siderophore import. It is likely that this phenomenon is relevant to additional siderophores, heavy metals, and bacterial species.

1.3.2 Heavy-metal bound siderophores as protection against reactive oxygen species

In addition to preventing copper toxicity, Cu^{2+}-Ybt complexes can act as a superoxide dismutase mimic, transforming oxygen radicals to more stable, less

dangerous forms [72]. In fact, Ybt from *E. coli* promotes intracellular survival in phagocytes that depends on both copper and the respiratory burst [72]. The superoxide dismutase activity of Cu^{2+}-Ybt complexes may facilitate the intracellular survival of some extracellular pathogens, including UPEC, which have higher intracellular survival than non-pathogenic strains [72, 73]. Purified Ybt is also capable of inhibiting Reactive Oxygen Species (ROS) production in innate immune cells, particularly in neutrophils and macrophages [74]. Aer and DFO were also shown to inhibit ROS production by neutrophils and macrophages, but at lower rates. The ability of apo-Ybt to inhibit ROS production was significantly greater than Fe-Ybt, suggesting that metal chelation is critical to this function. Whether the active ligand is Fe, Cu or another metal is unknown, and the mechanism of action of Ybt on phagocyte ROS production is unclear [74]. These data indicate specific iron-independent abilities for Ybt that separate it from other bacterial siderophores and aid in virulence in strains of bacteria able to produce Ybt.

1.3.3 Uptake of non-iron metals

Similar to the requirement for ferric iron is the cellular requirement for nutritional Zn^{2+}. The *Y. pestis* Zn^{2+} transporter ZnuABC is responsible for zinc uptake, however, z*nuBC* mutants remain virulent in certain murine models of the plague [75]. This has led to the suggestion of the presence of “zincophores,” molecules capable of scavenging zinc [76, 77]. A dedicated zincophore has yet to be discovered. However, two iron-binding siderophores have been shown to bind and utilize Zn^{2+} as well. *Pseudomonas putida* secretes pyridine-2,6-

bis(thiocarboxylic acid) (PDTC), a small siderophore capable of binding and delivering Fe^{3+} and Zn^{2+} to the bacteria [78, 79]. In a *Y. pestis znuBC* mutant, Ybt is required for Zn^{2+} uptake and growth in Zn^{2+} limited conditions [80]. This zinc transport requires the inner membrane receptor YbtX but not the ferric-Ybt receptor Psn. These data are the first to identify a role for dual metal-acquisition by a single siderophore and indicate a new role for siderophores during infection. It is likely that the binding of heavy metals other than iron by siderophores serves additional purposes for bacteria that are yet to be discovered.

1.3.4 Ability to disrupt host cell homeostasis

Since iron is imperative to many cellular processes, its chelation by siderophores could significantly affect host cellular homeostasis. Depending on the cellular response, siderophores can act as toxins causing cell death or immunomodulators. Such is the case with DFO, which has been evaluated as a cancer therapeutic because it can induce cell-cycle arrest and apoptosis, but can also induce inflammation via cytokine production in a variety of cell types [81-85].

1.4 Implications of siderophore specialization during infection

As reviewed above, siderophores can be produced in a variety of structures, lending to variability in their affinity for iron, ability to be sequestered by Lcn2, ability to bind and utilize other heavy metals, and capacity to initiate host cellular pathways. Thus, the combination of siderophores produced by a bacterium could affect its pathogenesis, localization during infection, and instigation of specific immune responses (Figure 1.3).

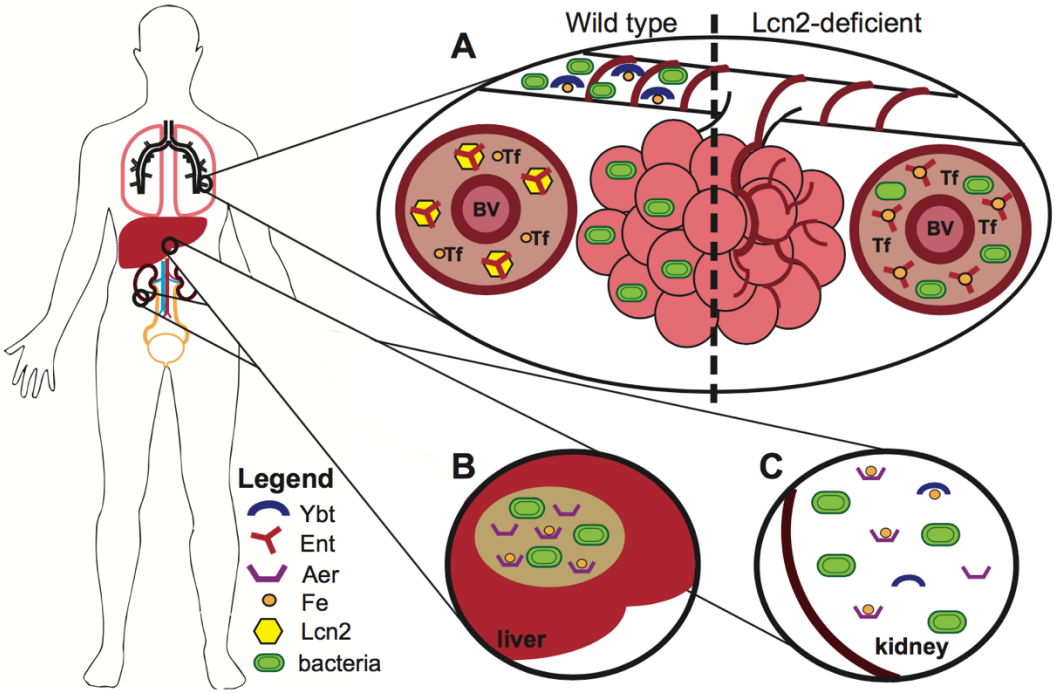

Figure 1.3: Siderophore production by bacteria can determine infection localization and "replicative niche."

A) During infection with K. pneumoniae, the ability to produce Lcn2-evasive siderophores, such as Ybt, results in bronchopneumonia but not perivascular growth (left). In a Lcn2-deficient mouse, Ent promotes a perivascular localization of infection by accessing iron from transferrin (Tf) for growth. B) Hypervirulent strains of K. pneumoniae that form pyogenic liver abscesses are associated with the secretion of Aer. C) The receptors for Aer and Ybt are involved in bacteria colonization during Uropathogenic E. coli ascending UTI. In fact, vaccination with the Ybt receptor FyuA is protective for the kidney in murine models of ascending UTI.

1.4.1 Ability of siderophores to evade Lcn2 mediates competition within the host

By using siderophores to acquire scarce host iron during infection, some bacteria can successfully compete for replicative niches in the intestines and the nasal cavity, allowing bacterial colonization. In fact, pathogens such as *Salmonella enterica* Serotype Typhimurium can exploit Lcn2 to outcompete other bacteria based solely on its ability to use Sal. *Raffatellu et al* first demonstrated that *S.* Typhimurium can outcompete an isogenic mutant of the Sal receptor, IroN, in the intestines [86]. Furthermore, by inducing IL-22 and expression of Lcn2, *S.* Typhimurium can outcompete commensal *E. coli* [87]. Probiotics, such as *E. coli* Nissle, may protect against diarrheal infections. In this case, *E. coli* Nissle has a greater diversity of Lcn2-resistant siderophores than *S.* Typhimurium and causes a reduction in *S.* Typhimurium colonization that depends on the presence of Lcn2 and iron uptake by *E. coli* Nissle [88]. In a nasal colonization model, *Streptococcus pneumoniae* and *Hemophilus influenzae* significantly induce Lcn2 but use siderophore-independent mechanisms to acquire iron [47]. This inability to produce Ent and instead uptake iron through other mechanisms could offer a competitive advantage by allowing colonization of a niche that is inhospitable to *Enterobacteriaceae*. By either not making siderophores or making more than a competitor, certain bacteria may leverage Lcn2 for their advantage [89].

1.4.2 Ability to produce multiple siderophores correlates with clinical disease

K. pneumoniae is a Gram-negative pathogen that requires siderophores for virulence and is capable of causing pneumonia, UTI, wound infections, and septicemia [90]. A comparison of isolates from various body sites of infected patients found increased prevalence of Ybt^+ strains from respiratory tract samples when compared to urine, blood, and stool samples [13]. Accordingly, Ybt production was sufficient to evade Lcn2 and cause pneumonia in a mouse model. Ent-dependent strains represent the predominant genotype of clinical isolates, but this genotype is inhibited in the wild-type mouse. In the LcnKO mouse, this genotype is highly virulent. Therefore, decreased Lcn2 levels would be predicted to put patients at increased risk from infection. Indeed, lung Lcn2 levels vary significantly in intensive care patients, and low levels correlate with worsened survival from Gram-negative pneumonia [91]. Similarly, Lcn2 levels rise in women with a UTI, and UPEC isolates with greater numbers of Lcn2-resistant siderophores are associated with greater bacterial density [49, 50].

A recent analysis of 57 carbapenem-resistant (CR) *K. pneumoniae* isolates of the epidemic sequence type (ST) 258 found an entire clade of ST258 strains with a deletion in the Ent exporter, *entS* [92]. This mutation could represent another form of Lcn2 evasion [92]. It is possible that these strains are "cheaters," who utilize siderophores made by other bacteria for iron acquisition and energy usually reserved for Ent export for other functions, or acquire iron through siderophore-independent mechanisms. This could represent another

situation in which bacteria utilize xenosiderophores to gain a competitive advantage in their replicative niche.

Whereas utilization of Ent may pose significant fitness tradeoffs, hypervirulent strains of *K. pneumoniae* causing severe liver abscesses in Asia are associated with carriage of multiple siderophore loci, including those for Ybt, Sal, and Aer [93]. In particular, secretion of Aer is highly associated with pyogenic liver abscess (PLA) isolates of *K. pneumoniae* and results in significantly higher siderophore production compared to non-PLA strains [94, 95]. In contrast, only 2% of *K. pneumoniae* strains isolated from the respiratory tract, urine, blood or stool from a U.S. hospital carried Aer [13]. It is possible that acquisition of Aer secretion could lead to more virulent strains of *K. pneumoniae* in the U.S. as well.

1.4.3 Siderophores can influence infection localization and determine bacterial "replicative niche"

The production of siderophores can influence the anatomic site and pattern of infection. In murine models of pneumonia, infection of WT mice with Ybt^+ strains of *K. pneumoniae* resulted in bronchopneumonia with moderate bacterial density in the lungs and spleen [96]. Infection with Ent^+ strains in WT mice resulted in low bacterial burden and airway localization of inflammation. However, infection of LcnKO mice with an Ent^+ or Ent^+Sal^+ mutant resulted in perivascular invasion by bacteria, high bacterial burden, invasion to the spleen, and poor survival of the mice [13, 96]. The perivascular space is rich with transferrin during infection, and the patterns of pneumonia correlated with the ability of Ent, but not Ybt, to

support replication with transferrin as an iron source. This indicates that, due to differences in iron-scavenging capabilities between siderophores, Ent is required for perivascular infiltration but can only do so if Lcn2 is deficient. These data also suggest that Lcn2 could partially protect from bacterial dissemination.

The ability of *E. coli* to cause UTI is significantly affected by its complement of siderophores. Models of competitive infection in mice have shown that receptors for non-catecholate siderophores are instrumental in the establishment of bacterial colonies in ascending UTI infections [97]. The receptors for Aer and Ybt, but not other siderophores, were shown to be critical for colonization of the bladder and the kidney [97]. To further demonstrate the importance of these siderophore receptors, murine studies involving vaccination with the Ybt receptor resulted in protection from ascending UTI, specifically in the kidney [98]. Successful vaccination with the Ybt receptor exemplifies the potential of siderophore-specific pathways as therapeutic targets during infection. Whether Aer or Ybt is more crucial in establishment of bladder or kidney infection has yet to be examined. However, Ybt genes are present among cystitis and pyelonephritis isolates at similar frequencies, suggesting that Ybt is equally important for infection in both the bladder and kidneys [99].

Y. pestis requires the presence of Ybt for full virulence depending on the route of inoculation. Ybt mutants are fully virulent when infected intravenously in murine models of septicemic plague as long as the Znu zinc-transport system is intact [80]. However, a Ybt mutant is essentially avirulent by subcutaneous injection, indicating the requirement of Ybt during a stage of bubonic plague

infection [100]. In a pneumonic plague model of infection, the absence of Ybt also decreased virulence of *Y. pestis* following intranasal infection with bacteria [101]. The differential requirement for Ybt based on infection site may stem from a complex interaction with Fe, Cu and Zn. For example, whereas Zn can be acquired by redundant mechanisms in septicemic plague, perhaps Cu^{2+}-Ybt or Fe^{3+}-Ybt complexes are instrumental in pneumonic plague. These data exemplify the ability to siderophores to aid in virulence based on route of infection, and further support the hypothesis that siderophores can determine infection localization and replicative niche.

1.4.4 Siderophores, hypoxia, and disease

Secretion of siderophores can modulate host pathways and transcription factors, as described above. One transcription factor that siderophores can modulate that may have interesting effects on the host is Hypoxia Inducible Factor-1α (HIF-1α). HIF-1α controls the transcription of many gene families, including inflammatory-cytokine, glycolysis, and angiogenesis genes [102, 103]. Under normoxia, HIF-1α is rapidly made and degraded by the proteasome through prolyl hydroxylation that requires both oxygen and iron. HIF-1α stabilization and subsequent dimerization with the β subunit is induced by either low oxygen or low iron, as iron is a required cofactor for its degradation [104, 105]. HIF-1α was initially shown to coordinate an adaptive response to hypoxia, which can occur directly from low oxygen or indirectly from low iron that compromises oxygen-dependent processes such as cellular respiration. Recently, HIF-1α has been shown to be

stabilized by Sal and Ybt, indicating that cellular iron chelation by siderophores can induce this pathway [106].

It is unclear what effect the stabilization of HIF-1α by siderophores, independent of hypoxia, would have on infection and pathogenesis. However, the ability of siderophores to induce host cell hypoxic responses has been shown to alter the outcome of infection. In a *Caenorhabditis elegans* infection model, *P. aeruginosa* killed worms in a pyoverdin-dependent manner that was associated with activation of a hypoxic host response. This response included hypoxia-dependent activation of HIF-1α that was partially protective, as a *hif-1* mutation exacerbated killing [107]. Similarly, *Y. enterocolitica* induces HIF-1α during orogastric infection of mice, and Hif-1a$^{-/-}$ mice have worsened survival [106]. Furthermore, pharmacologic activation of HIF-1α can protect against infection through enhancement of phagocyte function [108]. These results suggest that disruption of host cell homeostasis by siderophores can be lethal but can also serve as a danger signal and activate HIF-1α that may be protective. Further work must be done to uncover if there is a relationship between siderophore-dependent, hypoxia-independent stabilization of HIF-1α.

1.5 Gaps in knowledge

Significant progress has been made in the recent years to define the specialized characteristics of several siderophores, but many questions remain unaddressed. Siderophores are capable of binding non-iron heavy metals, but this has potential advantages and disadvantages to the bacteria. Recent work suggests that

siderophores bind heavy metals to detoxify its environment. However, it is unclear how the bacterium avoids transporting the heavy metal-siderophore complex into the cell. One unanswered question most relevant to this thesis revolves around the fact that siderophores can act as both toxins and immunomodulators, but it is unclear whether activation of host pathways such as HIF-1α-regulated gene expression is ultimately beneficial to the host or the bacterium. Finally, it has been shown that strains producing certain siderophores have heightened virulence, as is the case with strains of *K. pneumoniae* that secrete Lcn2-evasive siderophores. However, it is unknown what the specific effects of siderophores are *in vivo* beyond iron acquisition for the bacteria.

1.6 Outline of the Thesis

The central goal of this thesis is to define the host response to siderophores during infection with *K. pneumoniae*. The overarching hypothesis of this work is that the secretion of siderophores by *K. pneumoniae* results in the chelation of host iron, leading to the modulation of host responses that impact infection outcome independent of siderophore-mediated delivery of iron to bacteria. This work will aid in defining the mechanism by which siderophores and iron acquisition by *K. pneumoniae* alter the host response, leading to a better fundamental understanding of host-pathogen interactions during infection with Gram-negative bacteria. In Chapter II, the host cellular response to siderophores is characterized using purified components and an *in vitro* stimulation system. The regulation of gene families upon stimulation with purified Ent and Lcn2 is

characterized using microarray analysis. Furthermore, it is shown that the chelation of host iron by siderophores results in the secretion of IL-8, IL-6 and CCL20, as well as the stabilization of HIF-1α, within cultured respiratory cells. In Chapter III, the *in vitro* results are expanded upon by utilizing a murine model of pneumonia and a role for siderophores in the induction of the host immune response during *K. pneumoniae* infection is demonstrated. It is also shown that siderophore secretion causes bacterial dissemination to the spleen, and that this occurs through siderophore-dependent stabilization of HIF-1α in alveolar epithelial cells. In Chapter IV, the effect of a mutation in the Ent exporter in a set of CR *K. pneumoniae* clinical isolates is examined. The ability of the various isolates to secrete iron chelators and to grow in iron-limiting conditions is characterized. Additionally, genes that are differentially regulated between the isolates with intact or deleted entS, such as the hemin transport operon, are identified. In Chapter V, the findings of this thesis are dissected, and the implications of these findings for *K. pneumoniae* infection are discussed. Finally, further questions and experimentation to expand the understanding of siderophore-dependent effects on host-pathogen interactions are suggested.

1.7 Notes

The text and figures from sections 1.1-1.5 have been published and are reproduced with adaptations by permission of The Royal Society of Chemistry: Holden, VI and MA Bachman. 2015. Diverging roles of bacterial siderophores during infection. *Metallomics* 7: 986-995. http://pubs.rsc.org/en/content/articlelanding/2015/mt/c4mt00333k#!divAbstract

CHAPTER II

IN VITRO EFFECTS OF PURIFIED SIDEROPHORES AND LIPOCALIN 2 ON CULTURED RESPIRATORY EPITHELIAL CELLS

Summary

Iron is essential for many cellular processes and is required by bacteria for replication. To acquire iron from the host, pathogenic Gram-negative bacteria secrete siderophores, including Ent. However, Ent is bound by the host protein Lcn2, preventing bacterial reuptake of aferric or ferric Ent. Furthermore, the combination of Ent and Lcn2 (Ent+Lcn2) leads to enhanced secretion of IL-8 compared to either stimulus alone. Modified or structurally distinct siderophores, including Ybt and Sal, deliver iron to bacteria despite Lcn2. We hypothesized that the robust immune response to Ent and Lcn2 requires iron chelation rather than the Ent+Lcn2 complex itself, and can also be stimulated by Lcn2-evasive siderophores. To test this hypothesis, cultured respiratory epithelial cells were stimulated with combinations of purified siderophores and Lcn2, and analyzed by gene-expression microarrays, quantitative PCR, and cytokine immunoassays. Ent caused HIF-1α protein stabilization, induced the expression of genes regulated by HIF-1α and repressed genes involved in cell cycle and DNA replication, whereas Lcn2 induced expression of pro-inflammatory cytokines. Iron chelation by excess Ent or Ybt significantly increased Lcn2-induced secretion of

IL-8, IL-6 and CCL20. Stabilization of HIF-1α was sufficient to enhance Lcn2-induced IL-6 secretion. These data indicate that respiratory epithelial cells can respond to bacterial siderophores that evade or overwhelm Lcn2 binding by increasing pro-inflammatory cytokine production.

2.1 Introduction

Due to its ability to assume multiple oxidative states, iron is an essential element in many human cellular processes including DNA replication, oxygen metabolism, and electron transfer [2, 3]. Iron homeostasis represents a unique challenge since free ferric iron (Fe^{3+}) is insoluble and ferrous iron (Fe^{2+}) can be toxic to cells. Therefore, ferric iron is transported while complexed to transferrin, maintaining serum iron concentrations at ~10^{-24} M [5, 6, 109]. Bacteria require ~10^{-6} M of iron in their cytosol for cellular processes, a much higher concentration of iron than is readily available [6]. To acquire the iron necessary for growth in the iron-limiting conditions of the human body, Gram-negative pathogens such as *E. coli* and *K. pneumoniae* secrete the siderophore Ent. Ent is a prototypical catecholate siderophore with the highest known affinity for iron [6, 20, 109].

To counter the iron-scavenging effects of Ent, neutrophils and host mucosal cells secrete Lcn2 [43]. Lcn2 binds Ent in its binding pocket, either in its ferric (FeEnt) or aferric form, thereby disrupting bacterial iron acquisition and inhibiting bacterial replication [15, 19, 20, 43]. Lcn2 is critical for host defense, as

LcnKO mice rapidly succumb to infection with *E. coli* and *K. pneumoniae* isolates that depend on Ent for iron acquisition [13, 43, 48, 110].

As an evasion mechanism, some strains of *K. pneumoniae* and other Gram-negative bacteria secrete siderophores that are not bound by Lcn2, including Sal and Ybt. Sal is glycosylated Ent that cannot be bound by Lcn2 due to steric hindrance from added glucose groups [6]. Additionally, the glucose groups decrease the membrane partitioning ability of Ent, potentially altering the ability of Sal to access cellular iron [54]. Ybt is a phenolate siderophore with high iron affinity that is structurally distinct from Ent and promotes pneumonia despite Lcn2 [6, 13, 38]. Production of either Sal or Ybt by strains of *K. pneumoniae* is sufficient for bacterial growth during nasal colonization and pneumonia [13, 15].

The interaction between siderophores and Lcn2 can modulate the inflammatory response to infection. Ent and Lcn2 each induce secretion of the neutrophil chemoattractant IL-8 by cultured respiratory epithelial cells [45]. However, the combination of Ent+Lcn2 is highly pro-inflammatory, increasing IL-8 production above the combined effects of Ent and Lcn2 alone. During nasal colonization, Lcn2 enhances neutrophil influx in response to *K. pneumoniae* producing both Ent and Ybt [15].

Other siderophores also activate cytokine expression. For example, DFO, a non-pathogenic siderophore used therapeutically, induces IL-8 secretion through p38 Mitogen Activated Protein kinase (MAPK) signaling in a lung carcinoma cell line and an intestinal epithelial cell line [84, 111]. DFO also stabilizes the global transcriptional regulator HIF-1α. Expression of HIF-1α

protein is regulated through proline hydroxylation by prolyl hydroxylases, a reaction that targets the protein for rapid proteasomal degradation and requires iron and oxygen as cofactors. Thus, HIF-1α stabilization can be induced by both oxygen and iron starvation [112]. In turn, a wide variety of gene families can be activated, including genes involved in angiogenesis, iron metabolism, glycolysis, and inflammation [104, 105, 113, 114]. In contrast to DFO, the mechanism by which Ent induces cytokine production is unknown.

Whereas Lcn2 is known to induce IL-8 production and neutrophil recruitment in an Ent-dependent manner, Lcn2 is also an instrumental participant in the immune response to pathogens in an Ent-independent manner. During infection with *Mycobacterium tuberculosis*, Lcn2 induces alveolar macrophage expression of KC, a neutrophil chemoattractant, while inhibiting T cell accumulation and expression of the chemokine CXCL9 [115]. Additionally, Lcn2 promotes pro-inflammatory IL-1β and Interferon (IFN)-γ secretion, as well as granulocyte recruitment, during malaria infection [116]. These results indicate a role for Lcn2 in the inflammatory response to infections independent of its ability to bind Ent. Because iron chelation alone induces cytokine release, we hypothesized that the combined effects of siderophore-mediated iron starvation and the presence of Lcn2, rather than inherent properties of the Ent+Lcn2 complex, enhances inflammation in epithelial cells. The objective is of this study was to determine the mechanism by which siderophores and Lcn2 combine to induce inflammatory responses in respiratory epithelial cells. To accomplish this, inflammatory gene expression pathways induced in response Ent, Lcn2 and

Ent+Lcn2 were identified by microarray analysis of mRNA transcripts. To determine whether Lcn2 modulates inflammation specifically to Ent or more broadly in the context of iron starvation, respiratory epithelial cells were stimulated with the bacterial siderophores Ent, Ybt, and Sal in combination with Lcn2 and iron starvation responses and cytokine secretion were measured.

2.2 Results

2.2.1 Ent and Ent+Lcn2 induce distinct gene expression and cytokine secretion responses in respiratory epithelial cells

The combination of Ent+Lcn2 strongly induces secretion of IL-8, a pro-inflammatory cytokine responsible for neutrophil chemotaxis [45]. However, the mechanism of this inflammation and whether Ent+Lcn2 triggers additional cellular responses is unknown. To identify cellular pathways induced or repressed by combinations of Fe, Ent, Lcn2, or Ent+Lcn2, microarray analysis was performed on mRNA transcripts from stimulated A549 human respiratory epithelial cells. The array data and our statistical analysis have been deposited in NCBI's Gene Expression Omnibus (GEO) and are accessible through GEO Series accession GSE54962 [117]. We calculated the number of significant probe-set differences for many possible comparisons for 29096 probe-sets from our two experiments (Table 2.1). For comparisons that are the focus of this study, we collapsed the probe-sets to 19419 distinct genes (Table 2.2).

Table 2.1: Comparison of gene expression using 29096 non-control probe sets.

Experiment	Comparison	Selection p<.01,FC>1.3	
		Up	Down
exp1	LCN2 vs PBS	90	97
exp1	ENT+LCN2 vs PBS	491	400
exp1	ENT+LCN2+FE vs PBS	87	139
exp1	ENT+LCN2 vs LCN2	404	80
exp1	ENT+LCN2+FE vs LCN2	7	13
exp1	ENT+LCN2+FE vs ENT+LCN2	112	300
exp2	ENT vs PBS	1992	2536
exp2	FE vs PBS	78	44
exp2	ENT+FE vs PBS	992	1660
exp2	FE vs ENT	2081	1752
exp2	ENT+FE vs ENT	576	1133
exp2	ENT+FE vs FE	723	1124
exp2	interaction (ENT/PBS) / (ENT+FE/FE)	1320	931
selection #1	Ent+Lcn2 vs. both Lcn2 and FeEnt+Lcn2 in exp 1	261	42
selection #2	interaction (ENT/PBS) / (ENT+FE/FE) in exp 2	1320	931
selection #3	intersection of selection 1 and 2.	144	23

Table 2.2: Conversion of probe-sets to distinct genes.

	probe-sets up	probe-sets down	probe-sets altered	genes up	genes down	genes altered
Ent+Lcn2 vs. both Lcn2 and Fe-Ent+Lcn2 in exp 1	261	42	303	239	36	275
interaction in exp2, Ent/PBS is bigger than Fe-Ent/Fe	1320	931	2251	1152	812	1964
intersection of 1 and 2	144	23	167	137	21	158
exp2: Ent vs both PBS and Fe-Ent	876	527	1403	760	458	1218
exp1: Lcn2 vs PBS	90	97	187	56	80	136
total number of objects			29096			19419

Hereafter we report results in terms of distinct genes. To identify gene expression specific to the iron status of Ent, cells were stimulated with combinations of Fe and Ent and an interaction test was used to determine if the Ent vs. PBS difference was significantly larger, or smaller, than the Fe-Ent vs. Fe difference by a factor of at least 1.3, and with $p<0.01$ [(Ent/PBS)/(Fe-Ent/Fe)]. This interaction test demonstrated induction of 1152 genes and repression of 812 genes in response to aferric Ent. Gene ontology analysis indicated significant induction of genes related to MAPK phosphatase activity, apoptosis, and response to cytokine stimulus and repression of genes related to cell cycle, DNA replication, mitosis, and DNA repair (Table 2.3 and Figure 2.1).

Table 2.3: Gene ontology analysis of genes meeting selection criteria.

Selection criteria	Direction of change	Distinct genes in selection, with GO terms #	Title of Gene Ontology (GO) list *	Genes on list	Genes in intersection	p-value one-sided Fisher Exact test $	Rank of list in that list source	Estimated FDR (Q-value) @	Observed / expected for intersection
Ent/PBS > Ent+Fe/PBS	up	1112	protein binding	6758	541	6.92E-13	1	0.000	1.26
			cytoplasm	4576	383	9.42E-11	2	0.000	1.32
			MAP kinase tyrosine/serine/threonine phosphatase activity	13	8	2.44E-07	3	0.000	9.72
			positive regulation of smooth muscle cell proliferation	35	11	6.36E-06	4	0.000	4.96
			kinase activity	749	78	9.21E-06	5	0.000	1.64
			apoptosis	577	62	3.03E-05	6	0.005	1.70
			response to cytokine stimulus	64	14	3.72E-05	7	0.004	3.45
			positive regulation of anti-apoptosis	36	10	5.56E-05	8	0.006	4.39
	down	781	cell cycle	509	110	1.40E-45	1	0.000	4.86
			DNA replication	156	59	2.02E-39	2	0.000	8.50
			mitosis	219	65	6.89E-36	3	0.000	6.67
			cell division	291	72	6.32E-34	4	0.000	5.56
			DNA repair	260	63	3.21E-29	5	0.000	5.45
			chromosome, centromeric region	119	41	7.40E-26	6	0.000	7.75
			nucleoplasm	481	81	1.04E-25	7	0.000	3.79
			response to DNA damage stimulus	286	59	1.55E-23	8	0.000	4.64
ENT+LCN vs both LCN and ENT+LCN+Fe	up	235	glycolysis	44	9	5.573E-09	1	0.000	15.28
			response to hypoxia	160	14	3.279E-08	2	0.000	6.54
			endoplasmic reticulum	928	33	2.795E-07	3	0.000	2.66
			endoplasmic reticulum unfolded protein response	22	6	3.361E-07	4	0.000	20.38
			cholesterol biosynthetic process	28	6	1.587E-06	5	0.000	16.01
			sterol biosynthetic process	29	6	1.978E-06	6	0.000	15.46
			L-ascorbic acid binding	21	5	7.027E-06	7	0.000	17.79
			steroid biosynthetic process	58	7	1.183E-05	8	0.000	9.02
	down	36	mitotic prometaphase	2	2	4.078E-06	1	0.000	487.78
			condensed nuclear chromosome outer kinetochore	3	2	1.224E-05	2	0.010	325.19
Lcn2 vs PBS	up	46	immune response	334	10	1.203E-08	1	0.000	11.43
			extracellular space	724	12	2.358E-07	2	0.000	6.33
			extracellular region	1685	17	5.325E-07	3	0.000	3.85
			innate immune response	143	6	1.881E-06	4	0.000	16.02
			chemokine activity	41	4	3.887E-06	5	0.000	37.24
			cytokine activity	187	6	8.849E-06	6	0.008	12.25
			positive regulation of nitric oxide biosynthetic process	25	3	3.716E-05	7	0.010	45.81
			complement activation, classical pathway	27	3	4.709E-05	8	0.010	42.42
	down	72	None						

Enrichment testing performed after collapsing selections of significant probe-sets (of 29096 probe-sets) to be selections of distinct genes (19419 distinct genes).
* Top 8 hits are shown or until estimated false discovery rate >0.05
$ Tests were based on the intersection of genes we selected as altered, with gene lists from these other sources, and the size of the intersection judged based on one-sided Fisher Exact tests.
@ False discovery rate (FDR) estimates were based on analyzing 100 artificial gene lists that were like our own, but where gene labels were randomly permuted.

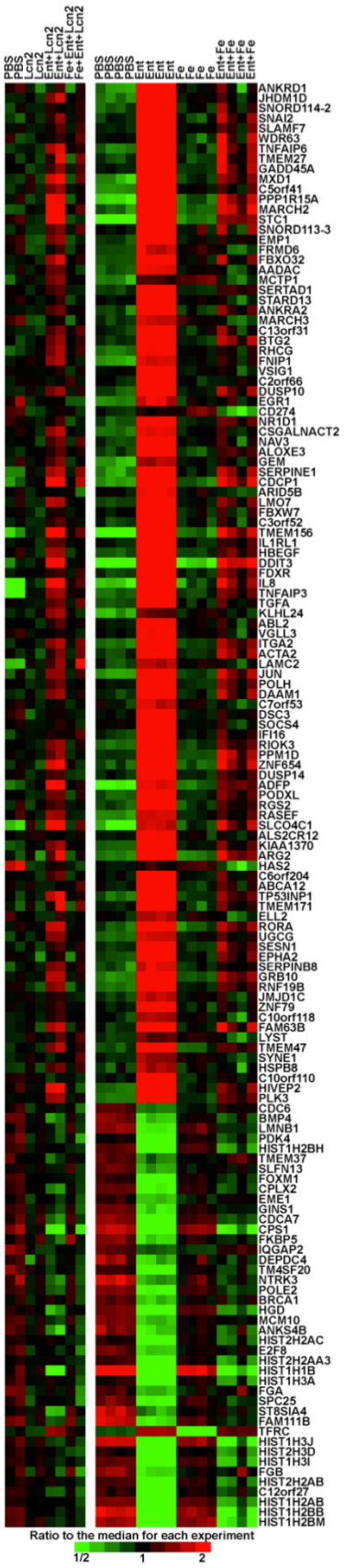
PBS
PBS
Lcn2
Lcn2
Ent+Lcn2
Ent+Lcn2
Fe+Ent+Lcn2
Fe+Ent+Lcn2
PBS
PBS
PBS
PBS
Ent
Ent
Ent
Ent
Fe
Fe
Fe
Fe
Ent+Fe
Ent+Fe
Ent+Fe
Ent+Fe
ANKRD1
JHDM1D
SNORD114-2
SNAI2
SLAMF7
WDR63
TNFAIP6
TMEM27
GADD45A
MXD1
C5orf41
PPP1R15A
MARCH2
STC1
SNORD113-3
EMP1
FRMD6
FBXO32
AADAC
MCTP1
SERTAD1
STARD13
ANKRA2
MARCH3
C13orf31
BTG2
RHCG
FNIP1
VSIG1
C2orf66
DUSP10
EGR1
CD274
NR1D1
CSGALNACT2
NAV3
ALOXE3
GEM
SERPINE1
CDCP1
ARID5B
LMO7
FBXW7
C3orf52
TMEM156
IL1RL1
HBEGF
DDIT3
FDXR
IL8
TNFAIP3
TGFA
KLHL24
ABL2
VGLL3
ITGA2
ACTA2
LAMC2
JUN
POLH
DAAM1
C7orf53
DSC3
SOCS4
IFI16
RIOK3
PPM1D
ZNF654
DUSP14
ADFP
PODXL
RGS2
RASEF
SLCO4C1
ALS2CR12
KIAA1370
ARG2
HAS2
C6orf204
ABCA12
TP53INP1
TMEM171
ELL2
RORA
UGCG
SESN1
EPHA2
SERPINB8
GRB10
RNF19B
JMJD1C
ZNF79
C10orf118
FAM63B
LYST
TMEM47
SYNE1
HSPB8
C10orf110
HIVEP2
PLK3
CDC6
BMP4
LMNB1
PDK4
HIST1H2BH
TMEM37
SLFN13
FOXM1
CPLX2
EME1
GINS1
CDCA7
CPS1
FKBP5
IQGAP2
DEPDC4
TM4SF20
NTRK3
POLE2
BRCA1
HGD
MCM10
ANKS4B
HIST2H2AC
E2F8
HIST2H2AA3
HIST1H1B
HIST1H3A
FGA
SPC25
ST8SIA4
FAM111B
TFRC
HIST1H3J
HIST2H3D
HIST1H3I
FGB
HIST2H2AB
C12orf27
HIST1H2AB
HIST1H2BB
HIST1H2BM
Ratio to the median for each experiment
1/2
1
2

Figure 2.1: Heat map of genes with expression specifically altered by aferric Ent.

Genes where the difference in gene expression in response to Ent vs. PBS was significantly larger, or smaller, than the Fe-Ent vs. Fe difference in gene expression [(Ent/PBS)/(Fe-Ent/Fe)] by a factor of at least 2, and with p<0.001, are shown. A549 human respiratory cells were stimulated and microarray analysis was performed as described below. The entire gene set used for analysis (p<0.01, fold change >1.3) is accessible through GEO Series accession GSE54962.

Consistent with iron starvation, aferric Ent specifically upregulated expression of *NDRG1*, a tumor metastasis gene that is induced in response to cell-permeable iron chelators (Figure 2.2A) [81]. Aferric Ent also significantly upregulated expression of *IL8.* In addition to down-regulation of cell cycle genes, Ent strongly reduced expression of the IL-1 receptor gene *IL1R1.* To confirm microarray findings, A549 cells were stimulated in an independent experiment with combinations of Fe, Ent, and Lcn2 and gene expression was measured by qPCR (Figure 2.2C, D). *NDRG1* was significantly induced by Ent compared to PBS (21.5 fold, p=1.1E-11), and met the selection criteria above where the increase from PBS to Ent was significantly more than the increase from Fe to Fe-Ent (35.8-fold more, p=1.4E-10). Similarly, *IL8* was induced by Ent compared to PBS (17 fold, p=3.4E-9) and met the interaction selection criteria used in the microarray (3-fold more, p=0.003; Figure 2.2F). Ent treatment repressed *IL1R1* expression significantly compared to PBS (0.29-fold, p=1.6E-5; Figure 2.2D), although it narrowly missed the interaction selection criteria (p=0.054).

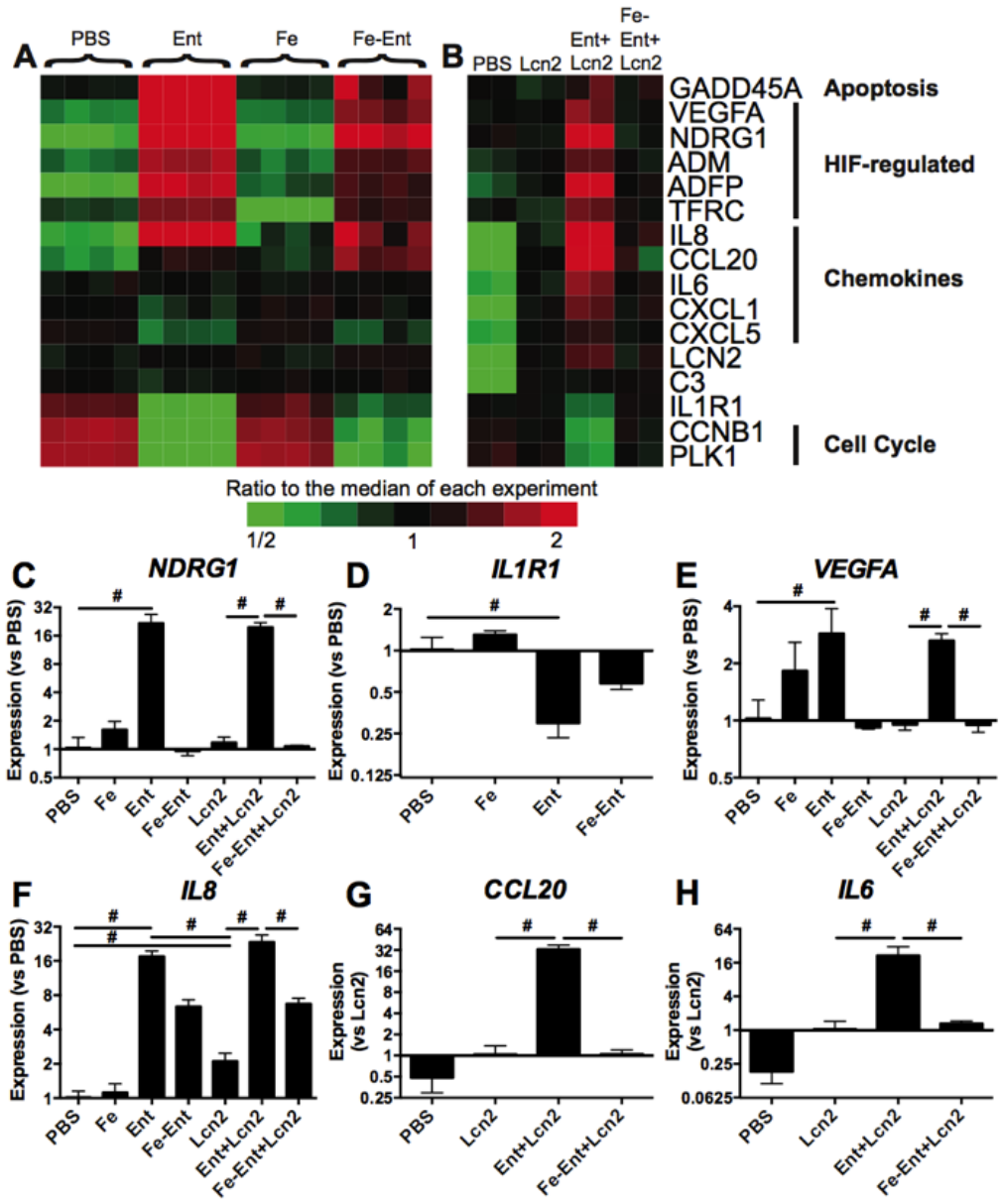

Figure 2.2: Ent and Ent+Lcn2 induce distinct gene expression patterns.

Heat maps of relative gene expression by A549 respiratory cells in response to combinations of 50 μM Enterobactin (Ent) and 50 μM Ferric Ammonium Citrate (Fe) alone (A), or with 25 μM lipocalin 2 (Lcn2) (B) as measured by microarray are shown. Red indicates upregulation of gene expression, whereas green indicates downregulation of gene expression, relative to the median of each experiment. Stimulations were repeated independently, and gene expression was validated by qPCR of NDRG1 (C), IL1R1 (D), VEGFA (E), IL8 (F), CCL20 (G), and IL6 (H) in response to combinations of Fe, Ent, and Lcn2. Data are shown as means +/- SEM of 3 replicate samples and are representative of at least 2 independent experiments. Statistics were calculated using ANOVA (#, $p<0.001$ for indicated comparison).

To identify gene expression uniquely altered by Ent+Lcn2, a second experiment was performed comparing responses to this stimulus with the response to both Lcn2 alone and Fe-Ent+Lcn2. Lcn2 alone significantly induced 56 genes and repressed 80 genes (selection criteria of $p<0.01$, fold-change >1.3), and gene ontology analysis demonstrated induction of genes involved with the immune response, innate immune response, chemokine and cytokine activity (Table 2.3, Figure 2.3). The set of repressed genes did not significantly overlap with a gene ontology group. Induced genes included the cytokines *IL8, IL6, CCL20, CXCL1*, *CXCL5*, complement component *C3,* and *LCN2* itself.

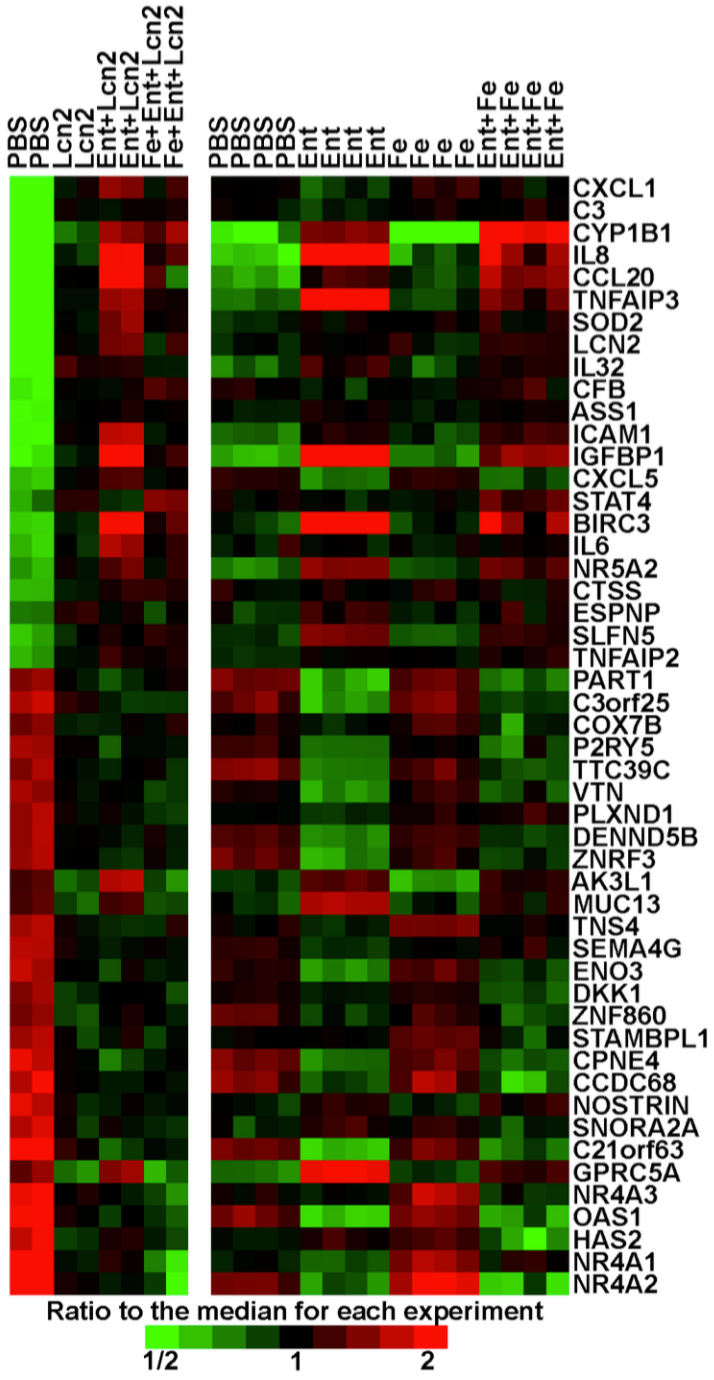

Figure 2.3: Heat map of genes with expression significantly altered by Lcn2.

Genes for which expression altered by a factor of at least 1.3 and with $p<0.01$ are shown. A549 human respiratory cells were stimulated and microarray analysis was performed as described below.

Ent+Lcn2 significantly induced expression of 239 genes and repressed 36 genes compared to Lcn2 and Fe-Ent+Lcn2 (p-value $p<0.01$ and fold-change >1.3 for both Ent+Lcn2 vs. Lcn2 and Ent+Lcn2 vs. Fe-Ent+Lcn2; Figure 2.4). The intersection of this gene set and the set induced by Ent described above contained 137 induced and 21 repressed genes ($p<1E-200$, Mantel-Haenszel Chi-Square statistic for association), indicating that the iron status of Ent conferred a strong effect on gene expression regardless of Lcn2. Accordingly, Ent+Lcn2 significantly induced *NDRG1* expression compared to both Lcn2 and Fe-Ent+Lcn2 (Figure 2.2C).

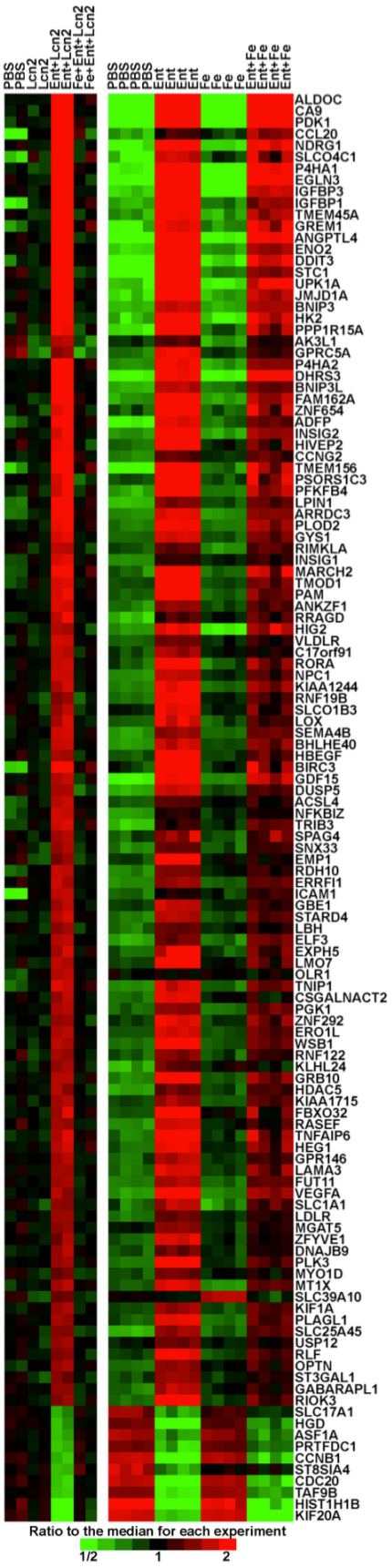
PBS
PBS
Lcn2
Lcn2
Ent+Lcn2
Ent+Lcn2
Fe+Ent+Lcn2
Fe+Ent+Lcn2
PBS
PBS
PBS
PBS
Ent
Ent
Ent
Ent
Fe
Fe
Fe
Fe
Ent+Fe
Ent+Fe
Ent+Fe
Ent+Fe
ALDOC
CA9
PDK1
CCL20
NDRG1
SLCO4C1
P4HA1
EGLN3
IGFBP3
IGFBP1
TMEM45A
GREM1
ANGPTL4
ENO2
DDIT3
STC1
UPK1A
JMJD1A
BNIP3
HK2
PPP1R15A
AK3L1
GPRC5A
P4HA2
DHRS3
BNIP3L
FAM162A
ZNF654
ADFP
INSIG2
HIVEP2
CCNG2
TMEM156
PSORS1C3
PFKFB4
LPIN1
ARRDC3
PLOD2
GYS1
RIMKLA
INSIG1
MARCH2
TMOD1
PAM
ANKZF1
RRAGD
HIG2
VLDLR
C17orf91
RORA
NPC1
KIAA1244
RNF19B
SLCO1B3
LOX
SEMA4B
BHLHE40
HBEGF
BIRC3
GDF15
DUSP5
ACSL4
NFKBIZ
TRIB3
SPAG4
SNX33
EMP1
RDH10
ERRFI1
ICAM1
GBE1
STARD4
LBH
ELF3
EXPH5
LMO7
OLR1
TNIP1
CSGALNACT2
PGK1
ZNF292
ERO1L
WSB1
RNF122
KLHL24
GRB10
HDAC5
KIAA1715
FBXO32
RASEF
TNFAIP6
HEG1
GPR146
LAMA3
FUT11
VEGFA
SLC1A1
LDLR
MGAT5
ZFYVE1
DNAJB9
PLK3
MYO1D
MT1X
SLC39A10
KIF1A
PLAGL1
SLC25A45
USP12
RLF
OPTN
ST3GAL1
GABARAPL1
RIOK3
SLC17A1
HGD
ASF1A
PRTFDC1
CCNB1
ST8SIA4
CDC20
TAF9B
HIST1H1B
KIF20A
Ratio to the median for each experiment
1/2
1
2

Figure 2.4: Heat map of genes with expression significantly altered by the combination of aferric Ent+Lcn2.

Genes for which expression is altered by a factor of at least 1.5 and p-value p<0.01 in response to Ent+Lcn2, compared to both Lcn2 alone and the combination of ferric ammonium citrate, Enterobactin, and Lipocalin 2 (Fe-Ent+Lcn2) are shown. A549 human respiratory cells were stimulated and microrarray analysis was performed as described. The entire gene set used for analysis (fold change >1.3; p<0.01) is accessible through GEO Series accession GSE54962.

Gene ontology analysis of Ent+Lcn2 induced genes indicated significant induction of genes involved in glycolysis, response to hypoxia, and the endoplasmic reticulum unfolded protein response and repression of genes related to mitotic prometaphase (Table 2.3). Induced genes that are associated with the response to hypoxia included *VEGFA*, *ADM, TFRC,* and *ELGN3* (Figure 2.2A, B; Figure 2.4). Independent stimulations of A549 cells indicated that Ent induced *VEGFA* relative to PBS and met the interaction selection criteria compared to Fe and Fe-Ent (p=4.4E-5) whereas Ent+Lcn2 induced significantly more expression than Lcn2 or Fe-Ent+Lcn2, as measured by qPCR (Figure 2.2E). Vascular Endothelial Growth Factor (VEGF) A is an angiogenesis gene regulated by HIF-1α, indicating that Ent and Ent+Lcn2 may activate HIF-1α, and *ELGN3* is a prolyl hydroxylase that regulates HIF function [104, 118]. Indeed, enrichment analysis for motif gene sets indicated Ent+Lcn2 induced HIF-1 responsive genes (Table 2.4).

Table 2.4: Enrichment analysis for motif gene sets.

Selection Criteria	Direction of Change	Distinct genes in selection #	Motif gene set title	Genes on list	Genes in intersection	p-value one-sided Fisher Exact test $	Rank of list in that list source	Estimated FDR (Q-value) @	Observed / expected for intersection
ENT+LCN vs both LCN and ENT+LCN+Fe	UP	239	GTGCCTT,MIR-506	606	25	1.4E-07	1	0.0000	3.35
			V$HIF1_Q3	167	11	7.3E-06	2	0.0000	5.35
			TTGTTT_V$FOXO4_01	1531	39	1.1E-05	3	0.0033	2.07
			V$AP1_01	204	11	4.7E-05	4	0.0075	4.38
			TGANTCA_V$AP1_C	860	25	6.3E-05	5	0.0060	2.36
			V$BACH2_01	214	11	7.3E-05	6	0.0067	4.18
			CTACTGT,MIR-199A	148	9	9.3E-05	7	0.0071	4.94
			TGASTMAGC_V$NFE2_01	149	9	9.8E-05	8	0.0063	4.91
			AAACCAC,MIR-140	91	7	1.3E-04	9	0.0056	6.25
			CTCAGGG,MIR-125B,MIR-125A	279	12	1.9E-04	10	0.0100	3.49
			V$IK1_01	212	10	3.1E-04	11	0.0127	3.83
			V$HIF1_Q5	177	9	3.6E-04	12	0.0125	4.13
			AAAGGAT,MIR-501	107	7	3.6E-04	13	0.0115	5.32
			ACACTAC,MIR-142-3P	111	7	4.5E-04	14	0.0129	5.12
			GCACTTT,MIR-17-5P,MIR-20A,MIR-106A,MIR-106B,MIR-20B,MIR-519D	496	16	4.5E-04	15	0.0120	2.62
			CTACTAG,MIR-325	13	3	4.8E-04	16	0.0125	18.75
			GAGCCTG,MIR-484	88	6	7.6E-04	17	0.0165	5.54
			V$AP4_Q5	205	9	0.0010	18	0.0244	3.57
			V$NFAT_Q4_01	205	9	0.0010	19	0.0232	3.57
			CAGTATT,MIR-200B,MIR-200C,MIR-429	387	13	0.0011	20	0.0230	2.73

Enrichment testing performed after collapsing selections of significant probe-sets (of 29096 probe-sets) to be selections of distinct genes (19419 distinct genes).

$ Tests were based on the intersection of genes we selected as altered, with gene lists from these other sources, and the size of the intersection judged based on one-sided Fisher Exact tests.

@ False discovery rate (FDR) estimates were based on analyzing 100 artificial gene lists that were like our own, but where gene labels were randomly permuted.

Two cytokine genes showed strong induction in response to Ent+Lcn2 compared to both Lcn2 and Fe-Ent+Lcn2: *IL6* and *CCL20* (Figure 2.2B). In contrast, neither cytokine was induced significantly by aferric Ent based on the interaction test (Figure 2.2A). Separate stimulation of A549 cells with combinations of Fe, Ent, and Lcn2 confirmed induction by Ent+Lcn2 compared to both Lcn2 and Fe-Ent+Lcn2, as measured by qPCR (Figure 2.2G, H). Based on the PBS control, basal transcription of *CCL20* and *IL6* was very low. Gene expression in response to combinations of Fe and Ent were similarly low and could not be reliably determined. Therefore, relative expression of *CCL20* and *IL6* was calculated by comparing each stimuli's transcript level to Lcn2, rather than PBS, as baseline expression. *IL8* was also significantly induced by Ent+Lcn2 compared to Lcn2 and Fe-Ent+Lcn2 when measured by qPCR ($p < 0.0001$). In contrast to the expression pattern of *IL6* and *CCL20*, aferric Ent strongly induced *IL8* expression as described above.

To correlate changes in gene expression with cytokine secretion, A549 cells were stimulated with combinations of Fe, Ent and Lcn2, and IL-6, IL-8 and CCL20 were measured by ELISA (Figure 2.5A-C). As previously reported, Ent and Lcn2 individually induced IL-8 secretion and the combination of Ent+Lcn2 induced IL-8 secretion that was greater than the response to either Lcn2 or Fe-Ent+Lcn2 (Figure 2.5A) [45]. However, this was in contrast to the expression pattern where Ent induced significantly more *IL8* expression than Lcn2 ($p=1.3E-7$, Figure 2.2F). This suggests that Lcn2 acts post-transcriptionally to increase IL-8 production or secretion. The patterns of CCL20 and IL-6 secretion differ from

the pattern of IL-8. CCL20 was secreted at lower levels than the PBS control in response to Ent or Fe-Ent ($p<0.001$; Figure 2.5B) whereas IL-6 was not detectable in response to either stimulus (Figure 2.5C). Similarly to the IL-8 response, Lcn2 induced secretion of CCL20 and IL-6 and Ent+Lcn2 induced greater secretion than Lcn2 or Fe-Ent+Lcn2. Together, the microarray data identify new gene targets induced and repressed by Fe, Ent, and Lcn2, and independent qPCR confirmation and ELISA data indicate IL-8, CCL20 and IL-6 as gene targets strongly activated in respiratory epithelial cells in response to the combination of Ent and Lcn2.

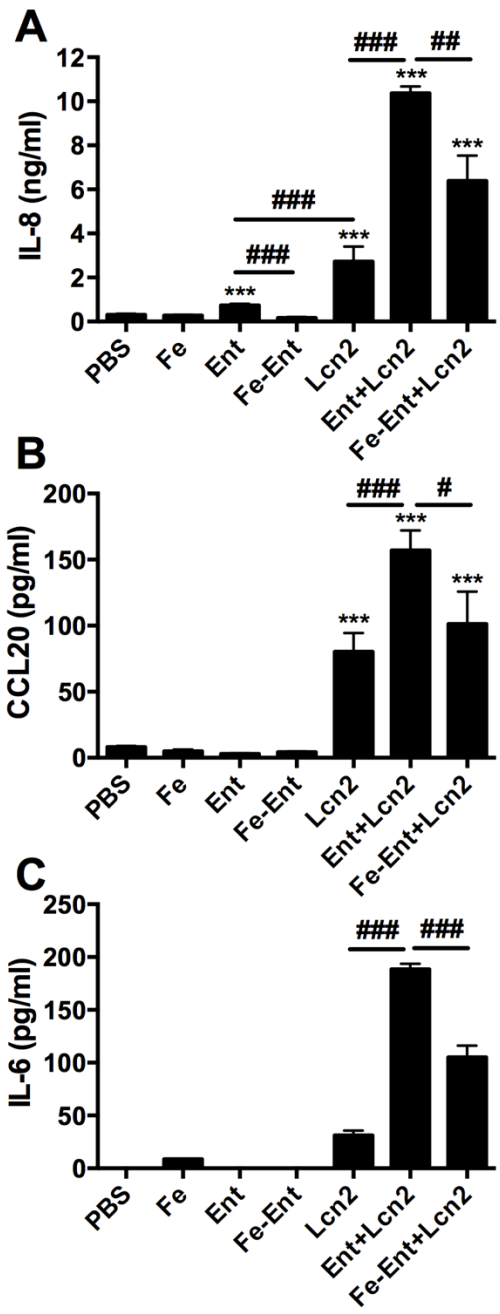

Figure 2.5: The combination of Ent and Lcn2 strongly induce cytokine production in A549 respiratory cells.

*Cells were stimulated for 16h with combinations of 50 μM FAC (Fe), 50 μM Ent, or 25 μM Lcn2. IL-8 (A), CCL20 (B), and IL-6 (C) secretion were measured by ELISA. Values shown are means +/- SEM of 3 replicate samples and are representative of at least 2 independent experiments. Statistics were calculated using one-way ANOVA (*** p<0.0001 induction relative to PBS; # p<0.05; ## p<0.01; ###, p<0.001 for indicated comparisons).*

2.2.2 Unbound Ent enhances Lcn2 induction of pro-inflammatory cytokines

The enhanced cytokine production induced by Ent+Lcn2 compared to Lcn2 and Fe-Ent+Lcn2 indicates that secretion is triggered by siderophore-dependent iron chelation (Figure 2.5A-C). This could be mediated either by Ent bound to Lcn2 in the binding calyx [45] or unbound Ent. To distinguish these possibilities, Ent and Lcn2 were incubated in a 2:1 ratio to allow binding and then spun through a 10 kilodalton (kDa) Molecular Weight cutoff column (MWCO) to retain Lcn2 (20.5 kDa) and Ent+Lcn2 complexes, but not Ent alone (669 Da). Consistent with the loss of unbound Ent, spinning Ent+Lcn2 in a MWCO column diminished its ability to stimulate IL-8 and IL-6 secretion ($p<0.0001$; Figure 2.6A and B), reducing IL-8 and IL-6 secretion to levels comparable to that of Lcn2 alone ($p=0.5$ and 0.1 respectively). The secretion of IL-8 and IL-6 correlated with *NDRG1* gene expression (Figure 2.6C). Addition of Ent to retained Ent+Lcn2 following spinning through a MWCO restored its ability to stimulate IL-8 and IL-6 secretion, indicating that the MWCO column has no effect on the stimulatory effect of Lcn2, and that unbound Ent is required to enhance secretion of IL-8 and IL-6. Additionally, simulation of respiratory epithelial cells with Ent and Lcn2 at a 4:1 and 2:1 ratio induced increased IL-8 secretion, whereas stimulation with Ent and Lcn2 at a 1:1 ratio did not. These data indicate that the combination of unbound Ent and Lcn2, rather than Ent+Lcn2 complexes themselves, stimulates robust IL-8 and IL-6 secretion.

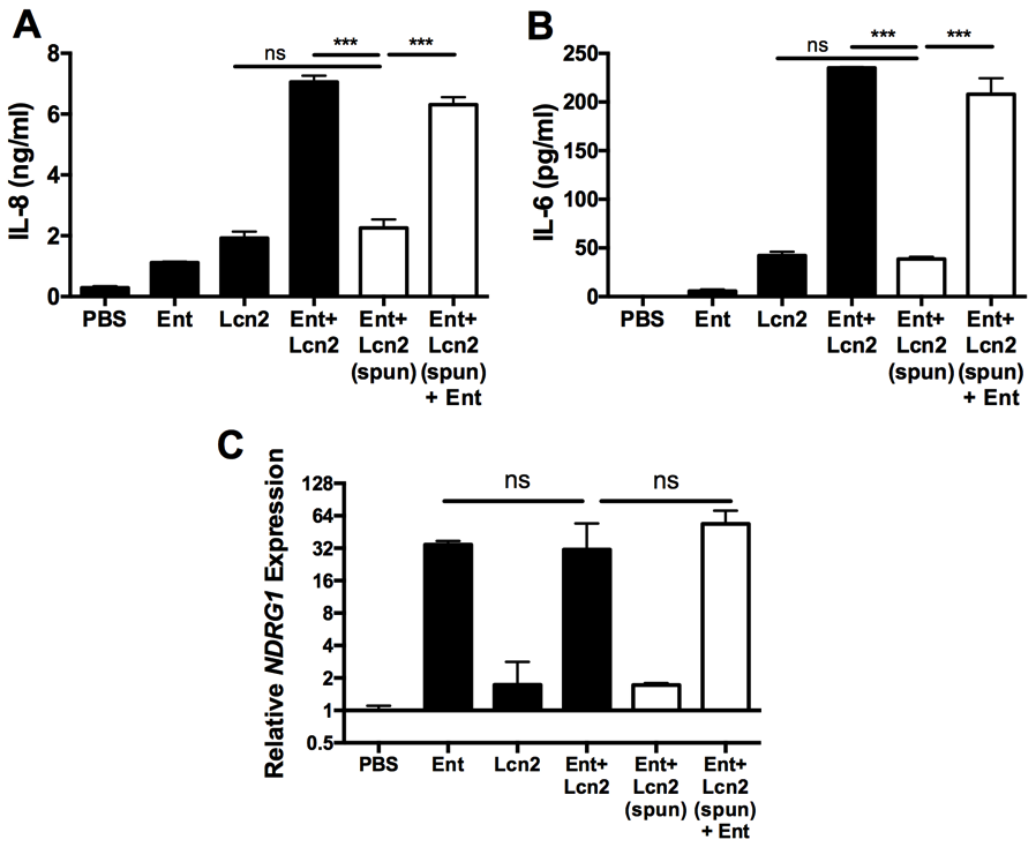

Figure 2.6: Unbound Ent in combination with Lcn2 is required for maximal IL-8 and IL-6 secretion in A549 cells and correlates to NDRG1 expression.

*Combinations of 50 μM Ent (669 Da) and 25 μM Lcn2 (20.5 kDa) were spun, as indicated, through a 10 kDa MWCO column, and cells were stimulated with the retentate, containing Lcn2 or Ent bound by Lcn2, for 16h. IL-8 (A) and IL-6 (B) secretion were measured by ELISA. Values shown are means +/- SEM of 3 replicate samples and are representative of at least 2 independent experiments. Statistics were calculated using one-way ANOVA (***, $p<0.0001$; ns $p>0.05$).*

2.2.3 Iron chelation by Ybt in combination with Lcn2 strongly induces cytokine secretion

The fact that unbound Ent enhances cytokine responses to Lcn2 suggests that this cellular response may also occur in response to iron chelation by siderophores to which Lcn2 cannot bind. To test this hypothesis, respiratory epithelial cells were stimulated with combinations of Fe and the Lcn2-evasive siderophores Ybt and Sal, and IL-8 secretion was assayed by ELISA (Figure 2.7A). Additionally, qPCR for the iron starvation gene *NDRG1* was performed (Figure 2.7B). Similar to Ent, Ybt strongly induced secretion of IL-8 and gene expression of *NDRG1*, which was reversed by Fe ($p<0.0001$). In contrast, Sal did not induce IL-8 or *NDRG1* ($p=0.6$). To verify the iron chelation ability of the siderophores, A549 cells were treated with calcein, a membrane-permeable ester that is cleaved upon entering a cell, causing fluorescence that is quenched by the cellular labile iron pool [119]. Addition of Ent and Ybt chelated iron away from calcein, increasing fluorescence, whereas addition of Sal did not (Figure 2.7C). Preloading the siderophores with Fe prevented induction of calcein fluorescence. Because Sal has different membrane-partitioning activities than Ent that could confer differing abilities to chelate intracellular iron, iron chelation in solution was measured by the chromogenic CAS Assay [120]. Ent and Ybt rapidly and efficiently induced a color change in the CAS reagent, whereas Sal did not. Combined, these data indicate the ability of Ent and Ybt to disrupt cellular iron homeostasis.

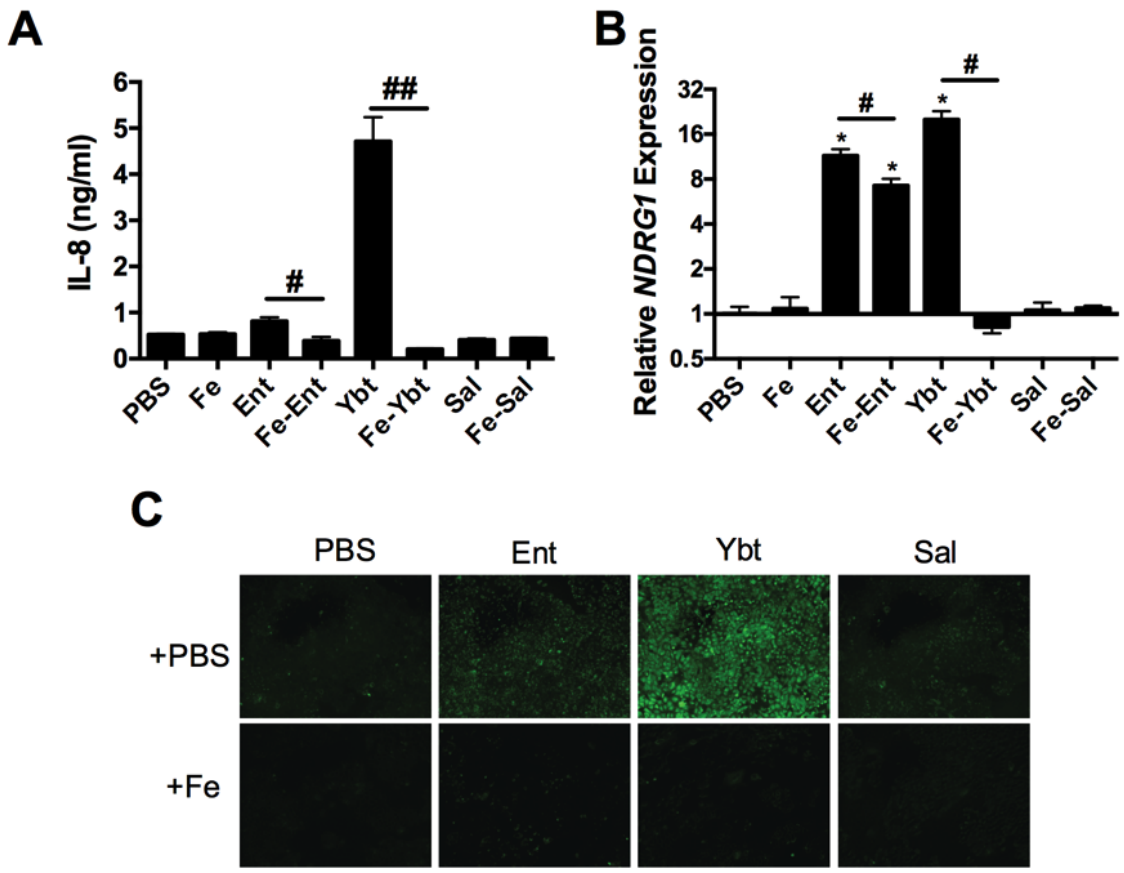

Figure 2.7: Ybt and Ent, but not Sal, induce expression of IL-8, the iron-starvation gene NDRG1 and calcein fluorescence.

(A) Cells were stimulated for 16h with combinations of 50 μM FAC (Fe), 50 μM Ent, 50 μM Ybt, or 50 μM Sal, and IL-8 secretion was assayed by ELISA. B) NDRG1 expression, a marker associated with iron chelation, was measured by qPCR. (C) Cells were stimulated for 16h with combinations of 100 μM FAC (Fe), 100 μM Ent, 100 μM Ybt, or 100 μM Sal, and calcein fluorescence was examined. Values shown are means +/- SEM of 3 replicate samples and are representative of at least 2 independent experiments. Statistics were calculated using one-way ANOVA (, $p<0.0001$ induction relative to PBS; #, $p<0.05$, ##, $p<0.01$ for indicated comparison).*

To determine if host iron chelation by non-ligand siderophores can induce increased cytokine release in presence of Lcn2, respiratory epithelial cells were stimulated with Ybt or Sal and Lcn2 (Figure 2.8). Ybt alone significantly increased IL-8 and IL-6 secretion, and induced CCL20 secretion whereas levels were undetectable in the control. Furthermore, Ybt+Lcn2 induced significantly more IL-8 (Figure 2.8A), IL-6 (Figure 2.8B), and CCL20 (Figure 2.8C) secretion than Lcn2 alone. Induction of cytokine secretion by Ybt and Ybt+Lcn2 correlated with host iron chelation, as measured by increased *NDRG1* gene expression (Figure 2.8D). Lcn2 alone had no effect on *NDRG1* expression. Neither Sal nor Sal+Lcn2 induced *NDRG1* expression. Additionally, Sal+Lcn2 did not induce IL-8, IL-6, or CCL20 secretion when compared to Lcn2, consistent with the inability of Sal to perturb intracellular iron levels (Figure 2.7). To determine if a pharmacologic iron chelator could induce increased cytokine release, we stimulated respiratory epithelial cells with DFO in the presence of Lcn2. DFO+Lcn2 induced secretion of IL-8, IL-6, and CCL20 that correlated with expression of *NDRG1* (Figure 2.8 E, F; Figure 2.9.) These data indicate that iron chelation by a siderophore other than Ent enhances Lcn2-dependent pro-inflammatory cytokine release in respiratory epithelial cells.

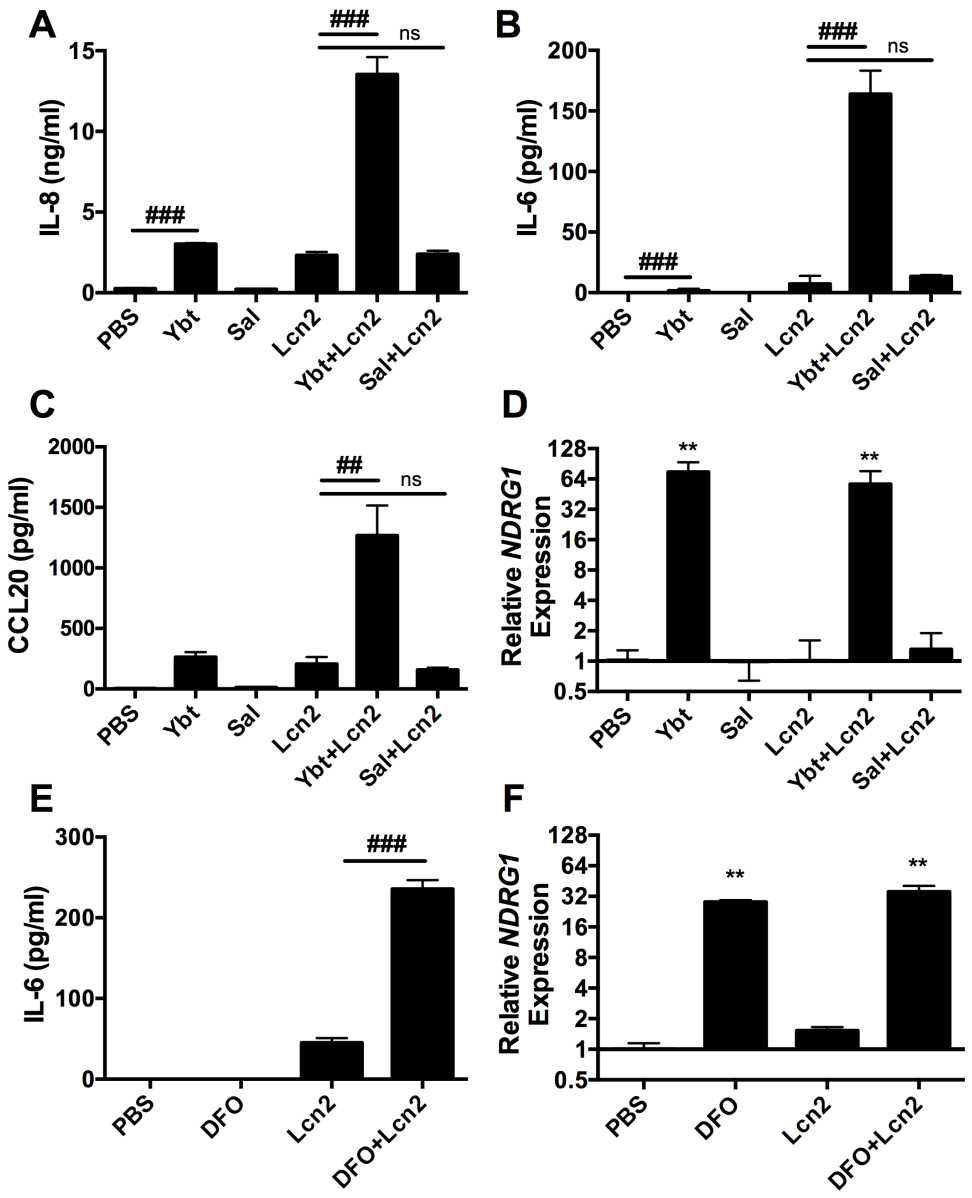

Figure 2.8: Ybt+Lcn2 and DFO+Lcn2 induce chemokine release by A549 respiratory cells.

*Cells were stimulated for 16h with combinations of 50 μM Ybt, 50 μM Sal, 200 μM DFO, or 25 μM Lcn2 and ELISA was used to measure IL-8 (A), IL-6 (B, E), and CCL20 (C) secretion. Relative NDRG1 expression (D, F) was assayed using qPCR. Values shown are means +/- SEM of 3 replicate samples and are representative of at least 2 independent experiments. Statistics were calculated using one-way ANOVA (** p<0.01 relative to PBS; ## p<0.01, ### p<0.001 for indicated comparison; ns p>0.05).*

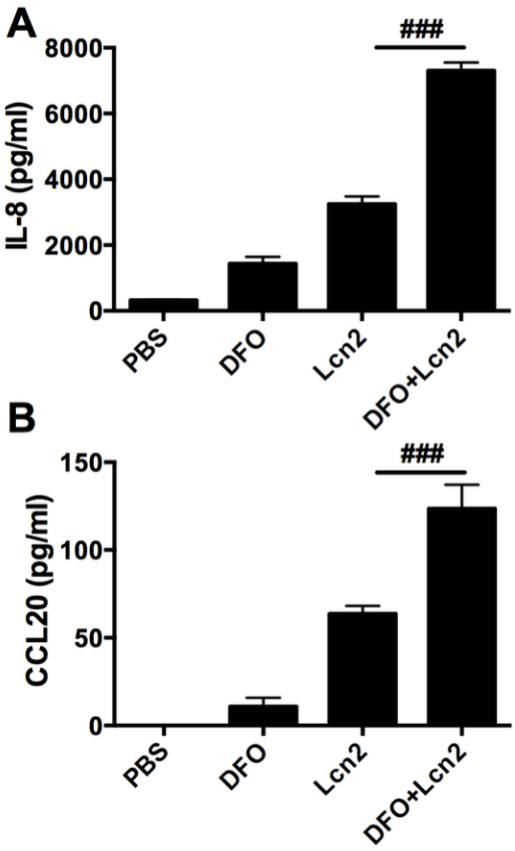

Figure 2.9: DFO+Lcn2 induces IL-8 and CCL20 secretion.

Cells were stimulated for 16h with combinations of 200 μM DFO or 25μM Lcn2 and ELISA was used to measure IL-8 (A) and CCL20 (B) secretion. Values shown are means +/- SEM of 3 replicates samples and are representative of at least 2 independent experiments. Statistics were calculated using one-way ANOVA (###, p<0.001 for indicated comparison).

2.2.4 Induction of HIF-1α stabilization in the presence of Lcn2 is sufficient to enhance inflammation

Gene expression analysis indicated that Ent and Ent+Lcn2 induced HIF-regulated genes, including *VEGFA* (Figure 2.2A, B, E). HIF-1α has been shown to regulate inflammation and enhance expression of cytokines including IL-6 [121, 122]. HIF-1α is rapidly targeted for degradation by prolyl hydroxylases, but is stabilized through inactivation of prolyl hydroxylases by iron limitation, hypoxia or the dioxygenase inhibitor Dimethyloxaloylglycine (DMOG) [123]. To determine if HIF-1α is stabilized by stimulation with Ent, Western blots on nuclear fractions were performed. Stimulation with Ent induced nuclear stabilization of HIF-1α, similar to the stabilization of HIF-1α observed in response to DMOG (Figure 2.10A). Additionally, stimulation with Ent+Lcn2, but not Lcn2 alone, induced nuclear stabilization of HIF-1α (Figure 2.10B, C). To determine if stabilization of HIF-1α through inactivation of prolyl hydroxlases is sufficient to enhance Lcn2-dependent inflammation, A549 cells were treated with DMOG alone or in combination with Lcn2. DMOG in combination with Lcn2 did not increase secretion of IL-8 compared to Lcn2 alone ($p=0.2$; Figure 2.10D) or CCL20, however, DMOG+Lcn2 stimulation induced IL-6 expression significantly above the level of Lcn2 alone ($p<0.01$) (Figure 2.10E). These data indicate that Ent induces stabilization of HIF-1α that, in combination with Lcn2, is sufficient to induce a pro-inflammatory immune response.

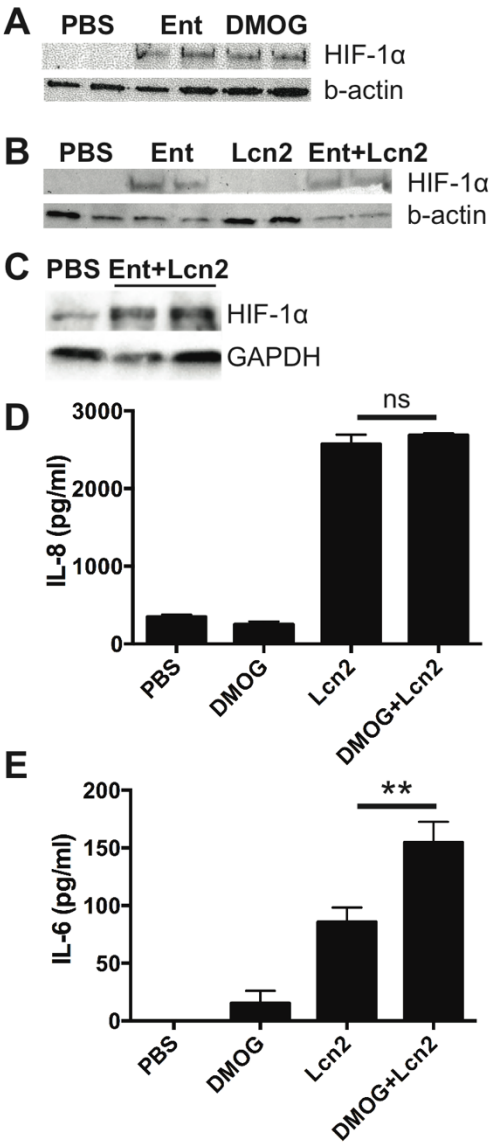

Figure 2.10: Ent stabilizes HIF-1α in A549 respiratory epithelial cells, which is sufficient to enhance Lcn2-dependent IL-6 secretion.

*Cells were stimulated for 16h with combinations of 50 μM Ent, 3 mM DMOG, or 25 μM Lcn2 and Western Blot or ELISA was used to measure HIF-1α stabilization (A, B, and C), IL-8 secretion (D) or IL-6 secretion (E), respectively. Western blot data are representative of 2 independent experiments. ELISA values shown are means +/- SEM of 3 replicate samples and are representative of at least 2 independent experiments. Statistics were calculated using unpaired two-tailed t tests (** $p<0.01$; ns $p>0.05$).*

2.2.5 Induction of immune response by siderophores + IL-1β

Because the immune response to Ent+Lcn2 was shown to be dependent on iron chelation by the siderophore rather than the siderophore itself, we hypothesized that Lcn2 was not required for the immune response to iron chelation. Instead, we hypothesized that the presence of a host inflammatory protein would be sufficient to induce pro-inflammatory cytokine secretion in the presence of iron chelation by a siderophore. To examine this hypothesis, A549 respiratory epithelial cells were stimulated with siderophores in combination with IL-1β for 16 hr, and then examined for the inflammatory response (Figure 2.11). Siderophores in combination with IL-1β caused secretion of IL-8 (Figure 2.11A), IL-6, (Figure 2.11B), and CCL20 (Figure 2.11C). The majority of the cytokine secretion correlated with the induction of *NDRG1* expression, indicating cellular iron chelation (Figure 2.11D). The combination of Sal+IL-1β resulted in a slight but significant increase in IL-8, IL-6, and CCL20 secretion despite Sal being unable to chelate host cellular iron as measured by *NDRG1* expression. These results are consistent with our hypothesis that an inflammatory host protein, such as Lcn2 or IL-1β, can induce an immune response in combination with cellular iron chelation by siderophores.

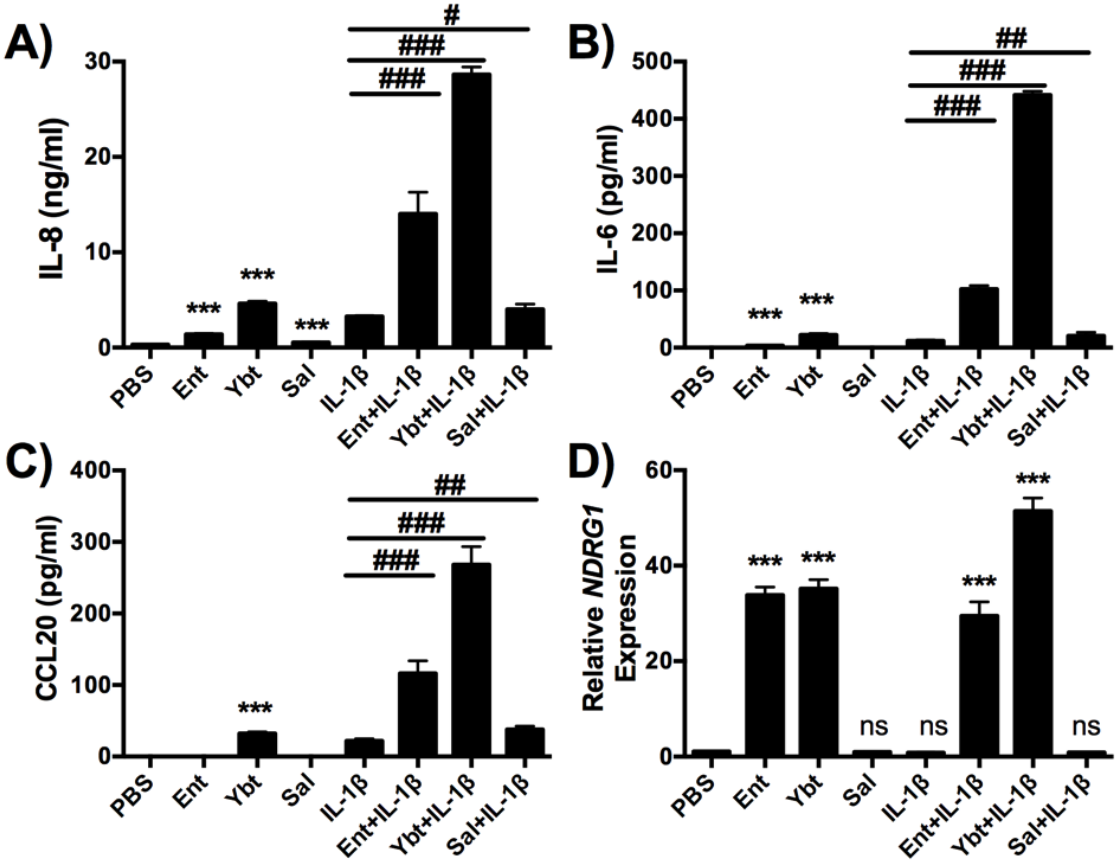

Figure 2.11: Siderophores + IL-1β induces IL-8, IL-6, and CCL20 secretion in A549 respiratory epithelial cells.

*Cells were stimulated for 16h with combinations of 50 μM Ybt, 50 μM Sal, 25 μM Lcn2 or 1 ng/mL IL-1β and ELISA was used to measure IL-8 (A), IL-6 (B), and CCL20 (C) secretion. Relative NDRG1 expression (D) was assayed using qPCR. Values shown are means +/- SEM of 3 replicate samples and are representative of 1 experiment. Statistics were calculated using one-way ANOVA (*** p<0.001, ns, p>0.05 relative to PBS; #, p<0.05, ## p<0.01, ### p<0.001 for indicated comparison).*

2.3 Discussion

2.3.1 Summary of findings

In addition to disrupting bacterial iron acquisition, Lcn2 enhances inflammation *in vitro* and *in vivo* in response to Ent [15, 45]. In this way, Lcn2 may tailor inflammation based on microbial iron metabolism. To determine the mechanism of inflammation induced by Ent and Lcn2, we performed a microarray analysis to identify genes modulated in response to Fe, Ent, and Lcn2 and confirmed changes in gene expression using qPCR and ELISA. We then determined whether the strong induction of cellular immune responses by Ent+Lcn2 was due to the ligand-protein complex or, more broadly, to iron chelation. We found that the host immune response is activated in response to Lcn2 and amplified through iron chelation by siderophores rather than in response to the Ent+Lcn2 complex itself. Furthermore, Ent induces HIF-1α stabilization alone and in the presence of Lcn2, and HIF-1α stabilization is sufficient to enhance Lcn2-dependent secretion of the cytokine IL-6. The inflammatory immune response may require iron chelation by siderophores in the presence of a host inflammatory protein, such as Lcn2 or IL-1β. These findings indicate a novel host response to microbial iron metabolism in which cellular stress induced by siderophore-mediated iron chelation and the presence of Lcn2 leads to activation of a limited set of cytokines, namely IL-6, IL-8 and CCL20. These findings also indicate a novel mechanism for siderophore-induced cytokine secretion, linking HIF-1α stabilization by pathogen-associated siderophores to IL-6 secretion.

2.3.2 Lcn2 and inflammatory cytokine secretion

Without its ligand, Lcn2 has been shown to modulate cytokine expression. In cells of the Central Nervous System, Lcn2 modulates lipopolysaccharide (LPS)-induced cytokine production, including IL-6 and CCL20, as well as adipokine production in adipocytes [124, 125]. In models of ischemia and reperfusion, Lcn2 controls neutrophil recruitment by regulating expression of chemokines, including IL-6, and their cell-surface receptors [126]. Consistent with these studies, our findings indicate that Lcn2 induces IL-6 and CCL20 secretion from respiratory epithelial cells. IL-6 is an inflammatory cytokine active in the regulation of the acute phase response in hepatocytes and is capable of upregulating expression of hepcidin [127]. Hepcidin regulates plasma iron concentrations by inhibiting enterocyte uptake of iron and iron recycling by macrophages, and is upregulated during infection and inflammation [128]. IL-6 is also a differentiation factor for Th17 lymphocytes that mediate protective immunity against siderophore-producing pathogens such as *K. pneumoniae* [129]. In turn, CCL20 is a lymphocyte chemoattractant, whose expression is amplified by IL-6 production, recruiting Th17 cells to sites of inflammation by binding to its cognate receptor CCR6. Thus, it is possible that expression of CCL20 initiates an adaptive immune response [130-132].

Lcn2-induced cytokines are also induced in response to disruptions in iron homeostasis. Iron chelation by DFO induces IL-8 and CCL20 production in intestinal epithelial cells [84, 133]. In respiratory epithelial cells, the combination of siderophores and Lcn2 induces robust expression of IL-6 and CCL20.

Therefore, the cytokine response to bacterial siderophores and Lcn2 could serve as a multi-faceted failsafe mechanism: First, IL-8 can recruit neutrophils to the site of infection. Second, IL-6 can upregulate hepcidin to limit further iron availability for invading bacteria. Finally, IL-6 and CCL20 can act in concert to attract mature Th17 to sites of infection and commit naïve T cells to the Th17 pathway.

2.3.3 Effect of Lcn2 during Gram-positive and Gram-negative infections

The presence or absence of siderophores is likely crucial to the effect of Lcn2 on inflammation. In recent work, stimulation of macrophages with *Streptococcus pneumoniae* induced IL-10 production in an Lcn2-dependent manner, which skewed macrophages towards a deactivated phenotype [91]. In human and animal models, increased Lcn2 correlated with worsening of pneumococcal pneumonia. These findings contrast the results of this work, which demonstrate pro-inflammatory effects of Lcn2, and previous work by our group and others demonstrating that Lcn2 is a crucial antimicrobial peptide that enhances survival during infection, particularly with *K. pneumoniae* [13, 15, 43, 48]. In addition, our microarray analysis did not indicate any change in the gene expression of IL-10 in response to Lcn2. We hypothesize that the difference in outcome is due to the fact that *S. pneumoniae* does not require siderophores for its pathogenesis, and thus Lcn2 cannot properly modulate inflammation during infection without siderophore-mediated iron chelation. In fact, patient survival from Gram-negative pneumonia correlated with increased Lcn2 in the bronchoalveolar lavage fluid [91].

2.3.4 Effect of iron chelators on host cell functions

Iron homeostasis and metabolism are tightly regulated systems that require the expression and function of many proteins, including transferrin, transferrin receptor, and ferritin. Disruption of these systems due to iron chelation exerts a wide range of pathologic effects on cells, including disruption of DNA replication, apoptosis, and cell-cycle arrest [81, 134, 135]. Although these properties of iron chelators show promise as anti-cancer therapies, our data suggest that bacterial siderophores may act as cytotoxins during infection. Clinical isolates of *K. pneumoniae* produce 50-100 μM of Ent in pure culture [13], quantities sufficient to induce the hypoxia and iron-starvation responses described herein. The induction of cellular stresses in response to siderophores and Lcn2 during infection may lead to significant pathologic effects during infection. However, our results indicate that Lcn2 can cooperate with these cellular stress responses to induce robust cytokine release and recruit inflammatory cells to combat the bacterial source of toxic siderophores.

Although the inflammatory response to siderophores and Lcn2 is activated in response to iron chelation, rather than a siderophore+Lcn2 complex, the cellular responses to Ent, Ybt, and Sal are distinct. Stimulation with Ybt or Ybt+Lcn2 induces more IL-8, IL-6, and CCL20 secretion and *NDRG1* gene expression compared to equimolar stimulation with Ent or Ent+Lcn2. This is surprising due to the fact that Ent has the highest known affinity for iron. In fact, stimulation of A549 cells with increasing molar concentrations of siderophores illustrates a higher threshold concentration to induce IL-8 secretion by Ybt

compared to Ent. This is consistent with the pattern shown in Figure 2.7A, in which Fe-Ent induces more *NDRG1* gene expression than Fe-Ybt: Despite equimolar addition of Fe to Ent, trace free Ent is capable of chelating cellular iron and inducing *NDRG1* expression. Sal may not induce cellular iron chelation or pro-inflammatory cytokine secretion because of its decreased membrane partitioning abilities [54]. Addition of Sal to an entirely siderophore-deficient strain of *K. pneumoniae* restores bacterial growth, indicating that Sal is able to acquire iron for bacterial growth [96]. Differential secretion of Ent, Ybt, and Sal during infection may cause dissimilar pathologic effects through triggering varied levels of cytokine production.

2.3.5 Siderophores and HIF-1α

Expression of HIF-1α protein is regulated through hydroxylation by prolyl hydroxylases, a modification that targets the protein for rapid proteasomal degradation [112]. Since prolyl hydroxylases require iron as a cofactor, HIF-1α stabilization can be induced by both oxygen and iron starvation [136]. Indeed, siderophores have previously been shown to induce HIF-1α stabilization [106, 137]. In a previous study, Ybt was shown to stabilize HIF-1α but effects on inflammation were not assessed. Sal was also reported to induce HIF-1α, but this required high concentrations of siderophores (≥200 μM) [106]. The current study demonstrates induction of HIF-1α stabilization by the prototypical siderophore Ent and Ent+Lcn2 at physiologic concentrations. Additionally, we illustrate that HIF-1α stabilization in combination with Lcn2 is sufficient for IL-6 secretion, linking HIF-1α-regulated genes with inflammatory pathways. HIF-1α stabilization

in combination with Lcn2 is not sufficient to induce IL-8 or CCL20 secretion, suggesting that additional pathways are activated in response to siderophore+Lcn2 stimulation that enhance inflammation. IL-8 production by epithelial cells is regulated by a combination of MAPK and NF-κB signaling pathways [111]. Microarray analysis in response to treatment with Ent indicated up-regulation of Dual Specificity Phosphatases (DUSPs), indicating that MAPK signaling might be involved in the IL-8 secretion in response to siderophores+Lcn2.

2.3.6 Proposed model and conclusions

In summary, our results introduce a novel role for Lcn2 as a rheostat that modulates the response to iron chelation by bacterial siderophores. We propose a model in which a low amount of Ent can be bound and neutralized by Lcn2 (Figure 2.12A), resulting in low levels of Lcn2-induced cytokine secretion. However, high levels of Ent (Figure 2.12B) or Ybt (Figure 2.12C) can overwhelm Lcn2 binding capacity, causing the accumulation of unbound siderophores. These siderophores chelate host cellular iron and, in combination with Lcn2, induce robust secretion of IL-6, CCL20, and IL-8 in airway epithelial cells. Ent induces HIF-1α stabilization, and HIF-1α in combination with Lcn2 is sufficient to induce IL-6. In contrast, HIF-independent pathways are likely required to augment IL-8 and CCL20 expression. DFO and Ybt also combine with Lcn2 or IL-1β to induce inflammation, indicating this is a generalized response to siderophore-mediated iron starvation in the presence of a host inflammatory protein. In this way, Lcn2 can prevent iron sequestration by Ent without triggering

a substantial immune response, but can potently upregulate inflammation when overwhelmed by siderophores that perturb epithelial cell iron homeostasis.

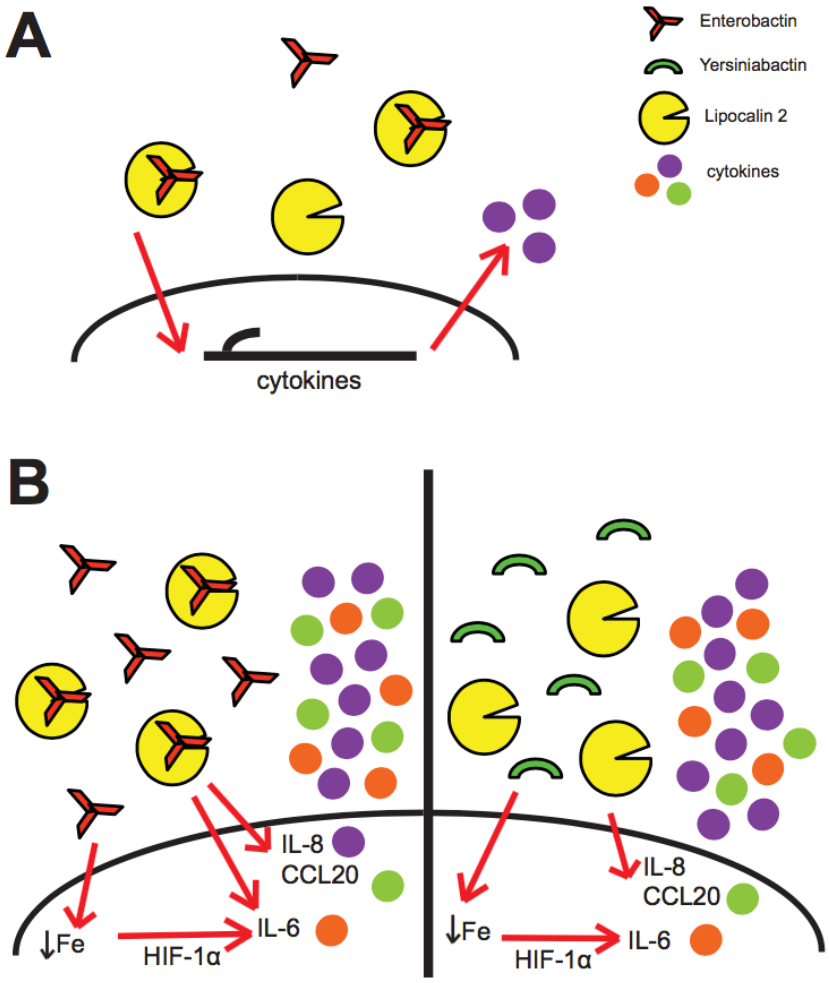

Figure 2.12: Proposed model.

Lcn2 acts as a sensor by modulating airway epithelial cell inflammatory cytokine secretion in response to iron chelation by unbound Ent and Ybt. (A) Low amounts of Ent can be bound and neutralized by Lcn2, leading to a low level of Lcn2-induced cytokine secretion in the airway. High amounts of Ent (B) or Ybt (C) evade Lcn2 binding, leading to altered host iron status and HIF-1α stabilization. The combination of cellular iron depletion and a host inflammatory protein, such as Lcn2, increases production of inflammatory cytokines, such as IL-8, IL-6, and CCL20.

2.4 Experimental Procedures

Cell Culture. A549 (ATCC CCL-185) cells, a human type II pneumocyte cell line, were cultured in F12K (Invitrogen, Carlsbad, CA) media supplemented with 10% fetal bovine serum (Invitrogen) and 1:100 penicillin streptomycin (Invitrogen).

Siderophore Stimulation Experiments. 24-well plates were seeded with A549 cells at a concentration of $3.5x10^4$ cells/well. After two days, cells were weaned from serum and antibiotics overnight. Cells were then stimulated overnight as previously described [45] with the indicated combinations of 50 μM Ferric ammonium citrate (FAC) (Sigma, St. Louis, MO), 50 or 100 μM Ent (Sigma or EMC Microcollections, Tubingen, Germany), 50 μM Ybt (EMC), 50 μM Salmochelin S4 (EMC), 200 μM DFO (Sigma), 3 mM dimethyloxaloylglycine (DMOG, Sigma) 1 ng/mL IL-1β (Sigma) or 25 μM Lcn2 in F12K media lacking serum or antibiotics. Prior to incubation with cells, siderophore+Lcn2 complexes were prepared by sequential incubation at room temperature of FAC and siderophore for 30 minutes followed by addition of Lcn2 and incubation for an additional 30 minutes. Where indicated, complexes were spun through a 10,000 MWCO centrifugal filter unit (EMD Millipore, Billerica, MA) prior to cell stimulation.

Cytokine Measurement. Cytokine secretion was measured from A549 supernatants as previously described [45]. Briefly, supernatants were collected from overnight A549 stimulations, cleared by centrifugation (1000 x g, 5 minutes

at 4°C) and assayed by ELISA according to manufacturers' directions for IL-8 (OptEIA, BD Biosciences, San Diego, CA), CCL20, and IL-6 (Duoset, R+D Systems) using TMB substrate (Life Technologies, Carlsbad, CA) for color development and measured using an Eon microplate spectrophotometer (BioTek, Winooski, VT).

RNA Extraction, cDNA synthesis, and qPCR. After collecting A549 supernatants, 700 µL Trizol Reagent (Ambion, Carlsbad, CA) was added to the cells and RNA was extracted according to the manufacturer's protocol. cDNA was synthesized using a High Capacity cDNA Reverse Transcription Kit (Applied Biosystems, Carlsbad, CA) and a 2720 Thermal Cycler (Applied Biosystems). Quantitative real-time PCR was conducted with Taqman Gene Expression Master Mix (Applied Biosystems) or SYBR Green POWER Master Mix (Applied Biosystems). Taqman Assays (Invitrogen) for *IL8* (Hs00174103_m1), *VEGFA* (Hs00900055_m1), *CCL20* (Hs01011368_m1), and *IL6* (Hs00985639_m1) were analyzed using a Realplex^2 machine (Eppendorf, Hauppauge, NY) with gene expression measured relative to the housekeeping gene *GAPDH* (Hs99999905_m1) or *GUSB* (Hs00939627_m1) using the comparative Ct method [138]. Relative expression of *NDRG1* (Hs.Pt.56a.4224283.g, Integrated DNA Technologies, Coralville, IA) and *IL1R1* (Hs.PT.58.15515070) was analyzed using a Realplex^2 machine with gene expression measured by SYBR Green relative to the housekeeping gene *GAPDH* (Hs.PT.39a.22214836) using the comparative Ct method [138].

Lcn2 Purification. Recombinant human Lcn2 was purified based on methods previously described [15, 139]. Briefly, *E. coli* strain BL-21, containing a plasmid encoding a human Lcn2-glutathione S-transferase (Lcn2-GST) fusion protein, was cultured to mid-logarithmic phase in Terrific Broth supplemented with 50 μM ferrous sulfate and Lcn2-GST expression was induced with 1mM IPTG for 3 hours at 37°C. Cells were pelleted by centrifugation, treated with lysozyme (0.5mg/mL; incubated on ice for 1 hour; Sigma), deoxycholate (2.8mg/mL; incubated at 37C for 20 minutes; Fisher Scientific, Pittsburgh, PA), DNAse (4.5 ug/mL; incubated at room temperature for 10 minutes; Roche, Branchburg, NJ) in lysis buffer (50mM Tris, 100mM NaCl, pH 7.5) supplemented with protease inhibitor (c0mplete EDTA-free cocktail tablets, Roche) and disrupted by sonication using a Model 505 Sonic Dismembrator (4 x 30 second pulses at 40% amplitude with a 30 second pause between pulses; Fisher Scientific). Lcn2-GST was purified from the lysate using a Glutathione Sepharose 4B bead column (GE Amersham, Piscataway, NJ) followed by elution with glutathione elution buffer (50mM Tris, 40mM reduced glutathione [Sigma], pH 8.5) and overnight cleavage using human thrombin (25 units per liter of *E. coli;* Sigma) during dialysis through a 10,000 MWCO membrane (Thermo) in buffered solution (50mM Tris, 100mM NaCl, pH 7.5). Digested protein was then sterilized using a 0.22 μM filter (EMD Millipore) and gel filtered using a Superdex 75 column attached to an AKTA FPLC system (GE Healthcare) using buffer containing PBS to remove GST. Biological activity of purified Lcn2 was confirmed by retention with Fe-Ent after centrifugation over a 10,000 MWCO column as measured by absorbance at 340

nm and growth inhibition of Lcn2-sensitive *K. pneumoniae* strain KP20 when added to human serum as previously described [13].

CAS Assay. The CAS assay was performed to determine the iron-chelating capabilities of Ent, Sal, and Ybt at concentrations between 1 to 200 μM as previously described [120].

Microarray Analysis. A549 cells were stimulated overnight as described above. RNA was purified using the miRNeasy kit (Qiagen) and submitted to the University of Pennsylvania Microarray facility for hybridization on the Affymetrix Human Gene 1.0ST gene chip (University of Pennsylvania Microarray facility). Transcript abundance was estimated with the Robust Multi-array Average (RMA) algorithm and log-transformed [140]. A cutoff for a significant difference in gene expression between experimental groups of a fold change of >1.3 with a p-value of 0.01 was used. Gene sets with significant changes were used for enrichment analysis by comparison with the Broad Institute Molecular Signatures Database (http://www.broadinstitute.org/gsea/msigdb/index.jsp) [141]. Gene ontology terms for each gene were obtained through downloads of “Annotation Files” from the Affymetrix web site (http://www.affymetrix.com/estore/index.jsp).

Calcein Treatment. A549 lung epithelial cells were seeded and serum-starved as above. Cells were washed twice with RPMI without phenol red (Invitrogen) and pre-treated with 1 μM Calcein (Sigma) for 30 minutes in a standard cell culture

incubator. Cells were then washed twice with RMPI without phenol red and treated overnight with siderophores with or without FAC. Fluorescence imaging was performed with the Olympus IX52 inverted microscope (Center Valley, PA), and images were analyzed with cellSens Entry imaging software (Olympus).

Western Blot. A549 lung epithelial cells were seeded, serum-starved, and stimulated as stated above. Following overnight stimulation, cellular fractionation was performed to collect nuclear proteins, as previously described [142], or with RIPA buffer (50mM Tris-HCl pH 7.5, 150mM NaCl, 2mM EDTA, 1% NP-40, 0.1% SDS) with protease inhibitors. Fractions were denatured in 6x sample buffer and separated on a 7.5% or 10% SDS-PAGE gel (BioRad, Hercules, CA) at 120 V for 1.5 hours. Protein was transferred onto PVDF or nitrocellulose membrane (Millipore) at 100 V for one hour, and immediately blocked in 5% nonfat milk in Tris-buffered saline with 0.1% Tween (TBST). Membranes were probed with α-HIF-1α (1:2000, R&D Systems or 1:1000, Santa Cruz Inc, Dallas, TX) and α-β-actin (1:5000, Novus Biologicals, Littleton, CO) or α-GAPDH (1:1000, Santa Cruz Inc) as a loading control overnight, followed by mouse IgG-HRP secondary antibody (1:1000, R&D Systems or 1:1000 Cell Signaling Technologies, Danvers, MA), in 5% BSA in TBST or 5% nonfat milk in TBST. Protein expression was detected using ECL Substrate (Pierce) and visualized on a ChemiDoc/RS+ Imaging System (BioRad). Protein concentration was determined by the Micro BCA Assay kit (Pierce).

Statistical Analysis. Array, qPCR, and ELISA data were log-transformed and fit to Analysis of Variance (ANOVA) models with one mean per group, and pairs of treatments were compared. Additionally, some comparisons of the difference of differences in two pairs of treatments were compared. Where indicated, unpaired, two-tailed t tests were performed using Prism 6 software (GraphPad Software, Inc).

2.5 Notes

This work has been adapted from the original published article and can be cited as follows:

Holden, VI, S Lenio, R Kuick, SK Ramakrishnan, YM Shah, MA Bachman. 2014. Bacterial siderophores that evade or overwhelm Lipocalin 2 induce Hypoxia Inducible Factor 1α and proinflammatory cytokine secretion in cultured respiratory epithelial cells. *Infect Immun* 82 (9): 3826-3836.

VI Holden designed and performed experiments, analyzed data, and wrote the paper; S Lenio performed experiments; R Kuick performed microarray and statistical analysis; SK Ramakrishnan and YM Shah performed experiments; and MA Bachman performed and designed experiments and wrote the paper.

CHAPTER III

IN VIVO EFFECTS OF SIDEROPHORES ON THE HOST UPON INFECTION WITH *KLEBSIELLA PNEUMONIAE*

Summary

K. pneumoniae, a Gram-negative bacterial pathogen, is responsible for a wide range of infections including pneumonia and bacteremia and is rapidly acquiring antibiotic resistance. *K. pneumoniae* requires secretion of siderophores, low molecular-weight, high affinity iron chelators, for bacterial replication and full virulence. The specific combination of siderophores secreted by *K. pneumoniae* during infection can impact tissue localization, systemic dissemination, and host survival. However, the effect of these potent iron chelators on the host during infection is unknown. *In vitro*, siderophores deplete epithelial cell iron, induce cytokine secretion, and activate the master transcription factor HIF-1α that controls vascular permeability and inflammatory gene expression. Therefore, we hypothesized that siderophore secretion by *K. pneumoniae* directly contributes to inflammation and bacterial dissemination during pneumonia. To examine the effects of siderophore secretion independent of bacterial growth, we constructed *tonB* mutants that persist *in vivo* but are deficient in siderophore import. Using a murine model of pneumonia, we found that siderophore secretion by *K. pneumoniae* induces the secretion of IL-6, KC, and MIP-2, as well as bacterial

dissemination to the spleen, compared to siderophore negative mutants at equivalent bacterial numbers. Furthermore, we identified that siderophore-secreting *K. pneumoniae* stabilized HIF-1α *in vivo*, and bacterial dissemination to the spleen required alveolar epithelial HIF-1α. Our results indicate that siderophores act directly on the host to induce inflammatory cytokines and bacterial dissemination, and that HIF-1α is a susceptibility factor for bacterial invasion during pneumonia.

3.1 Introduction

K. pneumoniae, a Gram-negative bacterium within the *Enterobacteriaceae* family, is the causative agent of a wide range of infections including pneumonia, UTI, wound infections, and bacteremia. As the third most common cause of hospital-acquired infections, *K. pneumoniae* represents a major healthcare threat [143]. Further compounding this concern, *K. pneumoniae* is rapidly acquiring resistance to all known antibiotics, thus becoming increasingly more difficult to treat. In particular, CR *K. pneumoniae* are resistant to all or nearly all antibiotics and exhibit a strikingly high mortality rate of 41% to 50% for bloodstream infections [144-147].

To establish infection, *K. pneumoniae* secretes molecules called siderophores that are critical for bacterial growth and replication [148, 149]. Siderophores are small, high-affinity iron-chelating molecules secreted by a wide variety of microorganisms that are critical for virulence in many Gram-negative bacteria [150]. Ent is the prototypic catecholate siderophore with the highest

known affinity for iron of any molecule, and effectively outcompetes host iron-binding proteins for iron [7]. To counter the effects of Ent, neutrophils and epithelial cells secrete Lipocalin 2, which binds Ent with subnanomolar affinity [19]. *In vivo*, the presence of Lcn2 has been shown to be bacteriostatic by preventing bacterial uptake of Ent [15, 43]. Bacteria have evolved to secrete Lcn2-evasive siderophores such as: Sal, a glycosylated Ent; Ybt, a structurally distinct phenolate siderophore; and Aer [13, 18, 150]. Ferric-siderophores are actively imported by bacteria through siderophore-specific outer membrane receptors, that are dependent on the TonB-ExuB-ExuD energy transducing system [151].

Because iron is critical for the function of many cellular processes, including DNA replication, oxygen metabolism, and as a cofactor for many cellular reactions, iron chelation by siderophores could have significant effects on host cells, including inflammation [2, 3]. However, the effects of siderophore-dependent manipulation of host iron homeostasis during bacterial infection are largely unknown. Iron chelation by siderophores in the presence of Lcn2 induces *in vitro* pro-inflammatory cytokine secretion of IL-8, IL-6, and CCL20 from lung epithelial cells [45, 152]. Siderophores also induce the stabilization of the master transcription factor HIF-1α *in vitro* [152]. HIF-1α regulates the expression of many genes, including those genes involved in glycolysis, inflammation, and angiogenesis, and is itself regulated by the availability of oxygen or iron within a cell [102, 103, 106, 153]. In normoxia, HIF-1α protein is targeted for degradation by prolyl hydroxlases, a reaction that requires iron [154]. However, in conditions

of low oxygen or low iron, HIF-1α protein is stabilized and translocates to the nucleus to activate gene expression [154-156]. In addition to roles in adaptation to hypoxia and tumor development, HIF-1α activation has recently been associated with innate immunity against infections. Infection with *P. aeruginosa* in a *C. elegans* model system identified a siderophore-dependent activation of a hypoxic host response that was partially protective [107]. In a murine UTI model, HIF-1α was protective against *Escherichia coli* infection through host innate immunity modulation [157]. These results indicate that siderophores have a broad and inflammatory effect on host epithelial cells in addition to their role as iron acquisition molecules for bacteria. However, a critical barrier to investigating this phenomenon *in vivo* is that siderophores allow bacterial proliferation, and an increase in bacterial CFU may indirectly increase inflammation, tissue damage, and bacterial dissemination.

In this study, we tested the hypothesis that *K. pneumoniae* siderophores disrupt iron homeostasis in host cells, leading to altered host responses to pneumonia. To study the effects of siderophore secretion independent of the indirect effects of siderophore-dependent bacterial growth, we constructed a *tonB* mutant that is capable of secreting siderophores but not utilizing them. By dissociating siderophore secretion from bacterial growth, we could directly compare the pro-inflammatory cytokine secretion, bacterial dissemination, and HIF-1α stabilization in response to infection with isogenic siderophore synthesis mutants at equivalent bacterial numbers.

3.2 Results

3.2.1 Siderophores induce bacterial dissemination and lung inflammation

To measure the overall contribution of siderophores to inflammation and bacterial dissemination, mice were infected with a WT strain of *K. pneumoniae* that secretes Ent, Sal, and Ybt or an isogenic siderophore negative *entB ybtS* mutant [96, 148]. Infection with WT *K. pneumoniae* resulted in increased lung bacterial load compared to infection with the *entB ybtS* mutant (Figure 3.1A). Furthermore, siderophores were required for *K. pneumoniae* dissemination to the spleen (Figure 3.1B). Additionally, siderophores were required for induction of pro-inflammatory cytokines: the WT, but not the *entB ybtS* mutant, induced IL-6, KC, MIP-2, IL-1β, and MIP-3α compared to mock-infected controls (Figure 3.1C-G).

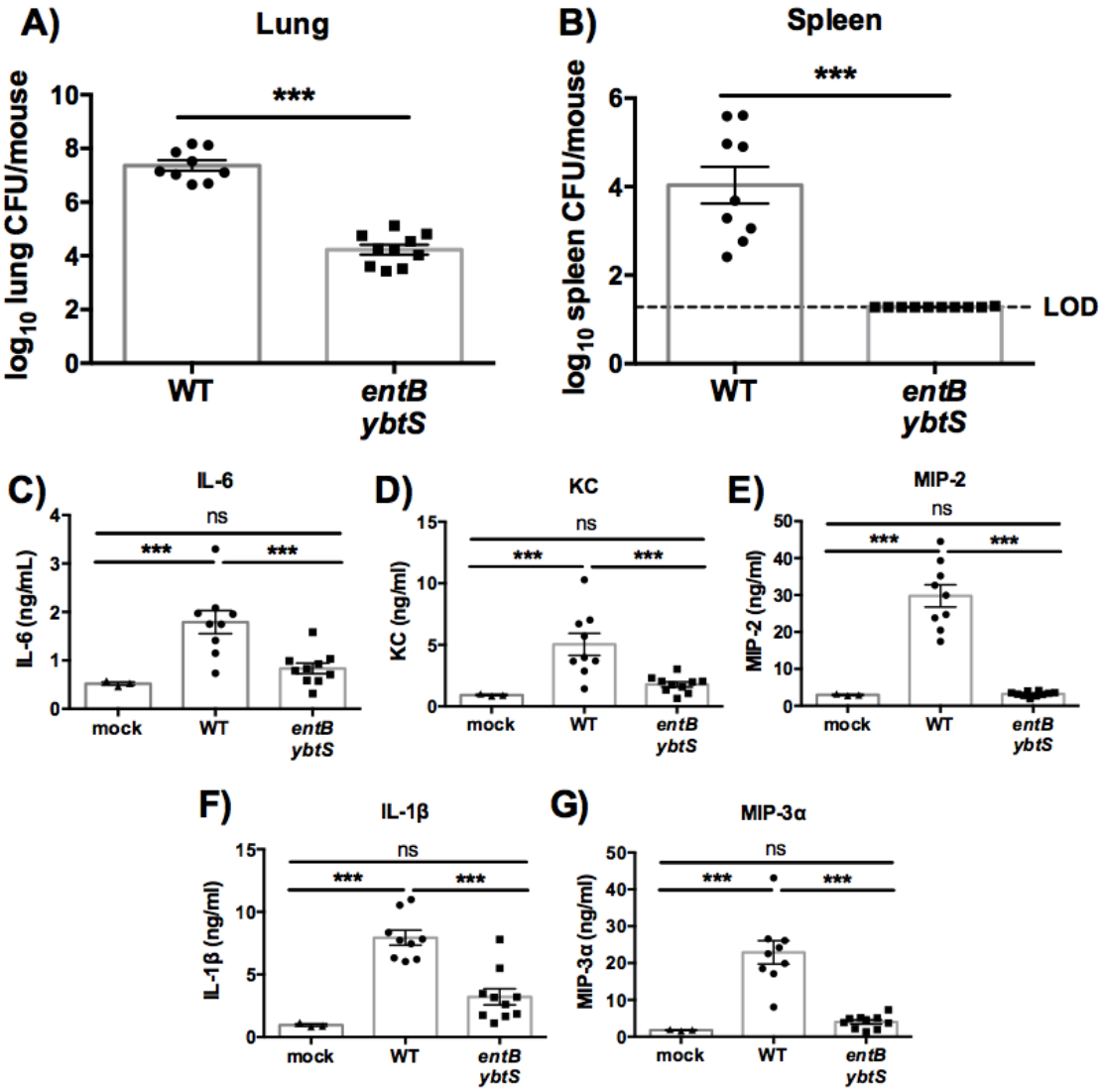

Figure 3.1: K. pneumoniae siderophores enhance bacterial growth and are required for cytokine secretion and bacterial dissemination.

*C57Bl/6 mice (n= 3-10 per group) were inoculated with (PBS) mock, 1x10^4 CFU wild-type K. pneumoniae or entB ybtS K. pneumoniae, a mutant deficient in siderophore production. At day 2, mice were euthanized, and organs were harvested for bacterial load in the A) lung and B) spleen. Lung homogenates were assayed by ELISA for C) IL-6, D) KC, E) MIP-2, F) IL-1β, and G) MIP-3α secretion. Statistics were calculated using one-way ANOVA with Fisher's post-test (***, p<0.001).*

The increase in bacterial dissemination and the inflammatory response during WT infection could be due to direct effects of iron chelation by siderophores on the host or an indirect effect due to increased bacterial CFU in the lungs. To examine the effects of siderophore secretion on the host independent of their ability to enhance bacterial growth through iron delivery, we constructed *tonB* mutants. TonB is required for the uptake of siderophores through the bacterial outer membrane [158]. The *tonB* mutant secreted siderophores, as indicated by the chrome azurol S (CAS) assay, but was not able to utilize endogenous or exogenous siderophores for bacterial growth (Figure 3.2). In effect, the *tonB* mutation uncoupled siderophore secretion from utilization.

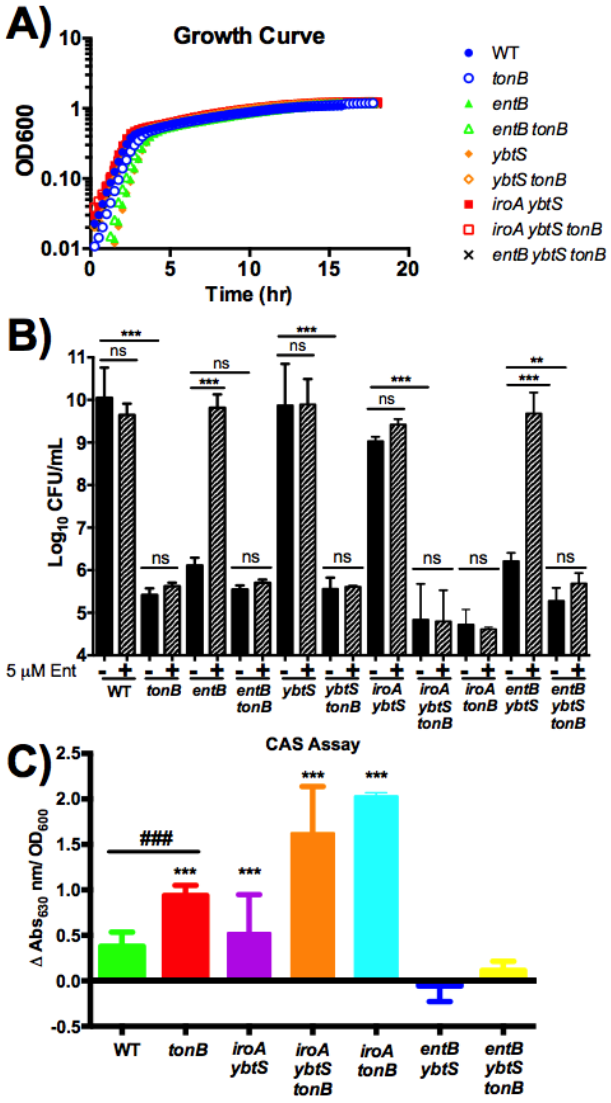

Figure 3.2: Mutants in tonB secrete siderophores but cannot uptake siderophores for growth.

*A) Bacteria were inoculated in LB in a 96-well plate and cultured overnight. OD_{600} readings were taken every 15 minutes. B) Bacteria were cultured overnight in LB medium, then subcultured into a 96-well plate with RPMI + 10% HI serum overnight to determine the strain's ability to grow in iron-limiting conditions. Strains were supplemented with exogenous Ent to examine if the siderophore could rescue growth. C) Bacterial strains were cultured overnight in M9 minimal medium. Supernatants were spun through a 0.2 micron filter to remove bacteria, and iron-chelating molecules were assayed via the CAS Assay. Statistics were calculated using one-way ANOVA with Fisher's post-test (***, p<0.001 vs entB ybtS tonB; ##, p<0.01, ###, p<0.001 as indicated).*

Since *K. pneumoniae* produces an antiphagocytic capsule, we hypothesized that a *tonB* mutant would persist in the lung and secrete siderophores, but not replicate [159]. To compare infection with *tonB K. pneumoniae* to infection with WT *K. pneumoniae*, C57Bl/6 mice were infected with $1x10^8$ CFU *tonB* or $1x10^4$ CFU WT *K. pneumoniae* for 24 or 48 hours. After 24 hours, *tonB K. pneumoniae* persisted in the lung and spleen, with a bacterial load comparable to 48 hr infection with WT *K. pneumoniae* (Figure 3.3A and B). At 24 hours, *tonB K. pneumoniae* infection also caused the induction of IL-6, KC, MIP-2, IL-1β, and MIP-3α secretion that was comparable to 48 hr infection with WT *K. pneumoniae* (Figure 3.3C-G). Additionally, we determined the concentrations of siderophores during infection with *tonB* and WT *K. pneumoniae* by performing mass spectrometry (Figure 3.3H). Micromolar concentrations of Sal were detected in whole lung homogenates. Ybt was detected in lower quantities in all lung samples, but Ent was not detected. Although bacterial growth dynamics differ, these results indicate that *tonB K. pneumoniae* can be used to examine the impact of siderophores on the host at concentrations and bacterial density that mimic WT *K. pneumoniae* infection.

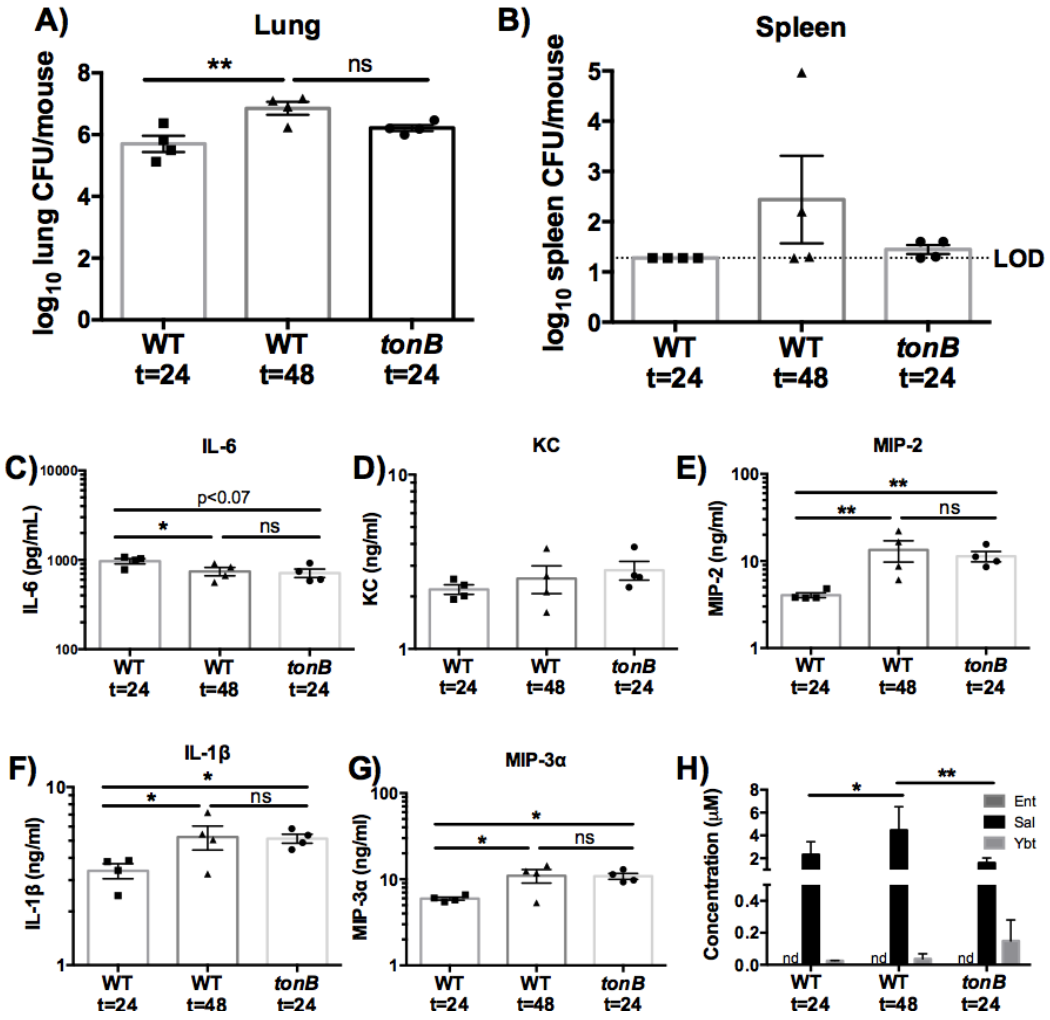

Figure 3.3: Twenty-four hour tonB K. pneumoniae infection is comparable to 48 hour wild-type infection.

C57Bl/6 mice (n=4 per group) were infected with 1x10^4 wild-type K. pneumoniae or 1x10^8 CFU tonB K. pneumoniae, a mutant that secretes, but cannot uptake, siderophores. Following 24 or 48 hr, mice were euthanized, and organs were harvested for bacterial load in the A) lung and B) spleen. Lung homogenates were assayed by for C) IL-6, D) KC, E) MIP-2, F) IL-1β, and G) MIP-3α secretion by ELISA and H) siderophore quantification by LC-MS/MS. Statistics were calculated using one-way (A-G) or two-way (H) ANOVA with Fisher's post-test (, p<0.05; **, p<0.01; ns, p>0.05).*

To determine the impact of siderophore secretion on dissemination and cytokine responses, C57Bl/6 mice were infected with isogenic *tonB* (siderophore secreting) or *entB ybtS tonB* (siderophore-negative) *K. pneumoniae*. Despite equivalent bacterial loads, infection with *tonB K. pneumoniae* resulted in increased bacterial dissemination and IL-6, KC, and MIP-2 secretion compared to infection with the *entB ybtS tonB* mutant (Figure 3.4A-C). Infection with *tonB* did not enhance secretion of IL-1β or MIP-3α compared to the *entB ybtS tonB* mutant (Figure 3.4C), suggesting that induction by WT compared to *entB ybtS* was attributable to differences in bacterial density (Figure 3.1F and G). *In vitro*, Lcn2 enhances induction of pro-inflammatory cytokines by siderophores [152]. To examine the contribution of Lcn2, Lcn2-deficient (LcnKO) mice were infected with *tonB* or *entB ybtS tonB K. pneumoniae*. The same pattern of cytokine induction and dissemination was observed in WT and LcnKO mice, indicating that Lcn2 was not required for siderophore-dependent dissemination and inflammation *in vivo* (Figure 3.4).

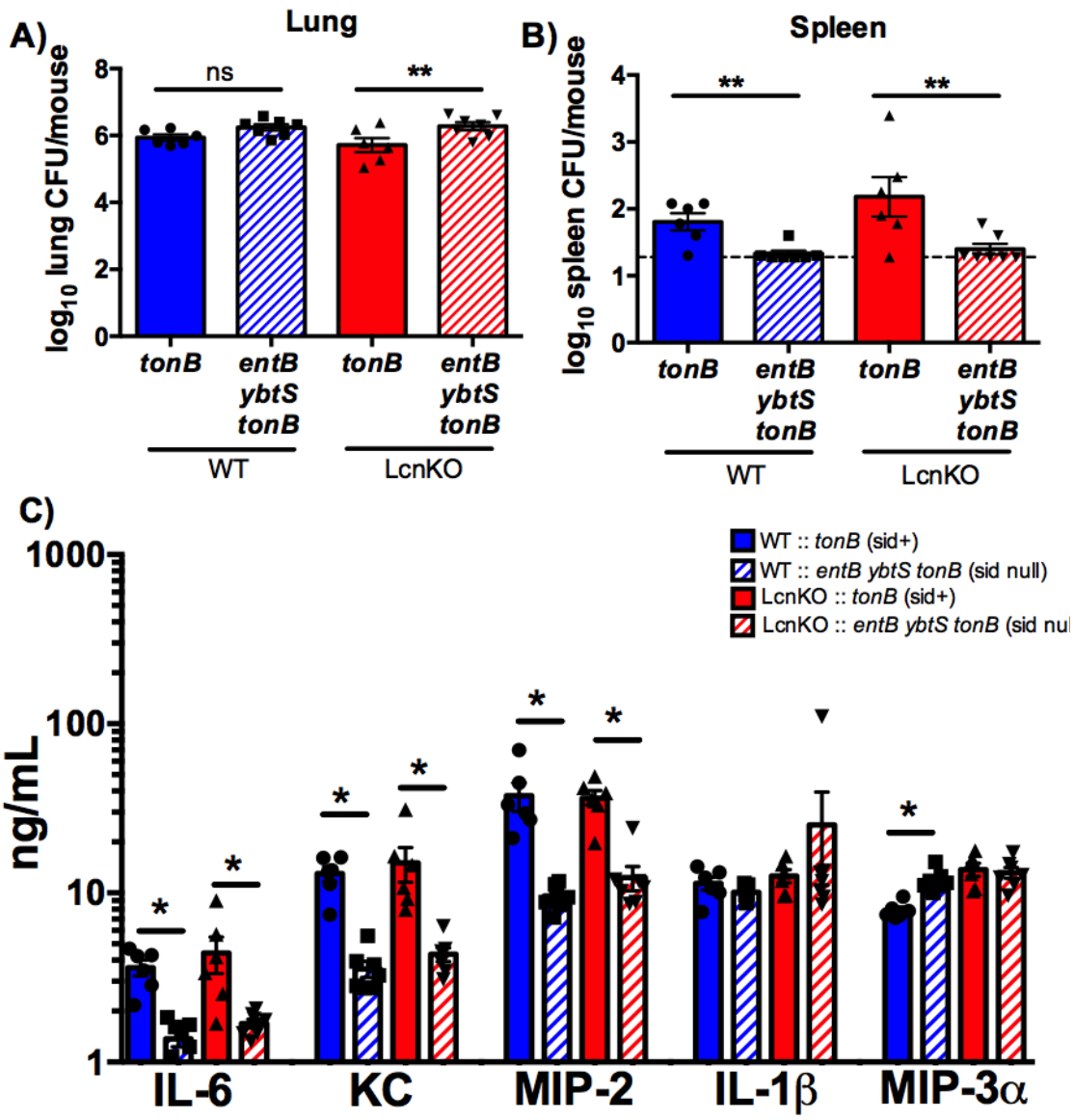

Figure 3.4: Siderophore secretion by K. pneumoniae results in bacterial dissemination and IL-6, KC, and MIP-2 secretion in a Lcn2-independent manner.

C57Bl/6 mice (n=6-7 per group) were infected with 1x10^8 tonB or entB ybtS tonB K. pneumoniae. Following 24 hr, mice were euthanized, and organs were harvested for bacterial load in the A) lung and B) spleen. Lung homogenates were assayed for C) IL-1β, IL-6, KC, MIP-2, and MIP-3α secretion by ELISA. Statistics were calculated using one-way ANOVA with Fisher's post-test (, p<0.05; **, p<0.01).*

3.2.2 Multiple siderophores are required for bacterial dissemination and cytokine secretion

In vitro, Ent and Ybt induced pro-inflammatory cytokine secretion, but Sal did not [152]. Because WT *K. pneumoniae* secretes Ent, Sal, and Ybt, it is unclear which siderophores are required to induce bacterial dissemination and inflammation during pneumonia. To test which siderophores were necessary for maximal dissemination and cytokine secretion, we created isogenic siderophore-secreting *tonB* mutants (Table 3.1) that secrete one or two siderophores and infected C57Bl/6 mice with each strain.

Table 3.1: K. pneumoniae mutants used in this work.

		Siderophore produced			
Strain	Description	Ent	Ybt	Sal	Reference
Wild-type	KPPR1; Rif^R derivative of ATCC43816	+	+	+	15
entB ybtS	VK089; KPPR1 *entB ybtS*	-	-	-	15
tonB	KP273; KPPR1 *tonB::kan*	+	+	+	this work
entB ybtS tonB	KP281; VK089 *tonB::kan*	-	-	-	this work
entB tonB	KP285; VK087 *tonB::kan*	-	+	-	this work
ybtS tonB	KP277; VK088 *tonB::kan*	+	-	+	this work
iroA ybtS tonB	KP2202; KP20 *tonB::hyg*	+	-	-	this work
iroA tonB	KP2227; KP25 *tonB::hyg*	+	+	-	this work

Importantly, infection with all mutants resulted in approximately equivalent lung bacterial load (Figure 3.5A). Consistently, infection with WT *tonB K. pneumoniae* induced significantly more dissemination to the spleen when compared to infection with the *entB ybtS tonB* mutant (siderophore-negative) (Figure 3.5B). No other siderophore mutant induced significant dissemination compared to the *entB ybtS tonB* mutant (siderophore negative). These data indicate that all

siderophores are required in combination for maximal bacterial dissemination to the spleen.

To determine if individual siderophores are sufficient to induce cytokine secretion, ELISAs were performed on lung homogenates taken at 24 hr post-infection. Infection with any of the isogenic siderophore *tonB* mutants was not sufficient to induce the secretion of IL-6, KC, or MIP-2 more than infection with *entB ybtS tonB* (siderophore negative), indicating that individual siderophores are not sufficient for secretion of these cytokines (Figure 3.5C-E). Consistent with Figure 3.4, siderophore secretion by the isogenic mutants did not specifically induce IL-1β or MIP-3α compared to infection with the *entB ybtS tonB* mutant (Figure 3.6).

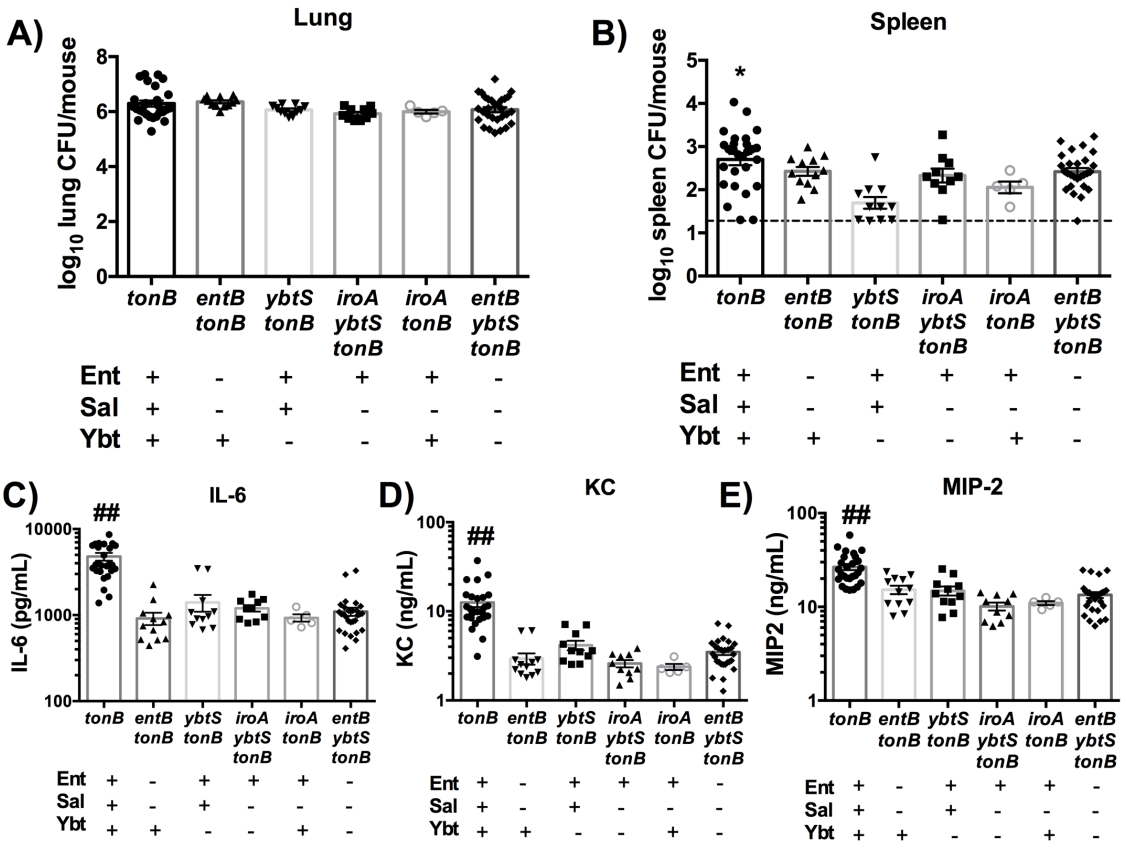

Figure 3.5: Multiple siderophores are required for bacterial dissemination and IL-6, KC, and MIP-2 secretion.

C57Bl/6 mice (n=5-18 per group) were infected with 1x10^8 isogenic tonB K. pneumoniae as indicated. Following 24hr, mice were euthanized, and organs were harvested for bacterial load in the A) lung and B) spleen. Lung homogenates were assayed for C) IL-6, D) KC, and E) MIP-2 secretion using ELISA. Statistics were calculated using one-way ANOVA with Fisher's post-test (, p<0.05 vs tonB; ##, p<0.001 vs all other conditions).*

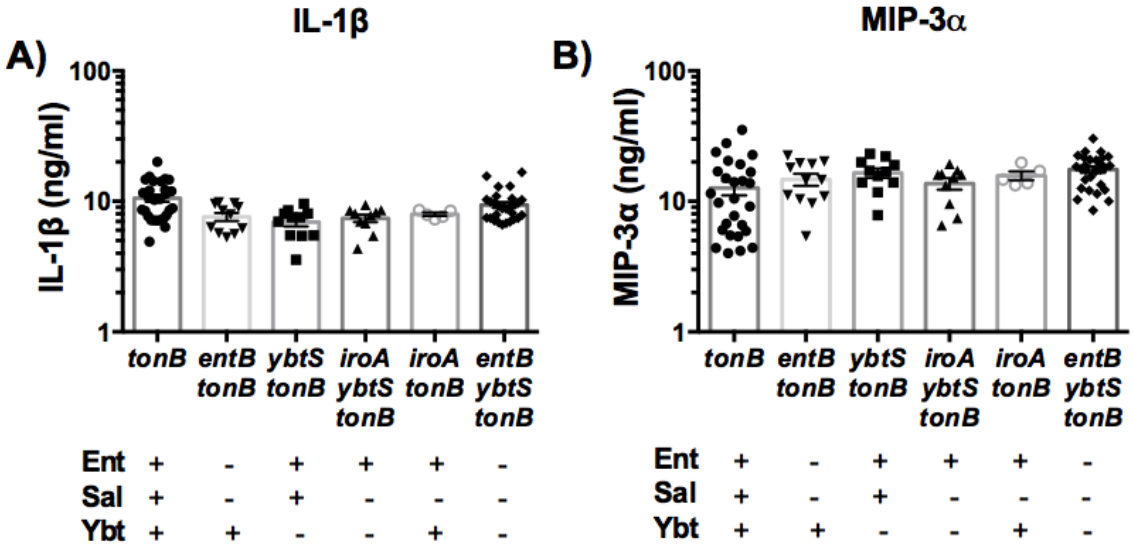

Figure 3.6: IL-1β and MIP-3α during lung infection with isogenic tonB mutants.

C57Bl/6 mice (n=5-18 per group) were infected with 1x10^8 isogenic tonB K. pneumoniae as indicated. Lung homogenates were assayed for A) IL-1β and B) MIP-3α secretion using ELISA. Statistics were calculated using one-way ANOVA with Fisher's post-test (, p<0.05; **, p<0.01; ***, p<0.001 vs tonB or as indicated.)*

Binding by Lcn2 could mask the effects of Ent on inflammation and dissemination. To test this hypothesis, we compared lung inflammation and dissemination in C57Bl/6 and LcnKO mice with *iroA ybtS tonB* (Ent+) *K. pneumoniae* (Figure 3.7). LcnKO mice did not display differences in spleen bacterial load or lung inflammation when compared to C57Bl/6 WT mice, indicating that Ent is not sufficient to induce dissemination or inflammation, even in the absence of Lcn2. Together, these results indicate that all siderophores are required to induce maximal secretion of IL-6, KC, and MIP-2.

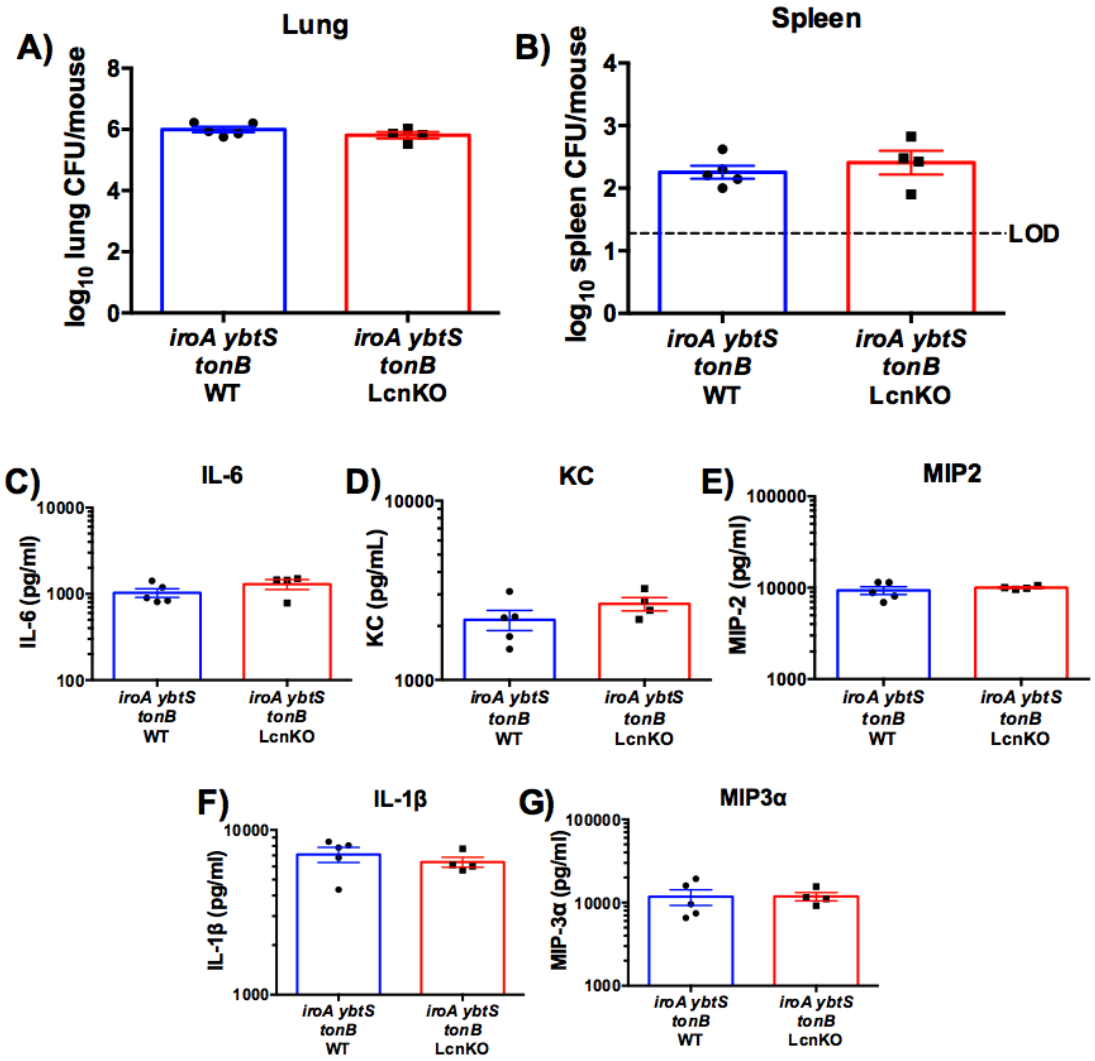

Figure 3.7: Lcn2 does not impact dissemination or inflammation by Ent-secreting tonB K. pneumoniae.

C57Bl/6 or LcnKO mice (n=4-5 per group) were infected with 1x10^8 CFU iroA ybtS tonB K. pneumoniae. Following 24 hr infection, mice were euthanized, and organs were harvested for bacterial load in the A) lung and B) spleen. Lung homogenates were assayed by ELISA for C) IL-6, D) KC, E) MIP-2, F) IL-1β, and G) MIP-3α secretion. There were no statistically significant differences, as calculated using unpaired, two-tailed t-tests.

3.2.3 Siderophores secreted by K. pneumoniae stabilize HIF-1α

To test the hypothesis that *K. pneumoniae* siderophores stabilize HIF-1α during pneumonia, we utilized a transgenic mouse model that expresses a fusion protein of luciferase with the Oxygen Dependent Domain (ODD) of HIF-1α ("ODD-Luc") that is subject to prolyl hydroxylation and becomes stabilized by low oxygen or low iron conditions [160-163]. Infection of ODD-Luc mice with WT *K. pneumoniae* induced increased bioluminescence in the lung when compared to the PBS vehicle control (Figure 3.8A). To determine whether siderophores secreted by *K. pneumoniae* induce HIF-1α stabilization *in vivo* during infection, ODD-Luc mice were infected with *tonB* (siderophore+) or *entB ybtS tonB* (siderophore negative) *K. pneumoniae*. Infection with *tonB* induced greater bioluminescence in the lung compared to infection with *entB ybtS tonB*, though infection with *entB ybtS tonB* did induce some bioluminescence when compared to the PBS vehicle control (Figure 3.8B). These results indicate that siderophores secreted *in vivo* can stabilize the transcription factor HIF-1α.

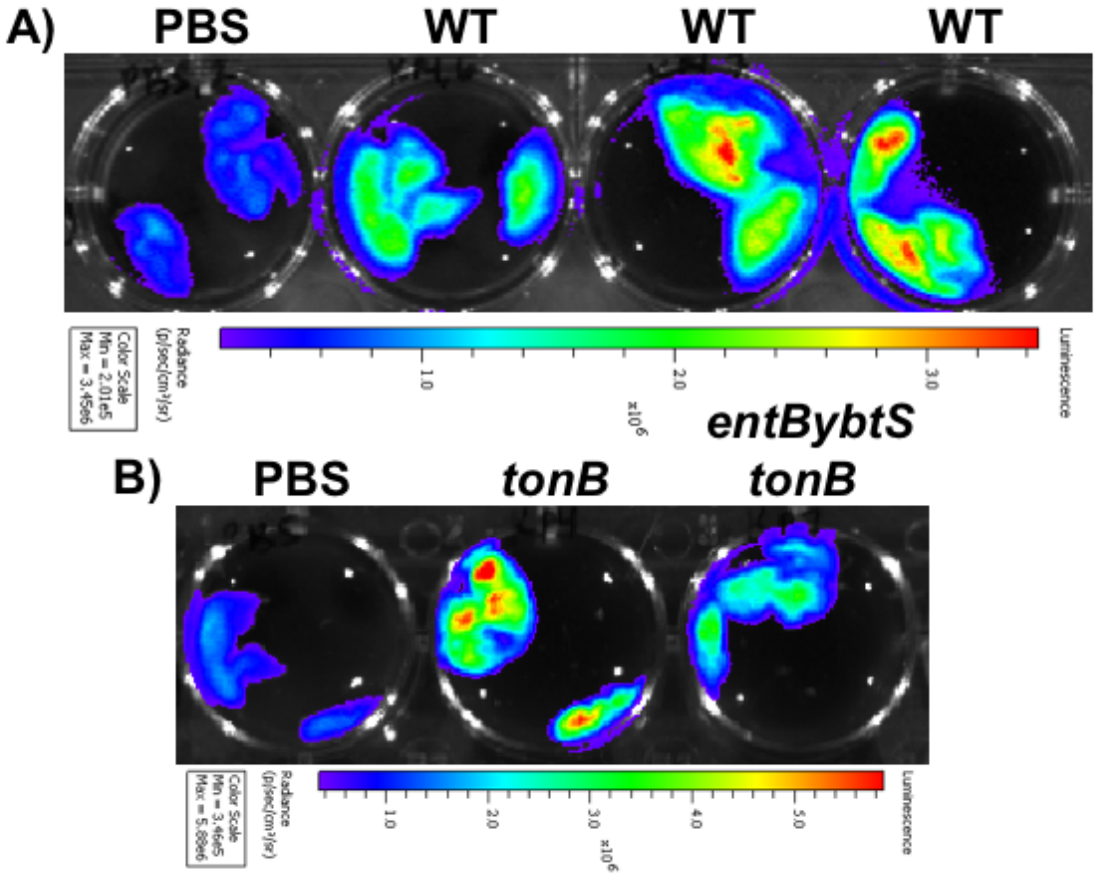

Figure 3.8: Wild-type K. pneumoniae and tonB K. pneumoniae induce HIF-1α stabilization in the lung as indicated by bioluminescence.

ODD-Luciferase mice were infected with A) $1x10^4$ CFU wild-type K. pneumoniae or B) $1x10^8$ CFU tonB or entB ybtS tonB K. pneumoniae for 24 hr. Mice were treated with luciferin, euthanized, and lungs were removed to image bioluminescence (p/sec/cm^2/sr). Bioluminescence intensity is indicated with blue representing low induction and red indicating high induction. Each well contains lungs from a single mouse. Data shown are representative of 3-7 individual mice.

We then sought to determine whether individual siderophores were capable of stabilizing HIF-1α. To do so, ODD-Luc mice were infected with isogenic siderophore *tonB* mutants, and bacterial load in the lung and spleen was quantified (Figure 3.9A and B). The *tonB* mutants had equivalent lung CFU but significantly higher spleen CFU than the *entB ybtS tonB* mutant, consistent with previous data. Additionally, luciferase expression in the lung homogenate was quantified as fold-change when compared to *entB ybtS tonB* (siderophore-negative). The *tonB* mutant induced significantly more luciferase expression when compared to infection with the other isogenic strains (Figure 3.9C). Infection with the *iroA ybtS tonB* (Ent+) strain had equivalent CFU to *tonB* and *entB ybtS tonB*, but did not significantly disseminate to the spleen or induce luciferase expression. ODD-Luc mice infected with *entB tonB* (Ybt+) displayed higher bacterial load in the lung upon infection, confounding comparisons to the other strains. This mutant induced increased luciferase expression for a few mice and had correspondingly high CFU in the spleen. We therefore hypothesized that HIF-1α stabilization in the lung correlates with bacterial load in the spleen, and that the outliers in the *entB tonB* mutant are the exceptions that prove the rule. To examine this hypothesis, spleen bacterial load as a function of luciferase in the lung was graphed, and the correlation was determined. This plot revealed a positive correlation between spleen bacterial load and luciferase expression during infection with *K. pneumoniae* across all siderophore mutant genotypes (Figure 3.9D). Altogether, these data indicate that HIF-1α is consistently stabilized only by *tonB K. pneumoniae* that produces all three siderophores, and

that stabilization of HIF-1α by *K. pneumoniae* secreting siderophores correlates with bacterial dissemination to the spleen.

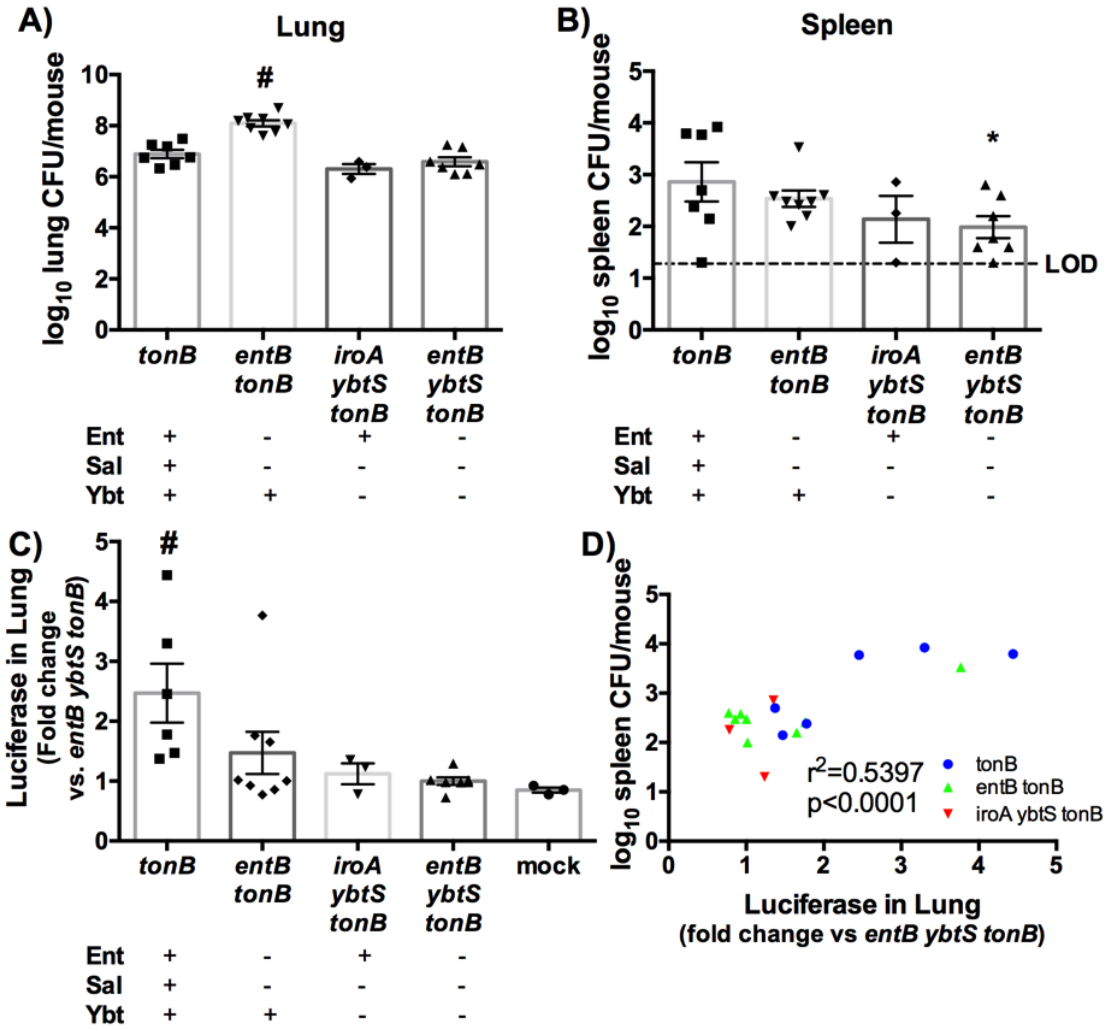

Figure 3.9: Siderophore secretion by K. pneumoniae induces HIF-1α stabilization, which correlates to bacterial dissemination to the spleen.

ODD-Luciferase mice (n=3-8 per group) were infected with 1x10^8 isogenic tonB K. pneumoniae as indicated. Following 24 hr, mice were euthanized, and organs were harvested for A) lung bacterial burden, B) spleen bacterial burden, and C) luciferase quantification. D) Correlation curves were plotted comparing spleen CFU as a function of luciferase in the lung. Statistics were calculated using one-way ANOVA with Fisher's post-test (, p<0.05 vs tonB; #, p<0.05 vs all other conditions) or Pearson r correlation curve.*

3.2.4 Lung epithelial HIF-1α is required for bacterial dissemination to the spleen

Because HIF-1α stabilization correlates with bacterial dissemination to the spleen, and because HIF-1α regulates vascular permeability and inflammation, we hypothesized that siderophores stabilize HIF-1α during infection, promoting bacterial dissemination and the host pro-inflammatory response. To test this hypothesis, we utilized transgenic mice that have an inducible lung epithelial cell-specific HIF-1α deletion, (SP-C-rtTA$^{-/tg}$/(tetO)^{7}-CMV- CRE$^{tg/tg}$/HIF1a$^{flox/flox}$), either induced with doxycycline postnatally ("Hif1a$^{-/-}$") or uninduced, wild-type littermates ("Hif1a$^{+/+}$"). To test the effect of HIF-1α on a productive infection with replicative *K. pneumoniae*, wild-type was compared to the *entB ybtS* mutant. Infection with wild-type *K. pneumoniae* did not cause HIF-1α-dependent differences in lung bacterial load (Figure 3.10A). However, Hif1a$^{-/-}$ mice displayed significantly less bacterial dissemination to the spleen after 24 hours, indicating that siderophore-dependent stabilization of HIF-1α promotoes bacterial dissemination to the spleen (Figure 3.10B). The siderophore negative *entB ybtS* mutant had lower lung and spleen CFU than the wild-type, which was not affected by the absence of lung epithelial HIF-1α (Figure 3.10A and B).

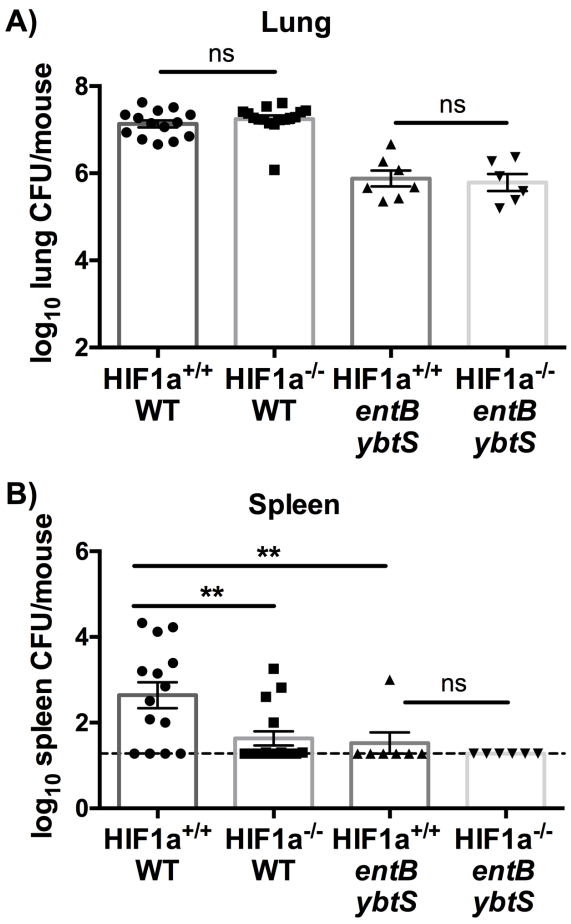

Figure 3.10: Lung epithelial HIF-1α is necessary for siderophore-dependent bacterial dissemination to the spleen.

*Hif-1a$^{+/+}$ or Hif-1a$^{-/-}$ mice (n=6-14 per group) were infected with 1x10^{4} CFU wild-type or entB ybtS K. pneumoniae. Following 24 hr, mice were euthanized, and organs were harvested for bacterial load in the A) lung and B) spleen. Statistics were calculated using one-way ANOVA with Fisher's post-test (**, p<0.01 as indicated).*

To examine the role of alveolar epithelial HIF-1α during infection with WT *K. pneumoniae,* cytokine secretion was assayed from murine lung homogenates. Infection with the wild-type *K. pneumoniae* induced significantly more IL-6 and MIP-2 than the *entB ybtS* mutant, consistent with siderophore-dependent effects observed above, and more IL-1β that may be attributable to higher bacterial density (Figure 3.11). However, there were no HIF-1α-dependent differences in lung cytokine secretion, indicating that lung epithelial HIF-1α is not required to induce IL-1β, IL-6, KC, MIP-2, or MIP-3α secretion during infection (Figure 3.11). These data suggest a role for epithelial HIF-1α stabilization by siderophores in the induction of bacterial dissemination, but secretion of IL-6, MIP-2, KC, IL-1β, or MIP-3α during *K. pneumoniae* infection.

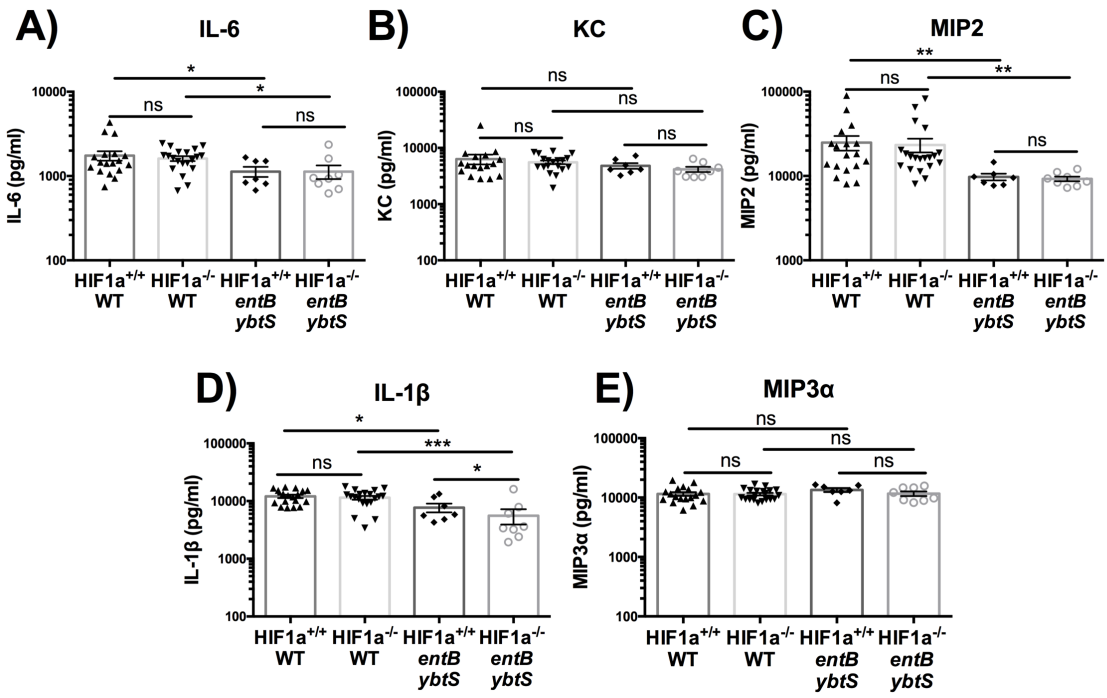

Figure 3.11: Lung epithelial HIF-1α is not necessary for siderophore-dependent cytokine secretion. Hif-1a$^{+/+}$ or Hif-1a$^{-/-}$ mice (n=6-14 per group) were infected with 1x10^{4} CFU wild-type of entB ybtS K. pneumoniae. Following 24 hr, mice were euthanized, and organs were harvested. Lung homogenates were assayed for A) IL-6, B) KC, C) MIP-2, D) IL-1β or E) MIP-3α secretion by ELISA. Statistics were calculated using one-way ANOVA wish Fisher's post-test (, p<0.05; **, p<0.01; ***, p<0.001; ns, p>0.05 as indicated.)*

3.3 Discussion

3.3.1 Summary of findings

K. pneumoniae is a Gram-negative bacterium that is rapidly acquiring resistance to all known antibiotics, including carbapenems. Developing novel therapies to combat antibiotic-resistant infections requires a more complete understanding of disease pathogenesis [164]. To determine the effect of siderophores on the host response to infection, we developed a *tonB* mutant that allowed us to uncouple siderophore secretion from bacterial growth. We show that *K. pneumoniae* siderophores are a major trigger of the inflammation and bacterial dissemination induced during lung infection with *K. pneumoniae*, independent of their ability to deliver iron to bacteria. Additionally, we show that the induction of bacterial dissemination by siderophores requires the stabilization of the master transcription factor HIF-1α in lung epithelial cells. These findings represent a novel function for bacterial siderophores in immune system modulation and bacterial dissemination, and a novel function for the host master transcription factor HIF-1α as a susceptibility factor for the development of sepsis.

3.3.2 Quantification of siderophores in lung homogenates

To confirm that the *tonB* mutant produces physiologically relevant levels of siderophores *in vivo*, we utilized mass spectrometry to quantify the secretion of siderophores during lung infection with WT and *tonB K. pneumoniae* (Figure 3.3H). This mass spectrometry analysis has been used to quantify Ent, Sal, and Aer in chicken air sacs during *E. coli* infection [165]. To our knowledge, these data represent the first published concentrations of siderophores from murine

lung homogenates. Measured concentrations were on the same magnitude as concentrations used *in vitro* by our group, as well as others, and provide context for prior findings using purified siderophores [45, 71, 106, 152, 166]. Although *tonB K. pneumoniae* secreted more siderophores *in vitro* than WT strains, the concentrations observed *in vivo* were equal or even slightly lower than WT, indicating that the *tonB* mutants can be used to assess the impact of siderophores on the host at physiologically relevant concentrations. Whereas micromolar concentrations of Sal and high nanomolar amounts of Ybt were detected, we were unable to detect Ent. We propose three possible explanations for this finding: 1) Ent is being sequestered by Lcn2, and is therefore undetectable; 2) bacteria convert all Ent to Sal *in vivo* to evade Lcn2; or 3) a combination of our two hypotheses, whereby bacteria are converting the majority of Ent to Sal, and the remaining Ent is sequestered by Lcn2. These data suggest that the majority of inflammation and bacterial dissemination is due to the secretion of Sal, but also suggests a role for Ybt. However, we could not test the contribution of Sal in isolation because it is not possible to create mutants that produce Sal without intact Ent synthesis genes, and we were unable to detect iron chelation by purified Sal *in vitro* [13, 152]. In contrast, a mutant making Ent alone (*iroA ybtS tonB*) had no detectable induction of cytokines or dissemination, with or without Lcn2. Together, these data implicate Sal and Ybt as significant inducers of inflammation and dissemination during pneumonia.

3.3.3 Impact of siderophore-dependent HIF-1α stabilization

Stabilization of the master transcription factor HIF-1α strongly correlated with siderophore-dependent bacterial dissemination to the spleen, which was found to occur in a lung epithelial HIF-1α-dependent manner (Figure 3.9 & 3.10). HIF-1α regulates the transcription of many genes, resulting in numerous possibilities for the downstream mechanism of HIF-1α-dependent bacterial dissemination. Most notably, HIF-1α regulates the induction of VEGFs that are responsible for vascular permeability and angiogenesis [104, 167, 168]. The secretion of various siderophores can determine *K. pneumoniae* localization during infection, including in the perivascular space with iron-rich serum exudate [96]. Therefore, it is possible that HIF-1α stabilization results in this vascular permeability by activating VEGF. *K. pneumoniae* may then be able to invade blood vessels, resulting in bacterial escape from the lung to the spleen. It is also possible that stabilization of HIF-1α disrupts the epithelial barrier, as shown for intestinal epithelial cells in a murine model of colitis [169]. By either mechanism, epithelial HIF-1α is a critical factor for invasion by *K. pneumoniae* during infection.

In this study, we illustrated that HIF-1α stabilization by siderophores results in bacterial dissemination to the spleen, an activity that is detrimental to the host. These results differ from prior work illustrating a protective response for HIF-1α stabilization by a pharmacological molecule, AKB-4924, during murine UTI [157]. These contrasting results may be due to differences in both pathogen and model system. For instance, treatment with AKB-4924 prevented internalization of *E. coli* by uroepithelial cells. *K. pneumoniae* is not readily

internalized by epithelial cells due to its capsule; therefore, preventing the uptake of bacteria through HIF-1α stabilization may not be an effective therapy against *K. pneumoniae* infection [170]. Additionally, the study primarily evaluated the contribution of the innate immune response and myeloid-cell HIF-1α during UTI, whereas we primarily examined the effects of siderophore secretion during *K. pneumoniae* infection. It is possible that HIF-1α activation in these different cell types have opposing effects on the outcome of infection. Together, these data illustrate the complexity of HIF-pathogen interactions, and highlight the importance of evaluating many various bacterial infections and model systems.

Whereas lung epithelial HIF-1α is instrumental in bacterial dissemination to the spleen, it was not shown to be required for the induction of the pro-inflammatory immune response. These results are divergent from our original hypothesis because HIF-1α is known to regulate the transcription of inflammatory genes, in particular IL-6, and differ from a study showing epithelial HIF-1α regulation of IL-6 and IL-1β secretion in a lung contusion model [171, 172]. Though lung epithelial HIF-1α is not involved in the cytokine response to siderophores, HIF-1α has been shown to be instrumental in the activity of myeloid-derived cell types, including myeloid cell development, phagocytosis, and antimicrobial production [105, 126, 173]. In addition to HIF-1α regulation of inflammation, HIF-2α can regulate macrophage function in tumor models, eosinophil function in the lung, and IL-6 secretion from endothelial cells [174-176]. Therefore, it is possible that another cell-specific source of HIF-1α or HIF-2α could be responsible for regulating inflammation via cytokine secretion and/or

bactericidal capacity in response to *K. pneumoniae* infection. Because HIF knockouts are embryonic lethal, testing other HIF isoforms and cell types would require multiple lineage-specific knockouts.

3.3.4 Siderophore-dependent cytokine induction

IL-6, KC, and MIP-2 has previously been shown to be protective upon lung infection with *K. pneumoniae* [177-179]. Here we attribute significant induction of IL-6, KC, and MIP-2 to the secretion of siderophores by the bacteria when compared to infection with siderophore-negative bacteria. These results are consistent with prior *in vitro* work illustrating that iron chelation by siderophores, as evidenced by depletion of the labile iron pool and induction of the iron starvation marker *NDRG1*, induces the secretion of the pro-inflammatory cytokines IL-8 and IL-6 from A549 lung epithelial cells [152]. Human and murine IL-6 act as an inflammatory cytokine involved in hepatocyte acute phase responses and can upregulate hepcidin, an iron homeostasis protein [127, 180, 181]. Murine KC and MIP-2 (CXCL1 and CXCL2, respectively) are neutrophil chemoattractants and are functionally similar to human IL-8 [182]. Prior microarray data illustrated that lung epithelial cell stimulation with Ent induces genes involved in the Unfolded Protein Response (UPR) [152]. The UPR has been implicated in the secretion of pro-inflammatory cytokines, including IL-6, and can act through NF-κB signaling, a common component in IL-6, KC, and MIP-2 secretion [183-188]. Additionally, the UPR and HIF-1α pathways interact and can potentiate downstream effects, potentially resulting in increased inflammatory cytokine secretion [189]. In this manner, iron chelation by

siderophores during lung infection may induce the secretion of pro-inflammatory cytokines.

3.3.5 Absence of Lcn2 requirement in vivo

Although Lcn2 was necessary for siderophore induction of cytokines *in vitro*, it was dispensible for the siderophore-dependent immune response to *K. pneumoniae in vivo* [152]. This may indicate differential ability of human and murine Lcn2 to modulate immune responses. Although they share 62% amino acid identity, murine Lcn2 lacks the ability to form covalent complexes, which may explain this discrepancy [190]. Alternatively, redundant signaling pathways may be activated during pneumonia so that inflammatory signaling by Lcn2 is dispensible. It may be that two signals are required for the maximal induction of cytokine secretion in response to infection with siderophore-secreting bacteria: 1) perturbation of iron homeostasis by siderophores, and 2) signaling by an inflammatory protein, including Lcn2. *In vivo*, many proteins could satisfy the requirement of the second signal, such as inflammasome activation or Toll-Like Receptor signaling activation by capsule and LPS [191, 192]. Our previous *in vitro* studies indicated that IL-1β could serve as the inflammatory protein from the host, corroborating this hypothesis (Figure 2.11). Although IL-1β and MIP-3α/CCL20 were secreted in response to *K. pneumoniae* infection, we showed that they were not secreted in a siderophore-dependent manner *in vivo*. Supporting these results are data indicating that IL-1β is induced in an NLRP3-dependent manner in response to *K. pneumoniae* capsule [191]. The lack of siderophore-dependent induction of MIP-3α/CCL20, a lymphocyte

chemoattractant, secretion is inconsistent with our previous *in vitro* results [193]. However, in these studies we examined whole lung homogenates rather than lung epithelial cell cytokine production, and differences in cell-specific secretion of MIP-3α/CCL20 may account for this discrepancy [193].

3.3.6 Proposed model and summary

Based on our data, we propose the following model: upon infection and iron starvation, *K. pneumoniae* produce and secrete siderophores. Siderophores serve to acquire host iron and deliver it to the bacteria, resulting in bacterial growth. In addition to supporting bacterial growth, chelation of host cellular iron by siderophores induces cellular stress. One stress response is the stabilization of the master transcription factor HIF-1α, resulting in bacterial dissemination to the spleen, potentially through vascular permeability as an acute response to deliver more iron from blood. An opposing stress response is secretion of the pro-inflammatory cytokines IL-6, KC, and MIP-2 within the lung that are necessary for protection from *K. pneumoniae*. These results indicate novel functions for bacterial siderophores during infection that are independent of their iron delivery capabilities and present siderophore molecules as a possible target for therapeutic intervention. Additionally, these results indicate a novel role for HIF-1α in *K. pneumoniae* pathogenesis as a susceptibility factor for development of systemic infection and illustrate the complex interplay between pathogen and host molecules during bacterial infection.

3.4 Experimental Procedures

Animal Strains and Ethics Statement. All work was approved by the University of Michigan Institutional Animal Care and Use Committee (IACUC). C57BL/6 and Lipocalin 2-deficient (LcnKO) mice were bred onsite. ODD-Luciferase (ODD-Luc) mice were obtained from Dr. Yatrik Shah [160], and conditional alveolar epithelial HIF-1α-deficient (SP-C-rtTA$^{-/tg}$/$(tetO)_7$-CMV- Cre$^{tg/tg}$/HIF1$^{flox/flox}$) mice were obtained from Dr. Krishnan Raghavendran [194].

To induce epithelial cell knockout of HIF-1α, newborn mice were treated as previously described [195]. Briefly, following birth lactating dams were given doxycycline-containing chow (625 mg/kg; Harlan Teklad, Madison, WI) and water (0.8 mg/ml, Sigma) until weaning to induce HIF-1α deletion. Upon weaning, mice were maintained on doxycycline-containing food and water until ~6 weeks of age (HIF-/-). Doxycycline treatment was terminated at least 7 days prior to bacterial infection. As controls (HIF+/+), littermates were given normal chow and water.

Growth Curves. K. pneumoniae strains were cultured overnight in LB medium. On the following day cultures were incubated in LB with a starting density of $2.6x10^7$ CFU/ml and cultured for 8 hours at 37^o C. OD_{600} readings were taken every 15 min using an Eon Microplate spectrophotometer with Gen5 software (BioTek, Winooski, VT).

Serum Growth Assay. To assess the ability of *K. pneumoniae* mutants to acquire iron, serum growth assays were performed as previously described [96].

CAS Assay. Following overnight growth, cultures of *K. pneumoniae* were diluted 1:100 and incubated for 2 hours with 10 μM 2,2′-dipyridyl (DIP) at 37° C, subcultured into M9 medium with 10^8 CFU, and incubated overnight. The following day, cultures were spun through 0.22 μm tube filters, and the supernatants were used for the CAS assay. CAS reagent was prepared as previously described. Briefly, 2 mM of chrome azurol S (CAS) agent was prepared. Next, iron (III) solution (1mM FeCl into 10 mM of HCl), 3 mM hexadecyltrimethrylammonium bromide (HDTMA) solution, and 1 mM anhydrous piperazine solution were prepared (Sigma). 7.5 mL of 10 M HCl was added to the piperazine solution, and 1.5 mL of the iron (III) solution was added to 7.5 mL of the 2 mM CAS solution. Finally, the acid-piperazine solution was poured into the iron-CAS-HDTMA solution, and the final volume was brought to 100 mL with ddH_2O (pH 5.6).

Bacterial Strains and Media. *K. pneumoniae* KPPR1 and isogenic mutants were cultured in Luria-Bertani (LB) broth at 37°C with shaking or 30°C on agar (Benton, Dickinson and Company, Sparks, MD) supplemented with kanamycin (25 μg/ml), rifampicin (30 μg/ml), or hygromycin (100 μg/ml) as indicated [196].

Murine Pneumonia Model. Six- to ten-week old C57BL/6, Lipocalin2-deficient (LcnKO), ODD-Luciferase (ODD-Luc), or HIF-/- mice were infected as previously described [149]. Briefly, mice were anesthetized with isoflurane, inoculated retropharyngeally with $1x10^4$ wild-type or $1x10^8$ of indicated isogenic *tonB* mutant

CFU of *K. pneumoniae* cultured under iron-limited conditions as described above for the CAS assay, and sacrificed at day 1 or day 2 post infection by CO_2 asphyxiation. To determine bacterial numbers in tissues, lungs and spleens were removed and homogenized into DPBS containing EDTA-free protease inhibitor (Roche) and cultured to obtain bacterial counts.

ELISA. Cytokine protein concentrations in lung homogenates were determined by ELISAs (Duoset Kits, R&D Systems) according to manufacturer's protocols.

Siderophore Quantification in Lung Homogenates. Siderophore concentrations were determined via Mass Spectrometry as previously described [165]. Briefly, homogenates were centrifuged at 3,200×g for 15 min. The supernatants were retained and 500 µL aliquots were then prepared with 5,6,7,8-tetradeutero-2-heptyl-3-hydroxy-4-quinolone as an internal control. Samples were analyzed three times by LC-MS/MS.

Multiple reaction monitoring (MRM) analyses were performed using a Waters 2795 Alliance HT instrument coupled to a Micromass Quattro Premier XE spectrometer (Micromass MS Technologies). Samples were injected onto a Kinetex 2.6-µm C8 4.6- by 100-mm column at a flow rate of 400 µl/min, with a linear gradient of water-acetonitrile with 1% acetic acid. The high-performance liquid chromatography effluent was directed to the mass spectrometer through a Valco T splitter. The analyses were performed in positive electrospray ionization mode with a cone voltage of 30 V. Monitoring of daughter ions from specific

pseudomolecular ions was performed by collision-induced dissociation with argon at different collision energies for each molecule ranging from 15-55 eV. The specific transition ions monitored from pseudomolecular ions to daughter ions of salmochelins SX, S1, linear diglucosyl-C-enterobactin (DGE) (S2), DGE (S4), S5, monoglucosyl-C-enterobactin (MGE), linear MGE, triglucosyl-C-enterobactin (TGE), and linear TGE were 404 > 299, 627 > 224, 1,012 > 224, 994 > 224, 789 > 386, 832 > 224, 850 > 224, 1,156 > 266 and 1,174 > 266 m/z, respectively. The transition ions monitored for enterobactin and its linear trimer [(DHBS)3], dimer [(DHBS)2], and monomer (DHBS) derivatives were 670 > 224, 688 > 224, 465 > 224, and 242 > 137 m/z, respectively. The transition ions monitored for the internal standard, aerobactin and yersiniabactin were 264 > 179, 565 > 205 and 482 > 295 m/z, respectively. Quantification of each compound was determined from the response factor of Ent for salmochelins and enterobactins corrected with the intensity of the signal of the internal standard. Quantification of Ybt was determined from the response factor of Ybt corrected with the intensity of the signal of the internal standard.

Bioluminescence. To determine the effect of *K. pneumoniae* infection on HIF-1α stabilization, six- to ten-week old ODD-Luc mice were infected as above for 24 hours. Following infection, mice were treated with 100 μL luciferin intraperitonally and euthanized as above. Lungs were removed for bioluminescent imaging and imaged on an IVIS bioluminescent imaging system at the Center for Molecular Imaging at the University of Michigan.

Luciferase Assay. ODD-Luc mice were infected with $1x10^8$ CFU of isogenic *tonB K. pneumoniae* for 24 hours. Following infection, mice were euthanized as above and lungs and spleens were collected. Lungs were homogenized with DPBS and protease inhibitor (Roche), and an aliquot was reserved for luciferase quantification. Luciferase cell lysis buffer (New England Biolabs, Ipswich, MA) was added to homogenate and incubated at room temperature for 15 minutes. Protein concentration was quantified using the BCA Assay (Thermo Fisher). 30 µg of protein was added to an opaque 96-well plate (Corning, Corning, NY) and luciferase buffer was added using a BioTek Synergy Multi Mode Plate Reader (BioTek). Luciferase buffer was composed of: 4.8 ml 0.11 mM Tris, pH 7.8, 50 µL 100 mM sodium luciferin; 60 µL 200 mM ATP, and 120 µL 0.5 M MgCl.

tonB Mutant Construction. PCR primers specific for conserved regions of the tonB gene were constructed by comparing DNA sequences from various *K. pneumoniae* species [15]. An internal 0.3 kb *tonB* PCR fragment was amplified and then cloned into the TA-based PCR cloning vector pCR2.1 (Invitrogen, Carlsbad, CA). The *tonB* fragment was then extracted using a gel extraction kit (Qiagen, Venlo, Limburg), purified with a PCR clean up kit (Qiagen), dephosphorylated, and ligated with a kanamycin-resistant derivative of the λpir-dependent suicide vector pGP704 [197]. This *tonB* suicide vector was transformed into *E. coli* strain BW20767 (ATCC 47084, RP4-2tet::Mu-1kan::Tn7-integrant uidA(DMlu1)::pir+ recA1 creB510 leu-63 hsdR17 endA1 zbf-5 thi) and subsequently conjugated into wild-type, *entB, ybtS,* and *entB ybtS* mutants of *K.*

pneumoniae to generate *tonB*, *entS tonB*, *ybtS tonB*, and *entB ybtS tonB* mutants. Integration of the suicide vector into the *tonB* gene was confirmed by generation of a PCR product using one primer on the vector (pGP704 MCS Pst.Xba) and a *tonB*-specific primer flanking the insertion site. Primers are listed in Table 3.2.

Lambda Red Mutant Construction. Lambda Red mutagenesis was performed as previously described [149]. Primers are listed in Table 3.2.

Statistical Analysis. Bacterial counts and ELISA data were log-transformed and analyzed using one- or two-way analysis of variance (ANOVA) models with one mean per group, and pairs of treatments were compared with Fisher's post-test (GraphPad Software, Inc). Luciferase assay data was analyzed using one-way ANOVA with Fisher's post-test. Correlation data were calculated using Pearson r correlation curve.

Table 3.2: Primers used for mutagenesis in this work

Use	Primer (5' --> 3')
tonB TOPO construct F	CTT TAT ACC TCG GTA CAT CAG GTT
tonB TOPO construct R	ATT CGC CGG CTG RGC RGA GAG
pGP704 MCS Pst>Xba	GGT CGA CGG ATC CCA AG
tonB Flank F	CGA CTG CGA TTT AGC CAT GC
tonB Flank R	GCT CTG GAG TGG AAA GCA CT
tonB Kan, co-integrant F	TTGCATTTAAAATCGGAGCATCATTTTTTCAACAGAAACGACTATGAGCGCAATGACCCTTGTGTAGGCTGGAGCTGCTTC
tonB Kan, co-integrant R	TCAGTTAATCTCGACGCCGTTCAGGCGGAATTTGATGGTCATCGTTACGCCGGTACCCGGATGGGAATTAGCCATGGTCC
tonB Hyg, lambda red F	TTGCATTTAAAATCGGAGCATCATTTTTTCAACAGAAACGACTATGAGCGCAATGACCCTTATGAGTAAACTTGGTCTGACA
tonB Hyg, lambda red R	TCAGTTAATCTCGACGCCGTTCAGGCGGAATTTGATGGTCATCGTTACGCCGGTACCCGGCAACCACTAAACCCACAGTA

3.5 Notes

VI Holden designed and performed experiments, analyzed the data, and wrote the chapter; P Breen performed experiments and analyzed the data; S Houle and CM Dozois performed mass spectrometry; MA Bachman designed experiments and proofread the chapter.

CHAPTER IV

IRON ACQUISITION BY CARBAPENEM-RESISTANT *KLEBSIELLA PNEUMONIAE*

Summary

K. pneumoniae is rapidly acquiring antibiotic resistance to all known antibiotics, including carbapenems. One multilocus sequence type, ST258, encodes the *K. pneumoniae* Carbapenemase on a transmissible plasmid, and is the most prevalent carbapenem-resistant *Enterobactericeae* (CRE) in the United States and has disseminated worldwide. Previously, whole genome sequencing identified core genome single nucleotide variants that divide ST258 into two distinct clades, ST258a and ST258b. One significant genetic difference between clades is that ST258b contains a deletion within the Ent exporter gene *entS*. Despite the predicted inability of ST258b strains to secrete the siderophore Ent, this clade is prevalent among clinical strains, indicating that it has alternative mechanisms of acquiring iron required to cause infection. To determine how ST258a and ST258b strains differentially respond to iron limitation, we performed RNASeq in minimal medium alone, or supplemented with iron or human serum and measured gene expression patterns. Iron limitation induced differential expression of novel iron-acquisition pathways when comparing ST258a and ST258b strains, including the upregulation of the hemin transport operon in the

ST258b isolates. Additionally, *in vitro* assays were performed to characterize growth patterns as well as iron chelation ability of ST258a and ST258b strains. We determined that both ST258a and ST258b strains grow under iron-deficient conditions and secrete iron-chelating molecules and catechols, despite the loss of the Ent exporter in the ST258b clade. These data may indicate a mechanism by which Ent export-deficient strains have evolved to acquire iron from the host by a combination of alternative Ent secretion and upregulation of other iron acquisition systems.

4.1 Introduction

CRE are resistant to all or nearly all antibiotics, are increasingly present worldwide, and are therefore designated as an urgent public health concern [198]. Infection with CR *K. pneumoniae* is of particular concern due to its high rate of mortality, approximately 41-50% for bloodstream infections [146, 147, 198]. *K. pneumoniae* causes a variety of infections, including pneumonia, UTI, and bacteremia, and represents the 3rd most common cause of healthcare-acquired infection, further contributing to its relevance to healthcare settings [143]. Despite epidemiological studies documenting the spread and patient risk factors associated with infection, the bacterial pathogenesis of CR *K. pneumoniae* is currently not well understood [144, 199, 200].

To measure the genomic diversity of CR *K. pneumoniae*, a cohort of 57 isolates was collected from hospitals within the Midwestern United States for whole genome sequencing. For all 113 strains isolated from infection and

colonization, molecular genotyping identified two predominant and distinct clades within the Multilocus Sequencing Typing (MLST) ST258, clade ST258a and clade ST258b [201]. ST258a isolates were significantly associated with the carbapenemase KPC-2, whereas ST258b isolates were associated with the carbapenamse KPC-3. Many significant epidemiological differences were present as well. ST258a isolates were more commonly tigecycline- and gentamicin-susceptible, whereas ST258b isolates were more commonly susceptible to amikacin [201]. Infection with ST258a isolates was also more likely to result in an increased length of hospital stay than ST258b infection, and ST258b infection was more commonly acquired from a skilled-nursing facility whereas ST258a infections were more commonly community-acquired [201]. To further expand on this work, 57 isolates from the collection of 113 ST258 isolates was analyzed via genome sequencing. Whole genome comparisons uncovered differences between the two clades within the capsular polysaccharide locus and extending into the *mdtABC* locus [92]. Significant differences were also found within the isolates' plasmid contents [92]. Intriguingly, a 97 bp deletion in the Ent exporter gene, *entS*, was found in ST258b isolates that was absent in ST258a isolates [92].

Ent is the prototypic catecholate siderophore, and is secreted by Gram-negative bacteria, including *K. pneumoniae*, to acquire iron [150]. Siderophores are a major virulence factor for infection; in particular, Ent has the highest known affinity for iron of any molecule [150]. To counter the iron-sequestering effects of Ent, host cells secrete Lcn2 that specifically binds to and sequesters Ent. As the

only known Ent exporter, a deletion in *entS* is predicted to result in an inability of bacteria to secrete Ent for iron acquisition [16]. Because ST258 *K. pneumoniae* isolates do not secrete additional siderophores, an inability to secrete Ent would be predicted to be a deleterious mutation. However, the prevalence of the ST258b clade among clinical isolates suggests otherwise, indicating that a deletion in *entS* may be neutral or even advantageous. It is currently unknown how ST258b isolates of either clade respond to iron-limiting conditions.

To understand iron acquisition by CR *K. pneumoniae*, we examined transcriptional and phenotypic responses of ST258 isolates to iron limitation induced by incubation in minimal medium and human serum. To study gene transcription in response to iron-replete and iron-depleted conditions, RNASeq was performed to identify differential gene expression based on iron status and *entS* deletion. Additionally, we performed *in vitro* assays to characterize the ability of ST258a and ST258b strains to grow in iron-limiting medium and to secrete iron-chelating molecules. These results serve to increase the general understanding of CR *K. pneumoniae* iron acquisition.

4.2 Results

4.2.1 Growth of K. pneumoniae ST258 strains in iron-replete and iron-depleted conditions

The strains utilized in this study are shown in Table 4.1 and include: KP4, a WT strain secreting Ent, Ybt, and Sal; KP7, an isogenic, siderophore-negative mutant of KP4; KP20, an isogenic, Ent-secreting mutant of KP4; UHKPC05, an ST258a

strain with a full-length *entS*; NJST258_1 and NJST258_2, ST258b strains with a full-length *entS*; and UHKPC48, DMC0526, and VAKPC297, ST258b strains that have a 97 bp deletion within *entS*.

Table 4.1: K. pneumoniae strains used in this work.

Strain	Description	ST258 Clade	*entS*
KP4	KPPR1; Ent+ Ybt+ Sal+	-	+
KP7	KPPR1 *entB ybtS;* siderophore-negative	-	+
KP20	KPPR1 *iroA ybtS*; Ent+	-	+
UHKPC05	Ent+	A	+
NJST258_1	Ent+	B	+
NJST258_2	Ent+	B	+
UHKPC48	Ent+	B	-
DMC0526	Ent+	B	-
VAKPC297	Ent+	B	-

To determine the ability of ST258 strains to grow under iron limitation, cultures were extensively diluted (1:100,000) into iron-depleted M9 minimal medium (M9/Chelex) and growth curves were performed. As expected, KP7, a siderophore-negative strain, was unable to grow likely due to its inability to acquire iron (Figure 4.1A). With addition of 100 μM Fe_2SO_4, the growth of all strains was rescued, including the siderophore-negative mutant KP7 (Figure 4.1B). To examine the ability of the strains to acquire iron in a physiologically relevant iron-limiting condition, growth curves were performed in M9/Chelex supplemented with 5% heat-inactivated serum. Within serum, iron is bound by the host protein transferrin, and iron acquisition for growth by WT KP4 requires siderophores [15]. All strains except KP7 grew in media containing 5% serum as

an iron source, indicating that ST258 strains are able to acquire iron from human serum for replication (Figure 4.1C). Additionally, doubling times for each strain in each medium were calculated (Table 4.2). Doubling time upon growth in iron-replete medium for each isolate was shorter than growth in either iron-depleted medium, except for UHKPC05, which experienced the shortest doubling time in M9/Chelex medium. In general, ST258 strains experienced slower doubling times in M9/Chelex and M9/Chelex+serum when compared to KP4, whereas ST258 strains were faster than KP4 in M9/Chelex+Fe. Some strains exhibited similar growth curves with different doubling times, such as KP4 and UHKPC48 in M9/Chelex. The shorter doubling time of KP4 in this media could be due to its ability to secrete Ent, allowing it to double more quickly compared to UHKPC48 that cannot secrete Ent. Together, these data document that all ST258 strains are able to grow in various iron-depleted and iron-replete growth conditions, although they did not grow as well as KP4. These conditions were then used to examine iron-responsive differences in the RNASeq analysis.

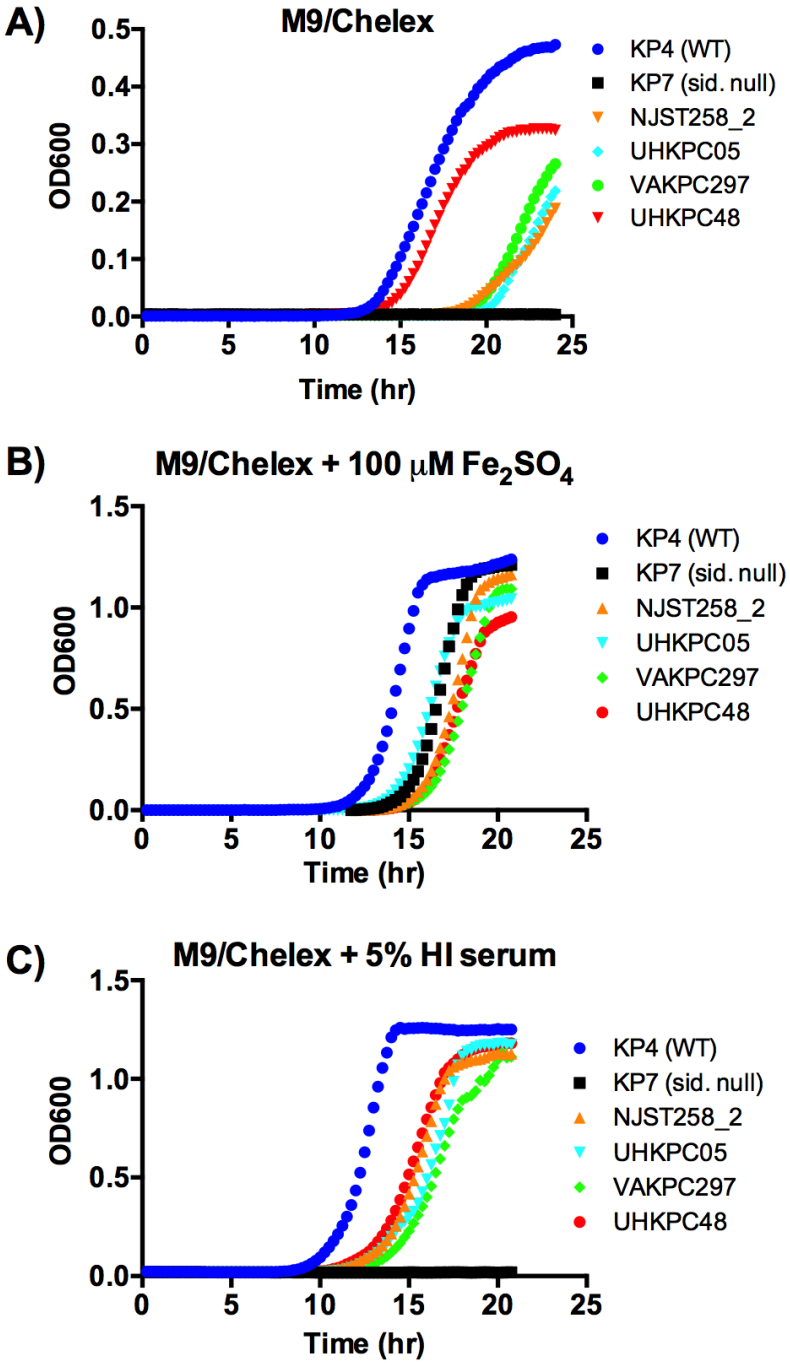

Figure 4.1: Growth curves for RNASeq stimulation conditions.

Strains were cultured overnight in LB, then subcultured at 1:100,000 into a 96-well plate for A) M9/Chelex, B) M9/Chelex + 100μM Fe_2SO_4, and C) M9/Chelex + 5% HI serum. Strains were cultured overnight and OD_{600} was read at 15 min intervals. Data are representative of at 2-3 individual replicates.

Table 4.2: Doubling time for isolates cultured in M9/Chelex, M9/Chelex+Fe, and M9/Chelex+serum.

	Doubling Time (min)		
Strain	**M9/C**	**M9/C+Fe**	**M9/C+serum**
KP4	34.89	42.33	48.56
KP7	NA	37.35	NA
NJST258_2	42.17	39.82	67.78
UHKPC05	32.61	34.93	59.58
VAKPC297	46.41	42.88	60.09
UHKPC48	46.01	33.32	63.05

4.2.2 RNASeq results identify genes up- and down-regulated in response to iron-depleted media

To investigate the effect of the *entS* deletion on growth in iron-limiting conditions, we analyzed bacterial transcription in response to available iron. Bacteria were cultured in LB broth overnight, subcultured 1:100 into LB broth, and cultured to mid-logarithmic phase ($3x10^8$ CFU). Bacteria were then subcultured 1:10 into each condition for 1 hour. A 1 hour timepoint was used to examine the initial transcriptional response to iron limitation rather than changes during growth by each bacterial strain in the individual media. To examine bacterial persistance in the various media, bacteria were plated for CFU following 1 hr stimulation in each condition ("M9/C", "M9/C+Fe", and "M9/C+serum", Figure 4.2). This was done as a quality control step to verify approximate number of bacterial cells reserved for RNA isolation. Because of slight differences in bacterial CFU by each strain in the various conditions, RNASeq samples were normalized based on OD_{600} values to collect approximately 10^8 bacteria for each strain and in each condition.

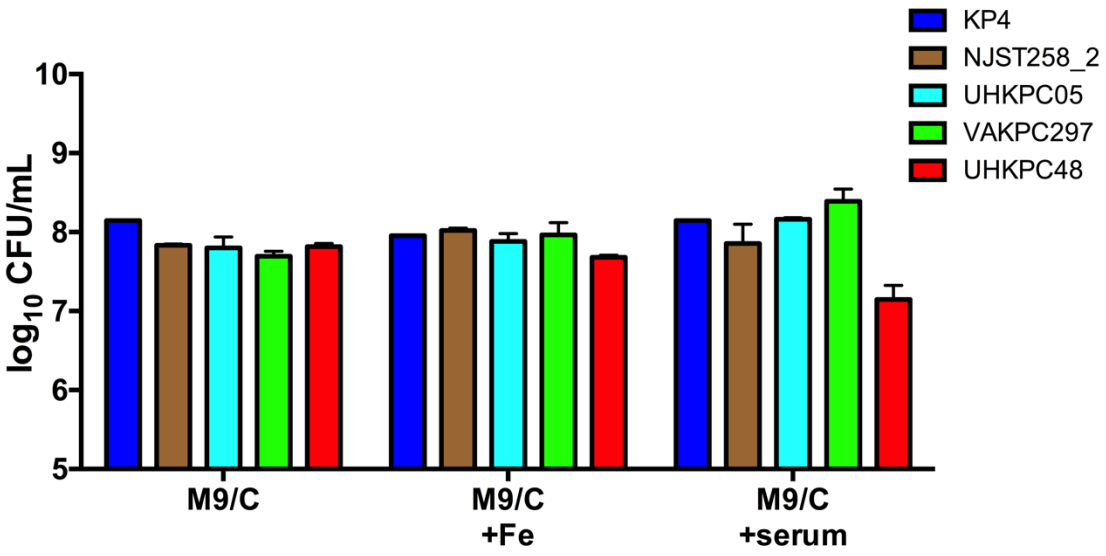

Figure 4.2: Bacterial CFU during RNASeq experiment.

Once bacteria reached mid-log growth phase, an initial aliquot was reserved and plated for CFU. Strains were then subcultured into M9/Chelex, M9/Chelex + 100μM Fe_2SO_4, and M9/Chelex + 5% HI serum. After 1 hr, aliquots were taken from each condition and plated for CFU. Data presented are means +/- standard deviation of 2 technical replicates of duplicate samples.

To identify genes among all ST258 isolates that were significantly modulated under iron-depleted conditions (M9/Chelex vs M9/Chelex+Fe), the DESeq2 package in R was used to analyze count data obtained from RNASeq (Table 4.3). Genes were considered to be significantly different if their expression was either up-regulated or down-regulated in response to iron (fold-change >1.5, adjusted p-value <0.05). Negative fold changes in red represent genes that were significantly down-regulated in response to iron depletion, whereas positive fold changes in blue represent genes that were significantly up-regulated in response to iron depletion. Genes with chronological cluster ID numbers represent potential loci and are separated into sections, such as the iron-sulfur cluster assembly locus (cluster IDs 311-314). Genes that were significantly down-regulated in response to iron-depleted media include the iron storage protein ferritin (cluster ID 37) and superoxide dismutase *sodB* that uses iron as a cofactor (cluster ID 470). The down-regulation of these iron-dependent genes serve as an internal validation. Genes that were significantly up-regulated in response to iron-depleted media include the Ent locus (cluster IDs 1883-1886), an iron-sulfur cluster assembly locus (cluster IDs 311-314), a TonB-dependent outer membrane ferric coprogen receptor *fitA* (cluster ID 348), a catecholate siderophore receptor *fiu* locus (cluster IDs 1190-1191), and a hemin transport system (cluster IDs 4314-4318). TPM values show up-regulation of *fitA* and *fiu* by ST258 isolates in response to iron-depletion (Figure 4.3). The genes identified in Table 4.3 represent genes that are regulated by the absence of iron in media by all ST258 isolates.

Table 4.3: Genes that are significantly down-regulated (negative fold change) or up-regulated (positive fold change) among all ST258 isolates upon iron depletion.

Cluster ID	Gene Name	Fold Change	P value	Adjusted P value
37	Ferritin	-2.17	6.88E-06	1.45E-03
70	zinc ABC transporter substrate-binding protein	-1.56	9.87E-08	5.76E-05
311	Iron-sulfur cluster assembly protein sufA	2.06	8.73E-07	3.40E-04
312	cysteine desulfurase	1.99	1.02E-06	3.41E-04
313	feS assembly ATPase SufC	1.67	4.70E-05	5.48E-03
314	feS assembly protein SufD	1.76	7.44E-06	1.45E-03
348	TonB-dependent outer membrane ferric coprogen receptor FitA	1.98	4.93E-06	1.20E-03
470	sodB	-2.25	3.79E-07	1.77E-04
1190	Catecholate siderophore receptor Fiu	1.87	1.95E-03	7.84E-02
1191	Iron-uptake factor	1.81	1.97E-04	1.53E-02
1883	entA	1.68	8.74E-05	9.27E-03
1884	Isochorismatase	1.53	1.14E-03	5.50E-02
1885	2,3-dihydroxybenzoate-AMP ligase	1.59	9.44E-04	4.79E-02
1886	isochorismate synthase	1.60	6.84E-04	3.55E-02
1896	Enterobactin synthase EntD component	1.53	5.16E-04	2.87E-02
1963	TonB-dependent receptor	1.64	2.46E-03	8.92E-02
1964	hypothetical protein	1.60	2.01E-03	7.84E-02
2074	ribosomal protein L31	-2.40	1.43E-08	1.11E-05
2554	hypothetical protein	1.68	6.43E-04	3.41E-02
3145	Putative exported protein	-1.65	5.13E-06	1.20E-03
4314	Hemin transport system ATP-binding protein hmuV	2.30	3.15E-04	1.99E-02
4315	Hemin transport system permease protein hmuU	2.03	1.74E-03	7.26E-02
4316	Hemin-binding periplasmic protein hmuT precursor	2.11	1.33E-03	5.86E-02
4317	hemin transporter	1.95	2.84E-03	9.63E-02
4318	TonB-dependent receptor	1.96	1.26E-03	5.67E-02
4396	ribonucleoside-diphosphate reductase subunit beta nrdF2	1.59	1.80E-05	2.45E-03
4397	Ribonucleoside-diphosphate reductase alpha chain	1.59	2.10E-05	2.58E-03
4398	nrdI protein	1.92	3.26E-06	9.51E-04
4399	Glutaredoxin	1.79	1.89E-05	2.45E-03
4459	Sulfite reductase [nadph] flavoprotein alpha-component	2.63	1.23E-08	1.11E-05

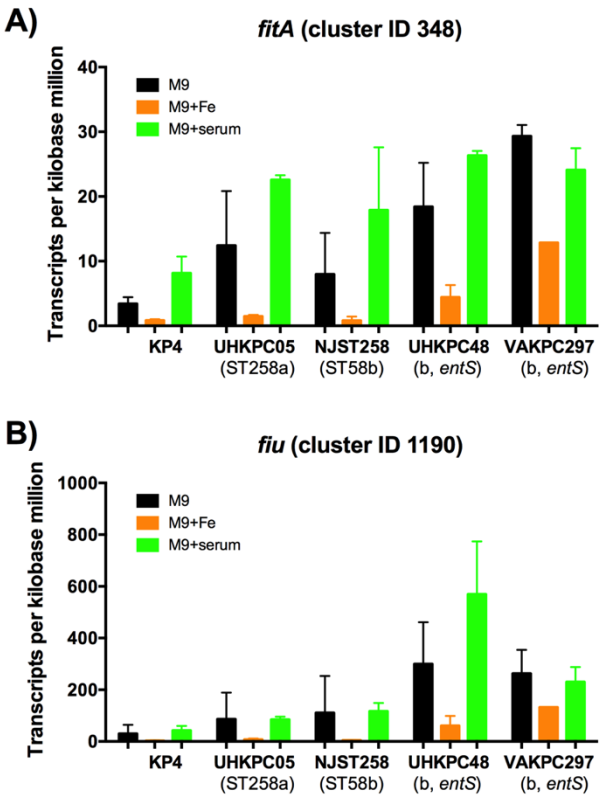

Figure 4.3: TPM values for each isolate illustrate up-regulation of fitA and fiu by ST258 isolates in M9/Chelex.

TPM values for each isolate were analyzed. The genes fitA (A) and fiu (B) were significantly upregulated by ST258 strains in M9/Chelex compared to M9/Chelex+Fe. Data were analyzed using the DESeq2 package in R.

To identify genes in *entS*+ and *entS*- isolates that were significantly modulated in response to M9/Chelex+serum, the DESeq2 package in R was used to analyze count data obtained from RNASeq (Table 4.4). The transcriptional response in M9/Chelex+serum was examined to identify genes that were differentially expressed in a physiologically relevant, iron-deplete condition. Genes were considered to be significantly different if their expression was either up-regulated or down-regulated when comparing between *entS*+ and *entS*- isolates (fold-change >1.5, adjusted p-value <0.05). Negative fold changes in red represent genes that were significantly up-regulated by *entS*- isolates in response to M9/Chelex+serum, whereas positive fold changes in blue represent genes that were significantly up-regulated by *entS*+ isolates in response to M9/Chelex+serum. Genes with chronological cluster ID numbers represent potential loci and are separated into sections, such as the nickel transport locus (cluster IDs 3521-3525). Genes that were significantly up-regulated by *entS*- isolates in response to iron-depleted medium include the β-lactamase locus (cluster IDs 877-879) and the hemin transporter *hmuS* (cluster ID 4317). Genes that were significantly up-regulated by *entS*+ isolates in response to iron-depleted medium include the *entS* transporter (cluster ID 1888) and the penicillin-binding protein 1C (cluster ID 4533). Upregulation of *entS* by the *entS*+ isolates also serves as internal validation of the analysis.

Although the aforementioned genes were significantly modulated in response to M9/Chelex+serum, the pattern of regulation was different between each genes. To further examine the regulation of these genes in

M9/Chelex+serum, TPM values were graphed (Figure 4.4). The β-lactamase gene (cluster ID 877) was up-regulated by the *entS*-deficient strains UHKPC48 and VAKPC297 in all media (Figure 4.4A). The hemin transporter *hmuS* was up-regulated in M9/Chelex+serum by the *entS*-deficient strains UHKPC48 and VAKPC297 (Figure 4.4B). This gene was also significantly upregulated by ST258 isolates in M9/Chelex when compared to M9/Chelex+Fe (Table 4.3). As internal validation, *entS* gene expression was down-regulated in M9/Chelex+serum by the *entS*-deficient strains UHKPC48 and VAKPC297 (Figure 4.4C). These data illustrate the patterns of gene expression by *entS*+ and *entS*- strains in response to M9/Chelex+serum.

Table 4.4: Genes that are differentially expressed by entS-deficient isolates (negative fold change) or full-length entS isolates (positive fold change) in iron-depleted medium, M9/Chelex+serum.

Cluster ID	Gene Name	Fold Change	P value	Adjusted P value
500	Electron transport complex protein rnfC	5.24	2.10E-28	1.88E-25
694	DNA-binding helix-turn-helix protein	3.10	1.36E-17	6.98E-15
877	beta-lactamase	-5.40	2.25E-153	8.10E-150
878	deoR C terminal sensor domain protein	-5.25	3.93E-130	7.06E-127
879	D-beta-hydroxybutyrate dehydrogenase	-1.76	1.16E-04	1.10E-02
1203	cell division activator CedA	2.10	8.76E-09	2.25E-06
1279	L-asparaginase	1.52	6.78E-06	9.02E-04
1390	hypothetical protein	1.55	2.56E-06	3.84E-04
1539	Cell division protein ftsK	1.69	1.83E-25	1.32E-22
1672	hypothetical protein	1.71	2.16E-03	9.81E-02
1888	entS MFS transporter	2.30	1.13E-08	2.72E-06
2181	hypothetical protein	2.26	1.95E-11	8.77E-09
2305	outer membrane lipoprotein	1.57	2.10E-08	4.44E-06
2513	Proline/betaine transporter	1.64	3.99E-04	2.89E-02
2901	phnA family protein	1.51	6.31E-09	1.74E-06
3166	regulator of ribonuclease activity A	1.75	1.62E-06	2.65E-04
3328	hypothetical protein	2.73	1.61E-09	4.82E-07
3399	ribosomal protein L28	3.01	1.08E-09	3.54E-07
3521	nickel-responsive transcriptional regulator NikR	2.04	6.60E-07	1.13E-04
3522	Nickel transport ATP-binding protein nikE	1.94	2.83E-07	5.08E-05
3524	Nickel transport system permease protein nikC	1.74	1.05E-04	1.03E-02
3525	Nickel transport system permease protein nikB	1.60	1.59E-04	1.40E-02
3540	sirA-like family protein	2.09	2.17E-06	3.39E-04
3654	translation elongation factor Tu	4.29	4.01E-68	4.80E-65
3729	hypothetical protein	1.98	4.31E-04	2.98E-02
3897	urease accessory protein UreF	1.59	3.09E-06	4.44E-04
4033	yecA family protein	1.94	2.98E-11	1.19E-08
4109	arsenical pump membrane protein	2.31	1.45E-07	2.74E-05
4243	gcvA transcriptional dual regulator	1.64	3.25E-05	3.77E-03
4266	sdaC serine STP transporter	1.74	2.70E-04	2.16E-02
4270	tRNA pseudouridine synthase C family protein	1.81	8.76E-04	5.44E-02
4317	hemin transporter	-1.71	1.23E-03	7.14E-02
4379	global regulator family protein	2.95	9.09E-11	3.27E-08
4533	Penicillin-binding protein 1C	2.94	2.84E-18	1.70E-15

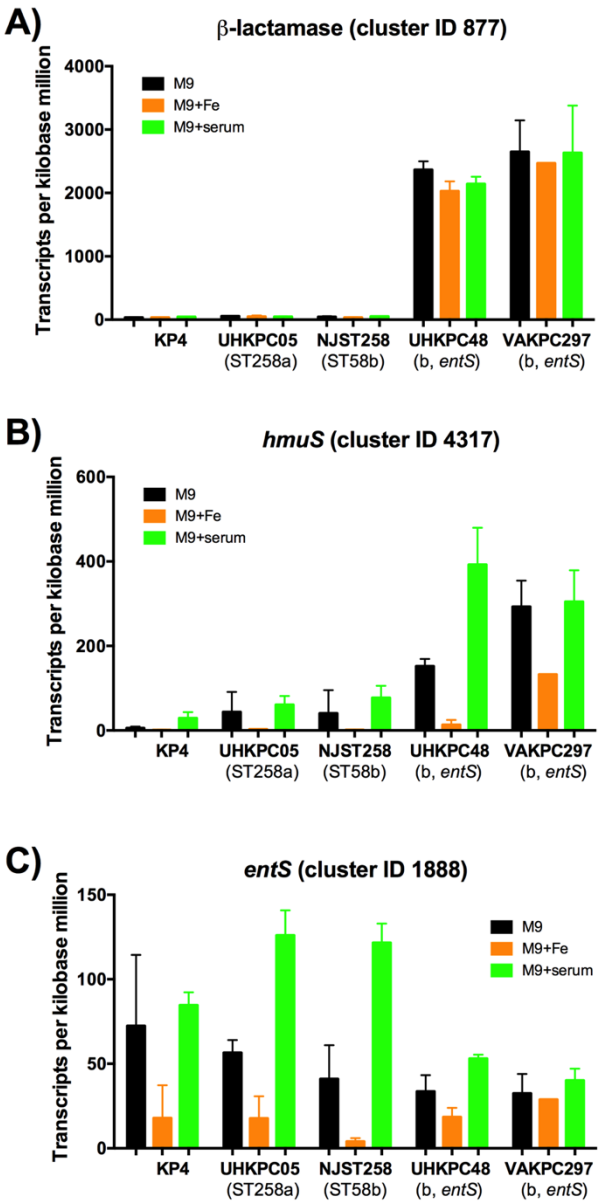

Figure 4.4: TPM values for each isolate illustrate gene regulation of β-lactamase, hmuS, and entS in M9/Chelex+serum.

TPM values for each isolate were analyzed. The β-lactamase gene (A) was significantly up-regulated in all media by entS-deficient isolates. The hemin transporter hmuS (B) was up-regulated by entS-deficient isolates in iron-depleted conditions, including M9/Chelex and M9/Chelex+serum. The Ent exporter entS (C) was down-regulated by entS-deficient isolates in M9/Chelex+serum. Data were analyzed using the DESeq2 package in R.

4.2.3 ST258 strains secrete iron-chelating molecules and catechols and are inhibited by Lcn2

To further characterize the relationship between iron and ST258 strains of *K. pneumoniae*, *in vitro* assays examining the secretion of iron-chelating molecules were performed. The CAS assay was used to detect iron-chelating molecules presence in bacterial culture [202]. Bacterial strains were cultured overnight in M9 medium, supernatants were filter sterilized, and bacteria-free supernatants were subjected to the CAS assay. Supernatants from all strains, except VAKPC297, secreted significantly more iron-chelating molecules as compared to KP7, the siderophore-negative control strain (Figure 4.5). Comparatively, UHKPC48 secreted significantly more iron-chelating molecules than KP7 despite containing a deletion in *entS*. A second *entS*-deficient strain, DMC0526, was also used. Similar to UHKPC48, DMC0526 secreted significant iron-chelating molecules. Strains of *E. coli* deficient in *entS* have been shown to secrete 2,3-dihydroxybenzoylserine, a component of Ent [16]. To determine if the CAS assay was identifying breakdown products of Ent, such as 2,3-dihydroxybenzoic acid (2,3-DHBA), 2,3-DHBA was assayed for iron-chelating ability. However, 2,3-DHBA did not induce a change in absorbance, indicating that it is not active in the CAS assay. Therefore it is still unknown whether strains are secreting 2,3-dihydroxybenzoylserine or 2,3-DHBA, which could account for the chelation of iron by these isolates.

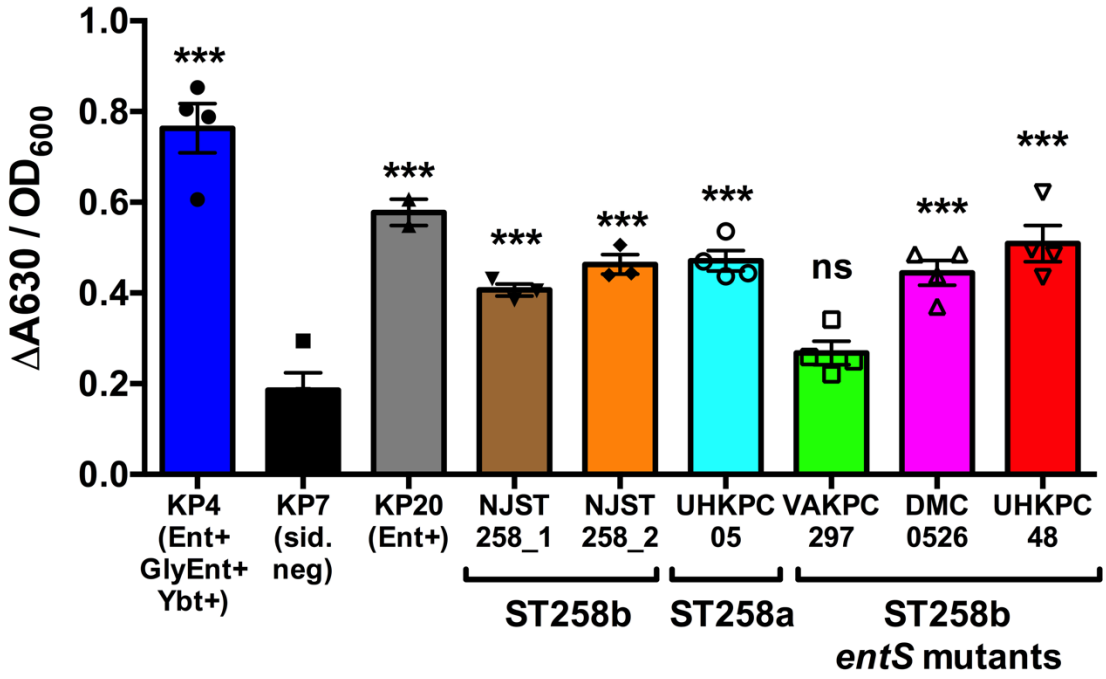

Figure 4.5: ST258a and entS-deficient ST258b strains, except VAKPC297, secrete iron-chelating molecules.

*To measure the relative concentration of iron-chelating molecules secreted by each strain, the CAS assay was performed. Bacteria were cultured overnight in M9 medium, the OD_{600} of each culture was read, and cultures were spun through a 0.2-micron filter tube to acquire bacteria-free supernatants. Supernatants were subjected to the CAS assay and the change in absorbance at 630 nm (ΔA630) was calculated. ΔA630 was normalized for bacterial growth using the OD_{600} for each strain. Data were analyzed using one-way ANOVA with Fisher's post-test (ns, $p>0.05$; ***, $p<0.0001$; compared to KP7).*

Whereas the CAS assay detects general iron-chelating molecules, the Arnow assay is able to detect catechols, such as Ent. To determine if ST258b strains secrete catechols, the Arnow assay was performed on bacteria-free culture supernatants. As expected, KP4 ($Ent^+Ybt^+Sal^+$) and KP20 (Ent^+) secreted significantly more catechols compared to KP7, the siderophore-negative strain (Figure 4.6). As stated above, DMC0526 was included to compare results between UHKPC48 and VAKPC297. NJST258_2, UHKPC05, DMC0526, and UHKPC48 all secreted significant amounts of catechols. NJST258_1 did not secrete significantly more catechols compared to KP7 despite secreting significantly more iron-chelating molecules (Figure 4.5). Consistent with CAS assay results, VAKPC297 also did not secrete significantly more catechols than KP7. These results indicate that ST258a and some ST258b strains are secreting iron-chelating molecules and catechols, despite the *entS* deletion in DMC0526 and UHKPC48.

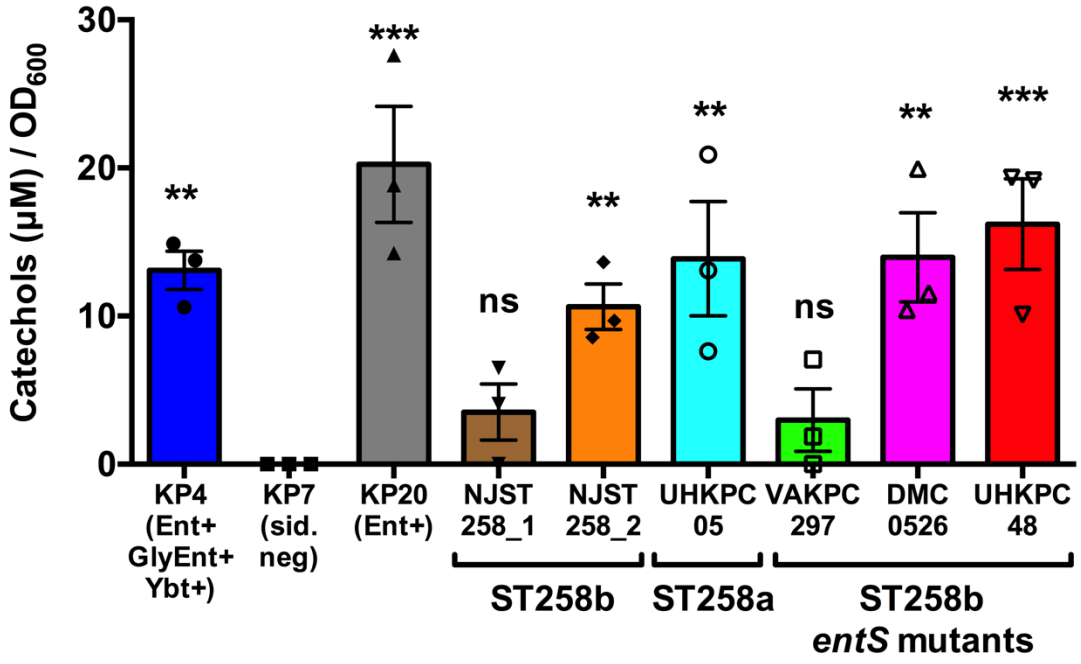

Figure 4.6: ST258a and entS-deficient ST258b strains, except VAKPC297, secrete catechols.

*To measure the concentration of catechols secreted by each strain, the Arnow assay was performed. Bacteria were cultured overnight in M9 medium, the OD_{600} of each culture was read, and cultures were spun through a 0.2-micron filter tube to acquire bacteria-free supernatants. Supernatants were subjected to the Arnow assay and the absorbance at 510 nm was calculated. A standard curve of 2,3-dihydroxybenzoic acid (2,3-DHBA) was used to determine catechol concentrations. Concentrations were normalized for bacterial growth using the OD_{600} for each strain. Data were analyzed using one-way ANOVA with Fisher's post-test (ns, $p<0.05$; **, $p>0.01$; ***, $p<0.001$; compared to KP7).*

Because the Arnow assay detects the presence of catechols, we hypothesized that ST258 strains, including *entS* ST258b strains, were releasing Ent. This Ent release, whether through an active exporter or another indirect method, could promote growth in iron-limited conditions. To examine this hypothesis, bacteria were examined using the serum growth assay. The serum growth assay examines the ability of bacteria to grow in serum, which is an iron-limiting condition due to the presence of transferrin as described above [15]. To measure growth that is attributable to Ent, the medium was supplemented with Lcn2, an innate immune protein secreted by host epithelial cells and neutrophils that specifically binds to and sequesters Ent [19]. KP4 that secretes multiple siderophores is not inhibited by the presence of Lcn2, whereas KP20 (Ent+) is inhibited by Lcn2 (Figure 4.7). The siderophore-negative mutant grows poorly regardless of Lcn2, consistent with 10% serum being a siderophore-dependent growth condition. Lcn2 inhibited growth of all ST258 strains, including the EntS deletion mutants. In particular, VAKPC297 growth was inhibited by Lcn2, which is in contrast with the lack of detectable iron-chelating molecules and catechols as illustrated by the CAS and Arnow assays. Because sequestration of Ent is the only known mechanism of growth inhibition by Lcn2, VAKPC297 could be secreting small amounts of Ent that are sufficient to promote growth. These results indicate that ST258 strains are able to grow in iron-limiting conditions, but that the host protein Lcn2 can inhibit the strains' mechanism of iron-acquisition.

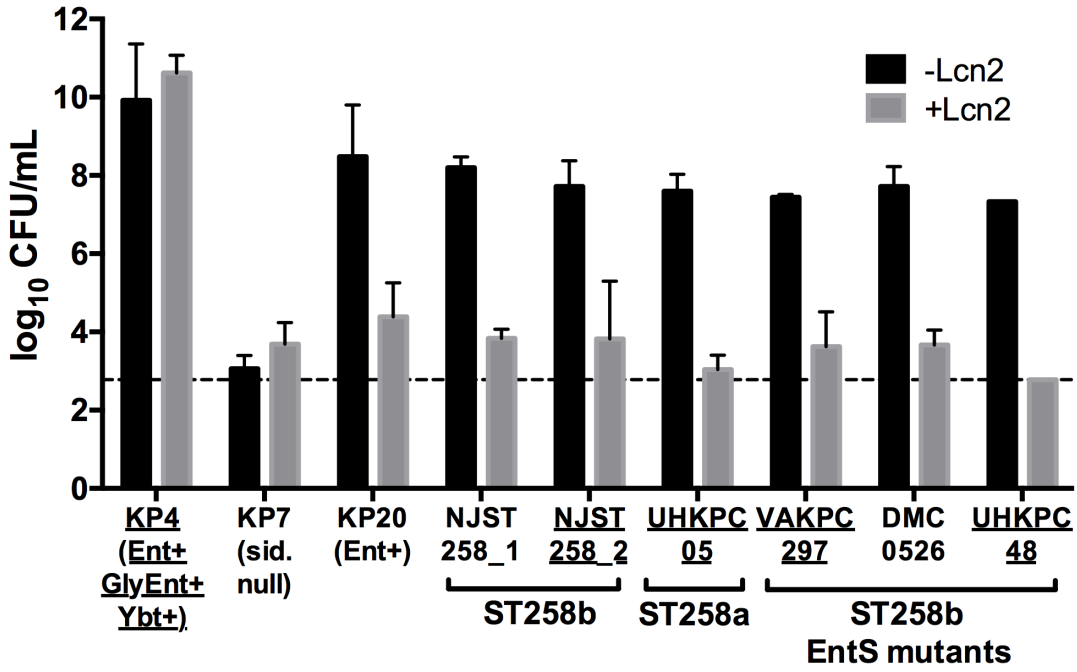

Figure 4.7: ST258 strains' growth in serum is inhibited in the presence of Lcn2.

To determine the ability of strains to grow in iron-limiting conditions, the Lcn2 growth assay was performed. Strains were cultured in LB overnight and plated in a 96-well plate with 10% serum in RPMI, with or without 5 μM Lcn2. Following an overnight incubation bacteria were plated for CFU. All clinical strains were able to cultured in the presence of serum, an iron-limiting condition, and showed susceptibility to Lcn2. Underlined strains were used in the RNASeq.

4.2.4 RNASeq analysis identifies transcript expression differences between UHKPC48 and VAKPC297

Although extremely similar genetically, UHKPC48 secreted significant amounts of iron-chelating molecules and catechols, despite its deletion in *entS*, whereas VAKPC297 did not (Figures 4.5 and 4.6). It was hypothesized that these differences may be due to an alternate exporter, which could be identified by comparing transcript expression patterns between the two isolates. To identify iron-dependent differences between these strains, an additional DESeq2 analysis was performed to compare transcript expression between UHKPC48 and VAKPC297 in iron-depleted conditions (Table 4.5). Negative fold changes in red represent genes that were significantly up-regulated by VAKPC297 isolates in response to iron depletion, whereas positive fold-changes in blue represent genes that were significantly up-regulated by UHKPC48 isolates. Genes with chronological cluster ID numbers represent potential operons and are separated into sections, such as the maltose receptor locus (cluster IDs 2985-2988). Genes significantly up-regulated by VAKPC297 in response to iron-depleted medium include an lrgB-like family protein (cluster ID 4813) and the tellurite resistance gene *tehB* (cluster ID 526). These data identify genes that are differentially regulated between UHKPC48 and VAKPC297. However, this analysis did not identify putative transporters for iron acquisition by VAKPC297 compared to UHKPC48.

Table 4.5: Genes that are differentially expressed by VAKPC297 (negative fold change) and UHKPC48 (positive fold change) in iron-depleted media.

Cluster ID	Gene Name	Fold Change	P value	Adjusted P value
128	hypothetical protein	-5.92	9.72E-42	1.32E-38
525	C4-dicarboxylate transporter/malic acid transport family protein	-1.77	9.31E-05	9.48E-03
526	Tellurite resistance protein tehB	-1.63	5.09E-06	7.41E-04
1009	hypothetical protein	-2.77	2.80E-08	7.13E-06
1181	Glycerate dehydrogenase	1.83	5.80E-04	4.32E-02
1293	hypothetical protein	1.84	2.85E-05	3.14E-03
1517	Hypothetical protein	-2.04	2.38E-07	5.11E-05
1727	hypothetical protein	3.03	1.16E-10	3.38E-08
1728	hypothetical protein	2.56	1.34E-07	3.04E-05
1729	regulator of acid resistance, influenced by indole	1.91	1.39E-04	1.29E-02
1944	beta-lactamase	1.90	2.41E-04	2.15E-02
2306	hypothetical protein	-4.56	1.17E-24	5.30E-22
2985	phage lambda receptor protein maltose high-affinity receptor	1.56	4.03E-04	3.35E-02
2986	malK	2.40	2.01E-05	2.36E-03
2988	malE	2.19	5.84E-06	8.21E-04
3635	CRP transcriptional dual regulator	-2.72	1.26E-14	4.28E-12
3790	phosphoglucosamine mutase	-5.03	2.79E-30	1.63E-27
3987	putative inner membrane protein	-3.38	2.56E-23	9.50E-21
4174	aldo/keto reductase family protein	-4.45	6.57E-37	4.46E-34
4233	cobalamin biosynthesis protein CbiQ	-2.78	1.07E-06	2.08E-04
4764	magnesium transporter	-1.89	3.29E-06	4.96E-04
4812	Cytidine deaminase	-5.40	6.47E-39	6.59E-36
4813	IrgB-like family protein	-2.37	5.58E-13	1.75E-10
4914	imidazole glycerol phosphate synthase, glutamineamidotransferase subunit	-1.58	2.51E-07	5.12E-05
4916	Histidinol-phosphate aminotransferase	-1.94	8.73E-08	2.09E-05
4917	Histidinol dehydrogenase	-6.21	1.05E-55	4.30E-52
5470	RND transporter, HAE1 family	-4.57	2.65E-38	2.16E-35
5471	Ribosomal-protein-serine acetyltransferase	-3.97	4.39E-26	2.24E-23
6023	ribonuclease P protein component	-2.80	3.40E-10	9.25E-08
6061	RES domain protein	-3.09	1.58E-24	6.43E-22
6249	putative membrane protein	-1.73	2.03E-05	2.36E-03

4.3 Discussion

4.3.1 Summary of findings

CR *K. pneumoniae* is resistant to all or nearly all antibiotics and represents a major healthcare concern [198]. One CR MLST type in particular, ST258, has disseminated worldwide. Previous studies have identified epidemiologic and genomic differences between two prevalent ST258 clades, clade ST258a and ST258b, including a 97 bp deletion in the Ent exporter *entS* [92, 201]. To further understand CR *K. pneumoniae* response to iron, we performed RNASeq in iron-depleted and iron-replete conditions to identify transcriptional differences. We identify potential mechanisms of iron-acquisition by CR *K. pneumoniae*: the hemin transport operon that has not been characterized previously in *K. pneumoniae*; a TonB-dependent outer membrane ferric coprogen receptor; and a catcholate receptor. Additionally, we characterized the growth patterns and secretion of iron-chelating molecules during iron-limiting conditions. We found that both ST258a and ST258b isolates could grow under iron-limiting conditions and secrete iron-chelating molecules, despite a deletion in *entS* in the ST258b isolates. However, VAKPC297, an *entS* ST258b isolate, was unable to secrete iron-chelating molecules. Further RNASeq analysis identified genes that were differentially expressed in response to iron-deplete conditions by UHKPC48 and VAKPC297, including the up-regulation of tellurite resistance genes by VAKPC297. These findings aid in the characterization of CR *K. pneumoniae* response to iron limitation and identify novel compensatory mechanisms by which CR *K. pneumoniae* acquires iron during infection.

4.3.2 Potential novel iron acquisition mechanisms

Data analysis from the RNASeq results identified multiple genes that were differentially regulated when all strains were compared for their transcriptional responses to iron (Table 4.3). Of particular interest is the upregulation of the hemin transport operon, which was shown to be up-regulated by all ST258 isolates in response to iron-depleted conditions. Additionally, it was shown to be significantly upregulated by *entS*- isolates compared to *entS*+ isolates in M9/Chelex+serum (Table 4.4). Previously uncharacterized in *K. pneumoniae*, the hemin transport operon can be used by Gram-negatives including *Yersinia enterocolitica* to acquire iron [203]. Acquisition of a siderophore-independent iron uptake system such as the hemin transport operon would allow ST258 isolates, especially *entS*-deficient isolates, to acquire iron during infection. Another gene of interest that was up-regulated by ST258 isolates upon iron-depletion is a TonB-dependent outer membrane ferric coprogen receptor FitA (Table 4.3). Within *E. coli*, the *fit* operon was found to be an iron acquisition mechanism commonly found in human pathogenic, but not commensal, clinical isolates [204]. The substrate for the *fit* operon is yet uncharacterized, however, Ent is not the substrate [204, 205]. The *fit* operon represents a mechanism by which ST258 isolates can acquire iron in an Ent-independent manner. A third gene locus of interest that was upregulated in response to iron-depleted conditions by ST258 isolates is the catecholate receptor Fiu (Table 4.3). The outer membrane receptor Fiu has been hypothesized to mediate uptake of hydrolytic products of Ent, such as 2,3-DHBA [206, 207]. It is possible that ST258 isolates, particularly

ST258b isolates that are deficient in *entS*, utilize Fiu to scavenge for and uptake hydrolytic products of Ent which may have been secreted through mechanisms other than the dedicated Ent exporter. This would be consistent with prior work illustrated that *entS* mutants in *E. coli* secrete 2,3-dihydroxybenzoylserine, a compound extremely similar to 2,3-DHBA [16]. Additionally, the secretion of this compound would be consistent with all *in vitro* phenotypes illustrated above. Together, these three genes/loci represent potential novel iron acquisition mechanisms utilized by ST258 isolates during infection. These RNASeq results must be verified by PCR and functional assays to determine if they are novel mechanisms that CR *K. pneumoniae* up-regulate to scavenge iron from its host environment during infection.

4.3.3 Secretion of iron-chelating molecules by ST258b isolates

In vitro characterization of the ST258 isolates identified interesting patterns of iron-chelating molecule secretion and growth in iron-limiting environments. Most surprising was the ability of ST258b isolates UHKPC48 and DMC0526 to secrete catechols despite encoding a deletion in *entS* (Figure 4.6). Inhibition of bacterial growth by Lcn2 in the serum growth assay also suggests that the secreted product is Ent. Additionally, it was interesting that NJST258_2 supernatants caused a change in the absorbance of the CAS assay but did not secrete catechols as detected by the Arnow assay (Figure 4.5 and 4.6). Mass spectrometry must be performed to definitively identify the iron-chelating molecules secreted by these isolates.

4.3.4 Differential gene expression between VAKPC297 and UHKPC48 may explain phenotypic differences

Although two ST258b strains deficient in *entS*, UHKPC48 and DMC0526, secreted iron-chelating molecules and catechols, one ST258b strain, VAKPC297, did not (Figure 4.5 and 4.6). This result is very surprising considering the extremely limited genetic differences between the two strains. To identify potential mechanisms of iron acquisition that differ between these strains, further RNASeq analysis was performed (Table 4.5). This analysis identified many genes that were differentially expressed in both M9/Chelex and M9/Chelex+serum. Overall, no genes identified by this analysis represent an obvious mechanism of regulation to explain the phenotypic differences. However, a few genes identified by this analysis are interesting and could warrant further examination. One potential locus that was strongly expressed by VAKPC297 in response to all media is a cytidine deaminase and a lrgB-like protein that is a murein hydrolyase. Murein hydrolases specifically cleave cell wall components within bacteria and are involved in cell growth and division as well as bacteria autolysis [208]. However, *lrgB* has specifically been shown to inhibit murein hydrolases that cleave cell wall components and promote tolerance to penicillin in *S. aureus* [208]. This gene could be up-regulated by VAKPC297 in order to prevent autolysis and bacterial death in all conditions. *In vitro* experiments and further analysis could potentially identify the gene or protein responsible for the differences responsible for the discrepancies in iron-chelating molecule secretion between VAKPC297 and UHKPC48.

4.3.5 Conclusion

In conclusion, we have identified potential novel and Ent-independent mechanisms for iron acquisition by CR *K. pneumoniae* clinical isolates, including the hemin transport operon, a ferric coprogen receptor *fitA*, and a catecholate receptor *fiu*. Furthermore, we have characterized the response of these isolates to iron-limiting conditions, including growth in serum, and determined their ability to secrete iron-chelating molecules as well as catechols. Finally, we have identified genes that are differentially regulated between UHKPC48 and VAKPC297, two *entS* deletion mutants that were found to have phenotypic differences in iron-chelation molecule and catechol secretion despite their genetic similarities. These genes may represent potential mechanisms to examine in an attempt to understand the phenotypic differences illustrated by the *in vitro* assays performed here. Together these results further the understanding of iron acquisition and pathogenesis during infection with CR *K. pneumoniae*. Future work can validate the novel iron acquisition pathways used by these isolates, which may provide potential therapeutic targets for infection with these antibiotic-resistant strains.

4.4 Experimental Procedures

Bacterial strains and media. Lab strains of *K. pneumoniae,* KP4, KP7, and KP20, have been previously described [96]. NJST258_1 and NJST258_2 were gifts from Dr. Barry Kreiswirth. ST258 strains of *K. pneumoniae*, UHKPC48,

DMCO526, UHKPC05, and VAKPC297, were isolated from Midwestern hospitals and have been described epidemiologically [201] and genetically [92].

As noted, bacterial strains were cultured in LB or M9 minimal media with and without additional supplementation. M9 minimal salts were diluted and prepared as described (ThermoFisher). To create iron-depleted medium, M9 was treated with Chelex 100 Resin for 1 hour at room temperature (Biorad). Following Chelex treatment, M9 was supplemented with D-glucose Sigma, $MgSO_4$, and $CaCl_2$ ("M9/Chelex", Sigma). M9/Chelex was supplemented with 100 μM Fe_2SO_4 or 5% heat-inactivated (HI) human serum ("M9/Chelex+Fe" or "M9/Chelex+serum", Sigma) where indicated.

Growth curves. Growth curves were performed as previously described [96].

Bacterial growth for RNASeq. Strains were cultured in duplicate overnight in LB broth and subcultured 1:100 into fresh LB until bacterial growth reached mid-log phase. At OD_{600}=~0.3, bacteria were plated for CFU and 10^8 bacterial were reserved as an initial RNA sample, though were not utilized in this RNASeq study. Additionally, bacteria were subcultured 1:10 from the mid-log LB culture into M9/Chelex, M9/Chelex+Fe, or M9/Chelex+serum in duplicate. Following 1 hour incubation, OD_{600} for each sample was read, samples were plated for CFU, and 2 aliquots of 10^8 bacteria were preserved into 2x volumes of RNAprotect Bacteria Reagent (QIAGEN). Additionally, 2 mL of bacterial culture was reserved for DNA isolation. Samples were frozen at -80°C until RNA was isolated.

RNA isolation and RNASeq. Samples were resuspended with 500 µL ice cold sterile DPBS to remove RNAprotect bacterial reagent. Samples were spun for 10 minutes at 10,000 RPM to repellet bacteria. RNA was isolated from 10^8 CFU bacteria using the MagJET RNA Purification kit (ThermoFisher) and then treated with an additional DNAse treatment. rRNA was depleted using Ribo-Zero (Illumina). Directional RNASeq library was constructed using PrepX RNA-Seq for Illumina library kit (Wafergen), which was then quantified and normalized using qPCR. Samples were sequenced using Illumina NextSeq 500 mid output kit (paired-end 75bp), and reads were mapped as paired-end to each respective genome using CLC. For each gene, raw counts and transcripts per million (TPM) values were calculated. Orthologs in each genome were identified using PanOCT to enable gene expression comparisons across genomes [209]. Differential expression analysis was conducted using DESeq2 package in R.

CAS Assay. The CAS assay was performed as previously described to determine iron-chelating capabilities of bacterial supernatants [152]. Briefly, bacteria were inoculated into M9 medium overnight. OD_{600} readings were taken, and bacteria cultures were spun through at 0.2 micron filter to remove bacteria. Supernatants were subjected to the CAS assay, and the change in absorbance at 630 nm was read. Results are expressed in $\Delta A630/OD_{600}$ for each culture to normalize for differences in bacterial growth.

Arnow Assay. The Arnow assay was performed as previously described to determine the secretion of catechols in bacterial cultures [210]. Briefly, cultures were cultured overnight in M9 medium, OD_{600} was read, and bacteria-free supernatants were acquired using 0.2 micro filters. Catechols were measured by creating an equal mix of sample, 0.5 N HCl, Nitrite-Molybdate Reagent (10% w/v of sodium nitrate and sodium molybdate), and 1 N NaOH. Absorbance was read at 510 nm, and samples were normalized for bacterial growth using the OD_{600} of each culture.

Lcn2 Growth Assay. The Lcn2 growth assay was performed as previously described [13].

Data analysis. Statistical analysis for *in vitro* assays was performed using GraphPad Prism. RNASeq results were analyzed using the DESeq2 in R.

4.5 Notes

VI Holden designed and performed experiments, analyzed data, and wrote the chapter; MS Wright and MD Adams performed RNASeq and DESeq2 analysis; and MA Bachman designed experiments, analyzed data, and proofread the chapter.

CHAPTER V

DISCUSSION

5.1 Summary of Thesis

Bacteria utilize many virulence factors to cause infection within their hosts, including LPS, capsule, fimbriae, and siderophores [211, 212]. Siderophores are small molecules that chelate and deliver iron to bacteria. Recent research has identified novel, non-iron-delivery functions for siderophores during infection, as described in Chapter I. The focus of this thesis was to determine the host response to siderophore secretion upon infection with *K. pneumoniae*. The central hypothesis was that the secretion of siderophores by *K. pneumoniae* modulates host pathways, resulting in inflammation and bacterial dissemination. Chapter II addressed this hypothesis using *in vitro* stimulations of respiratory epithelial cells with purified siderophores and Lcn2. Chelation of cellular iron by purified siderophores in the presence of Lcn2 caused the secretion of IL-8, IL-6, and CCL20 from a human respiratory epithelial cells. Additionally, purified siderophores could stabilize the master transcription factor HIF-1α, potentially leading to the secretion of IL-6. This *in vitro* work helped frame the hypothesis that siderophores secreted by *K. pneumoniae* can cause inflammation and bacterial dissemination through HIF-1α stabilization during infection.

Chapter III examined the effects of siderophore secretion by *K. pneumoniae* in a murine pneumonia model. To study siderophore secretion independent of their ability to cause bacterial growth, a mutant in *tonB* was developed. Strains deficient in *tonB* could secrete siderophores but were unable to utilize them for growth. Using these mutants, it was determined that siderophore secretion during infection with *K. pneumoniae* induced IL-6, KC, and MIP-2 secretion, as well as bacterial dissemination to the spleen. Siderophore-dependent induction of bacterial dissemination to the spleen was shown to occur via HIF-1α stabilization within alveolar epithelial cells. The inflammation and dissemination during infection required the secretion of all three siderophores produced by the WT strain: Ent, Sal, and Ybt. These results supported and built upon the *in vitro* work that indicated that siderophores could cause a host immune response and stabilize HIF-1α.

Chapter IV examined the response to iron limitation in CR *K. pneumoniae* human isolates. Within a large cohort of CR *K. pneumoniae* isolates acquired from Midwestern US, a portion of the isolates has a deletion in the Ent exporter *entS*. RNASeq was used to identify the impact of the *entS* deletion on gene transcription in response to iron-replete and iron-depleted conditions. Potential novel mechanisms of iron acquisition, such as the hemin transport operon, were identified. These iron acquisition systems may represent mechanisms that CR *K. pneumoniae* use to avoid immune system activation via siderophore secretion. This possibility, as well as other implications of siderophore secretion by *K. pneumoniae*, will be considered within this chapter.

5.2 Depletion of cellular iron by siderophores

Chapter II illustrated that the lung epithelial cell response to siderophores is dependent on the ability of siderophores to deplete cellular iron. This was shown using the cellular iron homeostasis reporter *NDRG1* and calcein dye that fluoresces upon depletion of iron within a cell's labile iron pool (Figure 2.7). Whereas it was shown that siderophores deplete cellular iron, the mechanism by which siderophores acquire cellular iron was not explored further. It is unclear if Ent, Ybt, and Sal enter a cell to chelate cellular iron and, if so, by which mechanism these siderophores enter a cell. DFO has been shown to enter cancer cells by passing through the cellular membrane and chelating iron from the labile iron pool, rather than from ferritin [213-216]. In contrast, studies with *E. coli* producing Ent have shown that iron is acquired from transferrin and lactoferrin rather than the cellular iron pool [217]. A follow-up study utilizing strains of *E. coli* that secrete both Ent and Aer determined that Aer preferentially chelates cell-derived iron rather than transferrin-bound iron [63]. Performing these studies with purified siderophores would verify the source of iron chelated by siderophores, and rule out any possible interactions between additional secreted bacterial products and host cellular iron. It is possible that the source of iron can influence inflammatory potential of siderophores, such that chelation from cell-derived iron results in a strong pro-inflammatory response, whereas chelation of transferrin-bound iron does not. This could potentially explain the differences in inflammatory profiles between DFO, Ent, Ybt, and Sal. For example, treatment of A549s cells with Ent results in moderate secretion of IL-8

and IL-6, whereas Ybt treatment results in high secretion of IL-8, IL-6, and CCL20 (Figure 2.11). Differences in the source of iron from the host could translate to the different patterns of cytokine induction by each siderophore. Further work must be performed to determine the preferential iron source for each siderophore. Studies could then determine if the preferred iron source within the host correlates with the pattern of inflammatory cytokine secretion. This would determine if chelation of iron from certain sources is more inflammatory than others.

One situation in which siderophores are present within a cell is following the binding of Ent by Lcn2. During infection, Lcn2 binds Ent and FeEnt with subnanomolar affinity, preventing bacterial uptake of Ent and iron [19]. Following this binding, Lcn2 delivers Ent to epithelial cells, likely via one of its two putative outer membrane receptors, 24p3R and Megalin [45, 218, 219]. However, it is unclear what happens to Ent following uptake of Ent+Lcn2 and FeEnt+Lcn2 by epithelial cells. Though bound by Lcn2, it is possible that Ent could still chelate cellular iron, resulting in the induction of a host immune response [220]. It would be interesting to determine the mechanism by which Ent is degraded upon entry into a cell. Ent+Lcn2 appears to be taken up through endocytic intracellular sorting pathways, which may result in the degradation of Ent [45]. Alternately, Ent could be degraded in human cells by esterases, a mechanism that would be similar to its degradation by bacteria [221]. However, because Lcn2 cannot bind to Sal or Ybt, examining this mechanism would not provide any additional clarity in the mechanism of iron chelation by Lcn2-evasive siderophores. Overall,

determining the mechanisms by which siderophores acquire cellular iron and host cells degrade Ent would provide additional insight to the interactions between host and pathogen during infection.

5.3 Overall effect of siderophores during infection

The traditional function of siderophores as iron acquisition molecules positions siderophores as a virulence factor by promoting bacterial growth during infection. However, work described in this thesis has attributed the immune response and bacterial dissemination during infection to siderophore secretion by *K. pneumoniae.* Whereas iron acquisition by siderophores aids in productive infection, it seems that these non-iron-acquisition functions of siderophores are more detrimental than helpful to a bacterium. For instance, siderophores induce the secretion of IL-8, IL-6, and CCL20 secretion in an *in vitro* model with human epithelial cells, and IL-6, KC, and MIP-2 in an *in vivo* model of murine *K. pneumoniae* infection. Because the secretion of IL-6, KC, and MIP-2 in murine models of pneumonia are important for host defense against *K. pneumoniae* infection, the immune response is likely more beneficial to the host rather than to the microbe [178, 179]. Additionally, work described within this thesis identified that siderophores induce bacterial dissemination to the spleen. Because bacteria need to proliferate and infect new hosts to survive as a species, it is likely that bacterial dissemination due to siderophores may be an undesirable effect during infection to both the bacteria and the host. This is in contrast to the inflammatory immune response induced by siderophores, which is harmful to the bacteria but

beneficial to the host. Rather than simply acquiring iron for the bacteria, siderophores may alert the host to bacterial infection, potentially leading to an immune response. Acquiring additional mechanisms of iron acquisition that do not result in an immune response and host death may be advantageous for bacteria during lung infection, such as utilization of the hemin transport system as shown by ST258 isolates (Table 4.3).

Bacteria can inhabit many different niches within a host, some of which may be beneficial to the bacteria (adaptive), and some of which may not (maladaptive). Because *K. pneumoniae* cannot be transmitted through the air, the lung is maladaptive niche for this bacterial species and likely represents an evolutionary "dead end" for *K. pneumoniae* [222]. Whereas the effects of siderophores on the host during infection seem to be negative for bacteria when in this maladaptive niche, it is possible that siderophore secretion may be advantageous at other sites of infection. The intestinal tract represents an adaptive niche in which siderophores may aid in the colonization and spread of *K. pneumoniae* to new hosts. An example of this is intestinal colonization of *Salmonella enterica* serovar Typhiurium. Secretion of Sal allows *S. enterica* serovar Typhimurium to survive and colonize in the intestinal tract [86]. Additionally, an inflammatory immune response is important for pathogen colonization during infection with *S.* Typhimurium; without IL-22 secretion, *Salmonella* would not be able to colonize the intestinal tract [87]. It is possible that the secretion of multiple siderophores by *K. pneumoniae* could lead to an inflammatory immune response, allowing the bacteria to colonize the intestinal

tract, as illustrated by *S.* Typhimurium. Therefore, it is plausible that in other infection locations, the secretion of siderophores and the corresponding immune response may be of benefit to the microbe.

5.4 Iron acquisition by CR *K. pneumoniae*

Previously it has been shown that the combination of Ent+Lcn2 is bacteriostatic of bacteria. Additionally, we show here that siderophores are responsible for IL-6, KC, and MIP-2 secretion and bacterial dissemination to the spleen. Therefore, it was extremely interesting that an entire clade (ST258b) of CR *K. pneumoniae* with a deletion in the only identified Ent exporter, *entS*, was discovered [92]. Because Ent is the only siderophore encoded by these isolates, a deletion in *entS* would render this clade of *K. pneumoniae* incapable of secreting any siderophores. However, these strains could also be capable of avoiding the bacteriostatic effects of Lcn2. Phenotypic analysis of the ST258b *entS* mutants identified disparity between strains in their secretion of iron-chelating molecules that appear to be Ent. Two strains of *entS* mutants, UHKPC48 and DMC0526, were shown to secrete iron-chelating molecules and catechols at similar degrees as WT KP4 (Figure 4.3 and Figure 4.4). In contrast, VAKPC297 was shown to be unable to secrete iron-chelating molecules and catechols. It is unclear whether secretion of these molecules in the absence of the Ent exporter is common to most ST258b isolates, or if the majority of these isolates do not secrete iron-chelating molecules. If *entS* deletion mutants commonly secrete iron-chelating molecules, this could mean that these isolates have a second exporter for Ent.

This possibility has been previously hypothesized, however, a secondary exporter for Ent is yet to be identified [16]. It is also possible that VAKPC297 has evolved a mechanism by which to shut off Ent production. Ent is very costly to produce, and ST258b isolates that produce Ent without the exporter could be expending energy to produce a molecule which they cannot secrete. Rather, strains that do not produce or secrete Ent but can still uptake it as a "freeloader" would be at an advantage during infection due to the presence of additional bacterial species within the lung [223]. Phenotypic characterization of the remaining ST258 isolates could identify which pattern of iron-chelating molecule secretion is more common.

Instead of relying on the Ent exporter, ST258 isolates may have evolved to utilize other mechanisms of iron acquisition, such as the hemin transport operon, as described in Chapter IV. Because the secretion of siderophores by *K. pneumoniae* may have a negative effect for the bacteria, the inability to secrete Ent by these isolates may be advantageous. Rather than secrete siderophores, these bacteria may utilize other mechanisms of iron acquisition, potentially preventing the induction of an inflammatory immune response. Quantifying inflammatory proteins within the lungs during infection with CR *K. pneumoniae* could test this hypothesis. Additionally, the absence of Ent secretion could prevent bacterial dissemination to the spleen, which may be an undesirable outcome for bacteria, as described above. In fact, infection with ST258a (*entS*+) isolates were more likely to be found in the blood stream whereas ST258b isolates were more likely to be isolated from the urine, though this was not a

statistically significant difference ($p<0.135$) [201]. Infection with ST258a isolates was also more likely to result in a longer length of hospital stay than infection with ST258b isolates ($p<0.043$), perhaps indicating that infection with ST258a isolates is more severe than infection with ST258b isolates [201]. Investigating a larger cohort of ST258a and ST258b isolates may identify a statistically significant effect on infection localization and infection outcome. However, careful work would need to be done to attribute these differences to the absence of the Ent exporter rather than other genetic differences between the clades. This could be done by examining infection with ST258b strains that encode a full-length *entS* in relation to infection with ST258a strains that encode a full-length *entS*. These results could then be compared to differences in infection between ST258b strains with the *entS* deletion and infection by ST258a strains. Such comparisons could uncover differences in infection that are specific to *entS*-deletion mutants. Additionally, this hypothesis could be examined by creating mutants in *entS* in isogenic lab strains that secrete siderophores. This would allow for direct comparisons between strains that only differ in the *entS* gene, as ST258 isolates have additional genomic differences among the clades. These data could potentially support the hypothesis that CR *K. pneumoniae* have evolved to utilize mechanisms of iron acquisition other than siderophores to evade the host immune response and prevent death of the host.

5.5 Requirement for multiple siderophores

Chapter III illustrated that the secretion of individual siderophores was not sufficient to induce the inflammatory response and bacterial dissemination to the spleen (Figure 3.5). This is surprising and is in contrast with the prevalence of *K. pneumoniae* strains that secrete only one or two siderophores, commonly Ent and Ybt [13]. It is well accepted that bacteria secrete additional siderophores to evade the effects of Lcn2 sequestration of Ent [18, 43]. However, the lack of inflammation and dissemination induced by Ent was not due to Lcn2-mediated sequestration of Ent (Figure 3.7). Additionally, Ent in combination with Sal or Ybt was not sufficient to induce inflammation and dissemination, indicating that secretion of Ent, Sal, and Ybt were all required for the immune response and dissemination to the spleen. It is not clear why the production of multiple siderophores would be required for the maximal secretion of pro-inflammatory cytokines and bacterial dissemination. One could postulate that the variety of siderophores produced permits the targeting of multiple pathways, such as the UPR, HIF stabilization, and MAPK, that a single siderophore is not capable of activating on its own. The presence of many different siderophores may simply overwhelm host cells, leading to a complete inability to regulate the secretion of cytokines and prevent bacterial dissemination.

As stated above, the majority of *K. pneumoniae* strains secrete one or two siderophores; the secretion of Ent, Sal, and Ybt by a clinical isolate of *K. pneumoniae* is rare, though not unheard of [13]. However, secretion of multiple siderophores by *K. pneumoniae* is highly associated with hypervirulent strains

that cause invasive, community-acquired infections [224]. Other characteristics of hypervirulent strains include K1 or K2 capsule and the presence of *rmpA* that can up-regulated capsule production [224]. These strains cause highly invasive infections, including PLA, meningitis, and endopthalmitis [224]. The WT strain used in these studies, KPPR1, is a Rifampin-resistant derivative of a human clinical isolate with similar virulent gene contents to the invasive strains described above, and likely represents a hypervirulent strain of *K. pneumoniae* [225]. This strain may be hypervirulent due to its thick mucoid capsule or other virulence factors [149]. However, the secretion of Ent, Sal, and Ybt may also contribute to the hypervirulent phenotype induced in response to infection with this strain. Therefore, while not relevant to infection with strains that secrete one or two siderophores, the results presented within this thesis are crucial for understanding infection with hypervirulent strains of *K. pneumoniae* that secrete multiple siderophores and are likely to cause significant morbidity.

A fourth siderophore that is commonly secreted by many Gram-negative bacteria is Aer. Aer is associated with morbidity but is not secreted by KPPR1, and therefore was not examined within this thesis [94, 95]. Strains that carry Aer, such as NTUH-K2044, are becoming more prevalent in Asia and cause severe liver abscesses [95]. Whereas Aer is commonly encoded in *K. pneumoniae* strains in Asia, it is still relatively rare in the US [13]. It would be interesting to determine if Aer is sufficient to induce inflammation and dissemination on its own in our murine model of pneumonia, or if this response would require the secretion of additional siderophores. Because Aer is thought to acquire iron directly from

host tissues rather than from transferrin, it is possible that Aer may be inflammatory even in the absence of the secretion of multiple siderophores [63]. However, if multiple siderophores were required, it would be interesting to examine the combinations of siderophores that are necessary for the induction of inflammation and dissemination during *K. pneumoniae* infection.

5.6 Siderophores as therapies

Siderophores are secreted by many species of Gram-negative bacteria, including *Klebsiella spp*, *E. coli*, *Yersinia spp*, and *Salmonella spp* [150]. Because siderophores are conserved among many species and are pro-inflammatory, it is possible that they could serve as a vaccine component to combat infection. Effective vaccines must utilize components that are associated with pathogens rather than commensals, are expressed during infection, and are immunogenic [226]. Chapter III illustrated that siderophores could induce IL-6 secretion during murine pneumonia. IL-6 can aid in the growth and differentiation of adaptive immune cells such as B cells and T cells, both of which are important in an immune response to a vaccine [227]. Siderophore-dependent induction of IL-6 secretion may therefore aid in the induction of an adaptive immune response. For this reason, siderophores could represent a direct vaccine target, however they could also be used as an adjuvant due to their ability to induce an immune response. Although Ent is commonly secreted by pathogens and commensals, both Ybt and Sal are more highly associated with pathogens [13, 18]. Additionally, because multiple siderophores were required *in vivo* for the maximal

secretion of cytokines, it is possible that multiple siderophores must be included in the vaccine to induce an immune response. The presence of multiple siderophores would also increase the range of bacterial species against which the vaccine could be effective.

Purified siderophores may represent a potential vaccine component, however, an attenuated strain of bacteria that secretes siderophores could also be considered. One example of an attenuated, siderophore-secreting strain is the *tonB* mutants generated and examined within Chapter III of this thesis. These bacteria persist within the lung, secrete siderophores, induce an immune response, but do not grow. Additionally, a *tonB* mutant in a hypervirulent strain of *K. pneumoniae* that produces multiple siderophores, NTUH-K2044, can induce an immune response that is protective upon secondary infection with WT *K. pneumoniae* infection [93]. However, because siderophores can also induce bacterial dissemination to the spleen, careful work would need to be performed to examine *tonB* mutants as vaccine components. For the studies described within this thesis, an extremely high inoculum of 10^8 bacteria was used, and it is possible that a lower inoculum could induce an immune response without inducing dissemination. This hypothesis is corroborated by the aforementioned study, in which mice were immunized with 10^5 NTUH-K2044 *tonB* bacteria. Upon secondary infection with 10^3 WT NTUH-K2044, 8/8 mice survived, whereas all non-immunized mice succumbed to infection [93]. Comparing immunization with *tonB K. pneumoniae* ($Ent^+Ybt^+Sal^+$) and *entB ybtS tonB K. pneumoniae* (siderophore-negative) could determine if secretion of siderophores by these

strains is responsible for the induction of the protective effect. Additionally, in our studies mice were infected with *tonB K. pneumoniae* retropharyngeally. An alternate site or method of administration, such as intramuscular injection or intranasal inoculation, could be preferential over retropharyngeal infection. Together, the data presented within this thesis, as well as studies previously performed by other groups, support further experimentation to examine the effectivity of siderophores and *tonB* strains of bacteria as vaccine candidates.

Another use for siderophores therapeutically may be in combination with antibiotics to combat biofilm formation. This is particularly attractive as a potential therapy to disrupt *P. aeruginosa* biofilms in patients with cystic fibrosis [228]. Cystic fibrosis patients have an extremely high concentration of iron available in the airway surface liquid of the lung, and iron chelators may disrupt the biofilm, allowing antibiotics to more effectively treat the infection [229]. Previously, DFO used in combination with the antibiotic tobramycin resulted in a decreased in bacterial burden and biofilm biomass, indicating that this may be a viable treatment option [230]. A stronger chelator, such as Ent, could represent a better siderophore to be used in combination with antibiotics due to its extremely high affinity for iron. However, the inflammatory response that may be initiated in response to the iron chelation could be problematic for patients suffering from cystic fibrosis. The inflammatory effects of any iron chelator used in combination with antibiotics should be examined to verify that cystic fibrosis patients will not suffer adverse effects from this potential therapy. In this way, siderophores may be used as one part of a therapy for cystic fibrosis patients infected with biofilms.

5.7 Conclusions

Although the first siderophores were discovered over half a century ago, the importance of siderophores as virulence factors during colonization and infection is still being uncovered today. Originally thought to be redundant iron-binding molecules, it is becoming more evident that individual siderophores can serve specific roles by evading Lcn2, binding non-iron heavy metals, initiating or inhibiting host cellular pathways, and determining the replicative niche during infection. Whether additional functions can be performed by distinct siderophores remains to be determined. Overall, more precise knowledge of the functions attributable to individual siderophores may allow for the development of novel therapeutics or vaccines.

The work presented in this thesis has defined a novel role for siderophores as inflammatory agents during infection with *K. pneumoniae*. This work also has identified a novel host-pathogen interaction between siderophores and the master transcription factor HIF-1α that leads to bacterial dissemination to the spleen. Finally, potentially uncharacterized mechanisms of iron acquisition have been identified in CR *K. pneumoniae* using RNASeq. Applications to exploit these newly characterized roles for siderophores during infection could be utilization of siderophores in vaccines and as drugs to combat infection. Together, these data have increased the understanding of *K. pneumoniae* infection and may aid in the discovery of novel therapeutics to combat disease caused by siderophore-secreting bacteria.

REFERENCES

1. Stein A, Hofmann H. Resonant Inverter Design for Stand-Alone Dynamic Active Piezoelectric Energy Harvesting. Applied Power Electronics Conference; Charlotte, NC: IEEE; 2014. p. 3265-71.
2. Pantopoulos K, Porwal SK, Tartakoff A, Devireddy L. Mechanisms of mammalian iron homeostasis. Biochemistry. 2012;51(29):5705-24. Epub 2012/06/19. doi: 10.1021/bi300752r. PubMed PMID: 22703180; PubMed Central PMCID: PMC3572738.
3. Gkouvatsos K, Papanikolaou G, Pantopoulos K. Regulation of iron transport and the role of transferrin. Biochim Biophys Acta. 2012;1820(3):188-202. Epub 2011/11/17. doi: 10.1016/j.bbagen.2011.10.013
S0304-4165(11)00267-4 [pii]. PubMed PMID: 22085723.
4. Crichton RR. Iron metabolism : from molecular mechanisms to clinical consequences. 3rd ed. Chichester, UK: John Wiley & Sons; 2009. xx, 461 p. p.
5. Correnti C, Strong RK. Mammalian siderophores, siderophore-binding lipocalins, and the labile iron pool. J Biol Chem. 2012;287(17):13524-31. Epub 2012/03/06. doi: 10.1074/jbc.R111.311829
R111.311829 [pii]. PubMed PMID: 22389496; PubMed Central PMCID: PMC3340207.
6. Fischbach MA, Lin H, Liu DR, Walsh CT. How pathogenic bacteria evade mammalian sabotage in the battle for iron. Nat Chem Biol. 2006;2(3):132-8. Epub 2006/02/18. doi: nchembio771 [pii]
10.1038/nchembio771. PubMed PMID: 16485005.
7. Crumbliss AL, Harrington JM. Iron Sequestration by Small Molecules: Thermodynamic and Kinetic Studies of Natural Siderophores and Synthetic Model Compounds. Adv Inorg Chem. 2009;61:179-250.
8. Sandy M, Butler A. Microbial iron acquisition: marine and terrestrial siderophores. Chem Rev. 2009;109(10):4580-95. Epub 2009/09/24. doi: 10.1021/cr9002787. PubMed PMID: 19772347; PubMed Central PMCID: PMC2761978.
9. Francis J, Macturk HM, Madinaveitia J, Snow GA. Mycobactin, a growth factor for *Mycobacterium johnei*. I. Isolation from Mycobacterium phlei. Biochem J. 1953;55(4):596-607. Epub 1953/11/01. PubMed PMID: 13115341; PubMed Central PMCID: PMC1269366.
10. Ratledge C, Dover LG. Iron metabolism in pathogenic bacteria. Annual review of microbiology. 2000;54:881-941. doi: 10.1146/annurev.micro.54.1.881. PubMed PMID: 11018148.

11. Hider RC, Kong X. Chemistry and biology of siderophores. Nat Prod Rep. 2010;27(5):637-57. Epub 2010/04/09. doi: 10.1039/b906679a. PubMed PMID: 20376388.
12. Vokes SA, Reeves SA, Torres AG, Payne SM. The aerobactin iron transport system genes in *Shigella flexneri* are present within a pathogenicity island. Mol Microbiol. 1999;33(1):63-73. Epub 1999/07/20. doi: mmi1448 [pii]. PubMed PMID: 10411724.
13. Bachman MA, Oyler JE, Burns SH, Caza M, Lepine F, Dozois CM, et al. *Klebsiella pneumoniae* yersiniabactin promotes respiratory tract infection through evasion of lipocalin 2. Infect Immun. 2011;79(8):3309-16. Epub 2011/05/18. doi: 10.1128/IAI.05114-11
IAI.05114-11 [pii]. PubMed PMID: 21576334; PubMed Central PMCID: PMC3147564.
14. Russo TA, Shon AS, Beanan JM, Olson R, MacDonald U, Pomakov AO, et al. Hypervirulent *K. pneumoniae* secretes more and more active iron-acquisition molecules than "classical" *K. pneumoniae* thereby enhancing its virulence. PLoS One. 2011;6(10):e26734. Epub 2011/11/01. doi: 10.1371/journal.pone.0026734
PONE-D-11-17203 [pii]. PubMed PMID: 22039542; PubMed Central PMCID: PMC3200348.
15. Bachman MA, Miller VL, Weiser JN. Mucosal lipocalin 2 has pro-inflammatory and iron-sequestering effects in response to bacterial enterobactin. PLoS Pathog. 2009;5(10):e1000622. Epub 2009/10/17. doi: 10.1371/journal.ppat.1000622. PubMed PMID: 19834550; PubMed Central PMCID: PMC2757716.
16. Caza M, Lepine F, Dozois CM. Secretion, but not overall synthesis, of catecholate siderophores contributes to virulence of extraintestinal pathogenic *Escherichia coli*. Mol Microbiol. 2011;80(1):266-82. Epub 2011/02/11. doi: 10.1111/j.1365-2958.2011.07570.x. PubMed PMID: 21306443.
17. Bearden SW, Fetherston JD, Perry RD. Genetic organization of the yersiniabactin biosynthetic region and construction of avirulent mutants in *Yersinia pestis*. Infect Immun. 1997;65(5):1659-68. Epub 1997/05/01. PubMed PMID: 9125544; PubMed Central PMCID: PMC175193.
18. Fischbach MA, Lin H, Zhou L, Yu Y, Abergel RJ, Liu DR, et al. The pathogen-associated iroA gene cluster mediates bacterial evasion of lipocalin 2. Proc Natl Acad Sci U S A. 2006;103(44):16502-7. Epub 2006/10/25. doi: 0604636103 [pii]
10.1073/pnas.0604636103. PubMed PMID: 17060628; PubMed Central PMCID: PMC1637611.
19. Goetz DH, Holmes MA, Borregaard N, Bluhm ME, Raymond KN, Strong RK. The neutrophil lipocalin NGAL is a bacteriostatic agent that interferes with siderophore-mediated iron acquisition. Mol Cell. 2002;10(5):1033-43. Epub 2002/11/28. doi: S1097276502007086 [pii]. PubMed PMID: 12453412.
20. Abergel RJ, Moore EG, Strong RK, Raymond KN. Microbial evasion of the immune system: structural modifications of enterobactin impair siderocalin recognition. J Am Chem Soc. 2006;128(34):10998-9. Epub 2006/08/24. doi:

10.1021/ja062476+. PubMed PMID: 16925397; PubMed Central PMCID: PMC3188317.
21. Pollack JR, Neilands JB. Enterobactin, an iron transport compound from *Salmonella typhimurium*. Biochem Biophys Res Commun. 1970;38(5):989-92. Epub 1970/03/12. doi: 0006-291X(70)90819-3 [pii]. PubMed PMID: 4908541.
22. O'Brien IG, Gibson F. The structure of enterochelin and related 2,3-dihydroxy-N-benzoylserine conjugates from *Escherichia coli*. Biochim Biophys Acta. 1970;215(2):393-402. Epub 1970/08/14. PubMed PMID: 4926450.
23. May JJ, Wendrich TM, Marahiel MA. The dhb operon of Bacillus subtilis encodes the biosynthetic template for the catecholic siderophore 2,3-dihydroxybenzoate-glycine-threonine trimeric ester bacillibactin. J Biol Chem. 2001;276(10):7209-17. Epub 2000/12/12. doi: 10.1074/jbc.M009140200 M009140200 [pii]. PubMed PMID: 11112781.
24. Carrano CJ, Raymond KN. Ferric Ion Sequestering Agents .2. Kinetics and Mechanism of Iron Removal from Transferrin by Enterobactin and Synthetic Tricatechols. Journal of the American Chemical Society. 1979;101(18):5401-4. doi: Doi 10.1021/Ja00512a047. PubMed PMID: ISI:A1979HH98100047.
25. Loomis LD, Raymond KN. Solution Equilibria of Enterobactin and Metal Enterobactin Complexes. Inorg Chem. 1991;30(5):906-11. doi: Doi 10.1021/Ic00005a008. PubMed PMID: ISI:A1991FA58700008.
26. Aisen P. Transferrin, the transferrin receptor, and the uptake of iron by cells. Met Ions Biol Syst. 1998;35:585-631. Epub 1998/01/28. PubMed PMID: 9444770.
27. Muller G, Matzanke BF, Raymond KN. Iron Transport in Streptomyces-Pilosus Mediated by Ferrichrome Siderophores, Rhodotorulic Acid, and Enantio-Rhodotorulic Acid. J Bacteriol. 1984;160(1):313-8. PubMed PMID: ISI:A1984TM02800047.
28. Muller G, Raymond KN. Specificity and Mechanism of Ferrioxamine-Mediated Iron Transport in Streptomyces-Pilosus. J Bacteriol. 1984;160(1):304-12. PubMed PMID: ISI:A1984TM02800046.
29. Moeschlin S, Schnider U. Treatment of Primary and Secondary Hemochromatosis and Acute Iron Poisoning with a New, Potent Iron-Eliminating Agent (Desferrioxamine-B). New Engl J Med. 1963;269(2):57-&. doi: Doi 10.1056/Nejm196307112690201. PubMed PMID: ISI:A19638598B00008.
30. Goodwin JF, Whitten CF. Chelation of Ferrous Sulphate Solutions by Desferrioxamine B. Nature. 1965;205:281-3. PubMed PMID: 14270711.
31. Schwarzenbach G, Schwarzenbach K. Hydroxamatkomplexe I. Die Stabilitat der Eisen(III)-Komplexe einfacher Hydroxamsauren und des Ferrioxamins B. Helv Chim Acta. 1963;46:1390-400.
32. Miethke M, Marahiel MA. Siderophore-based iron acquisition and pathogen control. Microbiol Mol Biol Rev. 2007;71(3):413-51. Epub 2007/09/07. doi: 71/3/413 [pii]
10.1128/MMBR.00012-07. PubMed PMID: 17804665; PubMed Central PMCID: PMC2168645.

33. Konetschny-Rapp S, Jung G, Meiwes J, Zahner H. Staphyloferrin A: a structurally new siderophore from staphylococci. Eur J Biochem. 1990;191(1):65-74. Epub 1990/07/20. PubMed PMID: 2379505.
34. Guerinot ML, Meidl EJ, Plessner O. Citrate as a siderophore in *Bradyrhizobium japonicum*. J Bacteriol. 1990;172(6):3298-303. Epub 1990/06/01. PubMed PMID: 2140566; PubMed Central PMCID: PMC209139.
35. Mino Y, Ishida T, Ota N, Inoue M, Nomoto K, Takemoto T, et al. Mugineic Acid-Iron(III) Complex and Its Structurally Analogous Cobalt(III) Complex: Characterization and Implication for Absorption and Transport of Iron in Gramineous Plants. J Am Chem Soc. 1983;(105):4671-6.
36. Drechsel H, Stephan H, Lotz R, Haag H, Zahner H, Hantke K, et al. Structure Elucidation of Yersiniabactin, a Siderophore from Highly Virulent *Yersinia* Strains. Liebigs Ann. 1995;(10):1727-33. PubMed PMID: ISI:A1995RZ25000002.
37. Cox CD, Rinehart KL, Jr., Moore ML, Cook JC, Jr. Pyochelin: novel structure of an iron-chelating growth promoter for *Pseudomonas aeruginosa*. Proc Natl Acad Sci U S A. 1981;78(7):4256-60. Epub 1981/07/01. PubMed PMID: 6794030; PubMed Central PMCID: PMC319768.
38. Perry RD, Balbo PB, Jones HA, Fetherston JD, DeMoll E. Yersiniabactin from *Yersinia pestis*: biochemical characterization of the siderophore and its role in iron transport and regulation. Microbiology. 1999;145 (Pt 5):1181-90. PubMed PMID: 10376834.
39. Harris WR, Carrano CJ, Raymond KN. Coordination Chemistry of Microbial Iron Transport Compounds .16. Isolation, Characterization, and Formation-Constants of Ferric Aerobactin. Journal of the American Chemical Society. 1979;101(10):2722-7. doi: Doi 10.1021/Ja00504a038. PubMed PMID: WOS:A1979GU65900038.
40. Barbeau K, Zhang G, Live DH, Butler A. Petrobactin, a photoreactive siderophore produced by the oil-degrading marine bacterium *Marinobacter hydrocarbonoclasticus*. J Am Chem Soc. 2002;124(3):378-9. Epub 2002/01/17. doi: ja0119088 [pii]. PubMed PMID: 11792199.
41. Cox CD, Adams P. Siderophore activity of pyoverdin for *Pseudomonas aeruginosa*. Infect Immun. 1985;48(1):130-8. Epub 1985/04/01. PubMed PMID: 3156815; PubMed Central PMCID: PMC261925.
42. Kjeldsen L, Johnsen AH, Sengelov H, Borregaard N. Isolation and primary structure of NGAL, a novel protein associated with human neutrophil gelatinase. J Biol Chem. 1993;268(14):10425-32. Epub 1993/05/15. PubMed PMID: 7683678.
43. Flo TH, Smith KD, Sato S, Rodriguez DJ, Holmes MA, Strong RK, et al. Lipocalin 2 mediates an innate immune response to bacterial infection by sequestrating iron. Nature. 2004;432(7019):917-21. Epub 2004/11/09. doi: nature03104 [pii]
10.1038/nature03104. PubMed PMID: 15531878.
44. Gomez-Casado C, Roth-Walter F, Jensen-Jarolim E, Diaz-Perales A, Pacios LF. Modeling iron-catecholates binding to NGAL protein. J Mol Graph Model. 2013;45:111-21. Epub 2013/09/11. doi: 10.1016/j.jmgm.2013.08.013

S1093-3263(13)00140-X [pii]. PubMed PMID: 24018130.
45. Nelson AL, Ratner AJ, Barasch J, Weiser JN. Interleukin-8 Secretion in Response to Aferric Enterobactin is Potentiatied by Siderocalin. Infect Immun. 2007;75(6):8.
46. Newton SM, Igo JD, Scott DC, Klebba PE. Effect of loop deletions on the binding and transport of ferric enterobactin by FepA. Mol Microbiol. 1999;32(6):1153-65. Epub 1999/06/26. doi: mmi1424 [pii]. PubMed PMID: 10383757.
47. Nelson AL, Barasch JM, Bunte RM, Weiser JN. Bacterial colonization of nasal mucosa induces expression of siderocalin, an iron-sequestering component of innate immunity. Cell Microbiol. 2005;7(10):1404-17. Epub 2005/09/13. doi: CMI566 [pii]
10.1111/j.1462-5822.2005.00566.x. PubMed PMID: 16153241.
48. Chan YR, Liu JS, Pociask DA, Zheng M, Mietzner TA, Berger T, et al. Lipocalin 2 is required for pulmonary host defense against *Klebsiella* infection. J Immunol. 2009;182(8):4947-56. Epub 2009/04/04. doi: 10.4049/jimmunol.0803282
182/8/4947 [pii]. PubMed PMID: 19342674; PubMed Central PMCID: PMC2708928.
49. Paragas N, Kulkarni R, Werth M, Schmidt-Ott KM, Forster C, Deng R, et al. alpha-Intercalated cells defend the urinary system from bacterial infection. J Clin Invest. 2014;124(7):2963-76. Epub 2014/06/18. doi: 10.1172/JCI71630
71630 [pii]. PubMed PMID: 24937428; PubMed Central PMCID: PMC4071397.
50. Steigedal M, Marstad A, Haug M, Damas JK, Strong RK, Roberts PL, et al. Lipocalin 2 Imparts Selective Pressure on Bacterial Growth in the Bladder and Is Elevated in Women with Urinary Tract Infection. J Immunol. 2014. Epub 2014/11/16. doi: 1401528 [pii]
jimmunol.1401528 [pii]
10.4049/jimmunol.1401528. PubMed PMID: 25398327.
51. Abergel RJ, Wilson MK, Arceneaux JE, Hoette TM, Strong RK, Byers BR, et al. Anthrax pathogen evades the mammalian immune system through stealth siderophore production. Proc Natl Acad Sci U S A. 2006;103(49):18499-503. Epub 2006/11/30. doi: 0607055103 [pii]
10.1073/pnas.0607055103. PubMed PMID: 17132740; PubMed Central PMCID: PMC1693691.
52. Holmes MA, Paulsene W, Jide X, Ratledge C, Strong RK. Siderocalin (Lcn 2) also binds carboxymycobactins, potentially defending against mycobacterial infections through iron sequestration. Structure. 2005;13(1):29-41. Epub 2005/01/12. doi: S0969-2126(04)00383-1 [pii]
10.1016/j.str.2004.10.009. PubMed PMID: 15642259.
53. Bister B, Bischoff D, Nicholson GJ, Valdebenito M, Schneider K, Winkelmann G, et al. The structure of salmochelins: C-glucosylated enterobactins of Salmonella enterica. Biometals. 2004;17(4):471-81. Epub 2004/07/21. PubMed PMID: 15259369.
54. Luo M, Lin H, Fischbach MA, Liu DR, Walsh CT, Groves JT. Enzymatic tailoring of enterobactin alters membrane partitioning and iron acquisition. ACS

Chem Biol. 2006;1(1):29-32. Epub 2006/12/14. doi: 10.1021/cb0500034. PubMed PMID: 17163637.
55. Cendrowski S, MacArthur W, Hanna P. *Bacillus anthracis* requires siderophore biosynthesis for growth in macrophages and mouse virulence. Mol Microbiol. 2004;51(2):407-17. Epub 2004/02/06. doi: 10.1046/j.1365-2958.2003.03861.x
MMI3861 [pii]. PubMed PMID: 14756782.
56. Pfleger BF, Kim Y, Nusca TD, Maltseva N, Lee JY, Rath CM, et al. Structural and functional analysis of AsbF: origin of the stealth 3,4-dihydroxybenzoic acid subunit for petrobactin biosynthesis. Proc Natl Acad Sci U S A. 2008;105(44):17133-8. Epub 2008/10/29. doi: 10.1073/pnas.0808118105
0808118105 [pii]. PubMed PMID: 18955706; PubMed Central PMCID: PMC2579390.
57. Zawadzka AM, Kim Y, Maltseva N, Nichiporuk R, Fan Y, Joachimiak A, et al. Characterization of a *Bacillus subtilis* transporter for petrobactin, an anthrax stealth siderophore. Proc Natl Acad Sci U S A. 2009;106(51):21854-9. Epub 2009/12/04. doi: 10.1073/pnas.0904793106
0904793106 [pii]. PubMed PMID: 19955416; PubMed Central PMCID: PMC2799803.
58. Vagrali MA. Siderophore production by uropathogenic *Escherichia coli*. Indian J Pathol Microbiol. 2009;52(1):126-7. Epub 2009/01/13. PubMed PMID: 19136808.
59. Visca P, Filetici E, Anastoasio MP, Vetriani C, Fantasia M, Orsi N. Siderophore production by *Salmonella* species isolated from different sources. FEMS Microbiol Lett. 1991;63(2-3):225-31. Epub 1991/04/15. PubMed PMID: 1829423.
60. Himpsl SD, Pearson MM, Arewang CJ, Nusca TD, Sherman DH, Mobley HL. Proteobactin and a yersiniabactin-related siderophore mediate iron acquisition in *Proteus mirabilis*. Mol Microbiol. 2010;78(1):138-57. Epub 2010/10/07. doi: 10.1111/j.1365-2958.2010.07317.x. PubMed PMID: 20923418; PubMed Central PMCID: PMC2951610.
61. Payne SM, Wyckoff EE, Murphy ER, Oglesby AG, Boulette ML, Davies NM. Iron and pathogenesis of *Shigella*: iron acquisition in the intracellular environment. Biometals. 2006;19(2):173-80. Epub 2006/05/24. doi: 10.1007/s10534-005-4577-x. PubMed PMID: 16718602.
62. Forman S, Paulley JT, Fetherston JD, Cheng YQ, Perry RD. Yersinia ironomics: comparison of iron transporters among *Yersinia pestis* biotypes and its nearest neighbor, Yersinia pseudotuberculosis. Biometals. 2010;23(2):275-94. doi: 10.1007/s10534-009-9286-4. PubMed PMID: 20049509.
63. Brock JH, Williams PH, Liceaga J, Wooldridge KG. Relative availability of transferrin-bound iron and cell-derived iron to aerobactin-producing and enterochelin-producing strains of *Escherichia coli* and to other microorganisms. Infect Immun. 1991;59(9):3185-90. Epub 1991/09/01. PubMed PMID: 1831796; PubMed Central PMCID: PMC258151.
64. Warner PJ, Williams PH, Bindereif A, Neilands JB. ColV plasmid-specific aerobactin synthesis by invasive strains of *Escherichia coli*. Infect Immun.

1981;33(2):540-5. Epub 1981/08/01. PubMed PMID: 6456229; PubMed Central PMCID: PMC350734.
65. Schalk IJ, Hannauer M, Braud A. New roles for bacterial siderophores in metal transport and tolerance. Environ Microbiol. 2011;13(11):2844-54. Epub 2011/09/03. doi: 10.1111/j.1462-2920.2011.02556.x. PubMed PMID: 21883800.
66. Crumbliss AL. Aqueous Solution Equilibrium and Kinetic Studies of Iron Siderophore and Model Siderophore Complexes. 1st ed. Winkelmann G, editor: CRC Press; 1991. 177-233 p.
67. Evers A, Hancock RD, Martell AE, Motekaitis RJ. Metal ion recognition in ligands with negatively charged oxygen donor groups. Complexation of iron(III), gallium (III), indium (III), aluminum (III), and other highly charged mteal ions. Inorg Chem. 1989;28(11):2189-95. doi: 10.1021/ic00310a035.
68. Braud A, Geoffroy V, Hoegy F, Mislin GL, Schalk IJ. Presence of the siderophores pyoverdine and pyochelin in the extracellular medium reduces toxic metal accumulation in *Pseudomonas aeruginosa* and increases bacterial metal tolerance. Environ Microbiol Rep. 2010;2(3):419-25. Epub 2010/06/01. doi: 10.1111/j.1758-2229.2009.00126.x. PubMed PMID: 23766115.
69. Braud A, Hannauer M, Mislin GL, Schalk IJ. The *Pseudomonas aeruginosa* pyochelin-iron uptake pathway and its metal specificity. J Bacteriol. 2009;191(11):3517-25. Epub 2009/03/31. doi: 10.1128/JB.00010-09
JB.00010-09 [pii]. PubMed PMID: 19329644; PubMed Central PMCID: PMC2681917.
70. Braud A, Hoegy F, Jezequel K, Lebeau T, Schalk IJ. New insights into the metal specificity of the *Pseudomonas aeruginosa* pyoverdine-iron uptake pathway. Environ Microbiol. 2009;11(5):1079-91. Epub 2009/02/12. doi: 10.1111/j.1462-2920.2008.01838.x
EMI1838 [pii]. PubMed PMID: 19207567.
71. Chaturvedi KS, Hung CS, Crowley JR, Stapleton AE, Henderson JP. The siderophore yersiniabactin binds copper to protect pathogens during infection. Nat Chem Biol. 2012;8(8):731-6. Epub 2012/07/10. doi: 10.1038/nchembio.1020
nchembio.1020 [pii]. PubMed PMID: 22772152; PubMed Central PMCID: PMC3600419.
72. Chaturvedi KS, Hung CS, Giblin DE, Urushidani S, Austin AM, Dinauer MC, et al. Cupric yersiniabactin is a virulence-associated superoxide dismutase mimic. ACS Chem Biol. 2014;9(2):551-61. Epub 2013/11/29. doi: 10.1021/cb400658k. PubMed PMID: 24283977; PubMed Central PMCID: PMC3934373.
73. Bokil NJ, Totsika M, Carey AJ, Stacey KJ, Hancock V, Saunders BM, et al. Intramacrophage survival of uropathogenic *Escherichia coli*: differences between diverse clinical isolates and between mouse and human macrophages. Immunobiology. 2011;216(11):1164-71. Epub 2011/08/02. doi: 10.1016/j.imbio.2011.05.011
S0171-2985(11)00109-4 [pii]. PubMed PMID: 21802164.
74. Paauw A, Leverstein-van Hall MA, van Kessel KP, Verhoef J, Fluit AC. Yersiniabactin reduces the respiratory oxidative stress response of innate immune cells. PLoS One. 2009;4(12):e8240. Epub 2009/12/31. doi:

10.1371/journal.pone.0008240. PubMed PMID: 20041108; PubMed Central PMCID: PMC2795162.
75. Desrosiers DC, Bearden SW, Mier I, Jr., Abney J, Paulley JT, Fetherston JD, et al. Znu is the predominant zinc importer in *Yersinia pestis* during in vitro growth but is not essential for virulence. Infect Immun. 2010;78(12):5163-77. Epub 2010/09/22. doi: 10.1128/IAI.00732-10
IAI.00732-10 [pii]. PubMed PMID: 20855510; PubMed Central PMCID: PMC2981304.
76. Hood MI, Skaar EP. Nutritional immunity: transition metals at the pathogen-host interface. Nat Rev Microbiol. 2012;10(8):525-37. Epub 2012/07/17. doi: 10.1038/nrmicro2836
nrmicro2836 [pii]. PubMed PMID: 22796883; PubMed Central PMCID: PMC3875331.
77. Cerasi M, Liu JZ, Ammendola S, Poe AJ, Petrarca P, Pesciaroli M, et al. The ZupT transporter plays an important role in zinc homeostasis and contributes to *Salmonella enterica* virulence. Metallomics. 2014;6(4):845-53. Epub 2014/01/17. doi: 10.1039/c3mt00352c. PubMed PMID: 24430377; PubMed Central PMCID: PMC3969385.
78. Cortese MS, Paszczynski A, Lewis TA, Sebat JL, Borek V, Crawford RL. Metal chelating properties of pyridine-2,6-bis(thiocarboxylic acid) produced by *Pseudomonas spp.* and the biological activities of the formed complexes. Biometals. 2002;15(2):103-20. Epub 2002/06/06. PubMed PMID: 12046919.
79. Leach LH, Morris JC, Lewis TA. The role of the siderophore pyridine-2,6-bis (thiocarboxylic acid) (PDTC) in zinc utilization by *Pseudomonas putida* DSM 3601. Biometals. 2007;20(5):717-26. Epub 2006/10/27. doi: 10.1007/s10534-006-9035-x. PubMed PMID: 17066327.
80. Bobrov AG, Kirillina O, Fetherston JD, Miller MC, Burlison JA, Perry RD. The *Yersinia pestis* siderophore, yersiniabactin, and the ZnuABC system both contribute to zinc acquisition and the development of lethal septicaemic plague in mice. Mol Microbiol. 2014;93(4):759-75. Epub 2014/07/01. doi: 10.1111/mmi.12693. PubMed PMID: 24979062; PubMed Central PMCID: PMC4132657.
81. Le NT, Richardson DR. Iron chelators with high antiproliferative activity up-regulate the expression of a growth inhibitory and metastasis suppressor gene: a link between iron metabolism and proliferation. Blood. 2004;104(9):2967-75. Epub 2004/07/15. doi: 10.1182/blood-2004-05-1866
2004-05-1866 [pii]. PubMed PMID: 15251988.
82. Richardson DR, Milnes K. The potential of iron chelators of the pyridoxal isonicotinoyl hydrazone class as effective antiproliferative agents II: the mechanism of action of ligands derived from salicylaldehyde benzoyl hydrazone and 2-hydroxy-1-naphthylaldehyde benzoyl hydrazone. Blood. 1997;89(8):3025-38. Epub 1997/04/15. PubMed PMID: 9108424.
83. Richardson DR, Tran EH, Ponka P. The potential of iron chelators of the pyridoxal isonicotinoyl hydrazone class as effective antiproliferative agents. Blood. 1995;86(11):4295-306. Epub 1995/12/01. PubMed PMID: 7492790.

84. Choi EY, Kim EC, Oh HM, Kim S, Lee HJ, Cho EY, et al. Iron chelator triggers inflammatory signals in human intestinal epithelial cells: involvement of p38 and extracellular signal-regulated kinase signaling pathways. J Immunol. 2004;172(11):7069-77. Epub 2004/05/22. PubMed PMID: 15153529.
85. Choi EY, Park ZY, Choi EJ, Oh HM, Lee S, Choi SC, et al. Transcriptional regulation of IL-8 by iron chelator in human epithelial cells is independent from NF-kappaB but involves ERK1/2- and p38 kinase-dependent activation of AP-1. J Cell Biochem. 2007;102(6):1442-57. Epub 2007/05/02. doi: 10.1002/jcb.21367. PubMed PMID: 17471497.
86. Raffatellu M, George MD, Akiyama Y, Hornsby MJ, Nuccio SP, Paixao TA, et al. Lipocalin-2 resistance confers an advantage to *Salmonella enterica* serotype Typhimurium for growth and survival in the inflamed intestine. Cell Host Microbe. 2009;5(5):476-86. Epub 2009/05/21. doi: 10.1016/j.chom.2009.03.011
S1931-3128(09)00108-5 [pii]. PubMed PMID: 19454351; PubMed Central PMCID: PMC2768556.
87. Behnsen J, Jellbauer S, Wong CP, Edwards RA, George MD, Ouyang W, et al. The cytokine IL-22 promotes pathogen colonization by suppressing related commensal bacteria. Immunity. 2014;40(2):262-73. Epub 2014/02/11. doi: 10.1016/j.immuni.2014.01.003
S1074-7613(14)00029-6 [pii]. PubMed PMID: 24508234; PubMed Central PMCID: PMC3964146.
88. Deriu E, Liu JZ, Pezeshki M, Edwards RA, Ochoa RJ, Contreras H, et al. Probiotic bacteria reduce *Salmonella typhimurium* intestinal colonization by competing for iron. Cell Host Microbe. 2013;14(1):26-37. Epub 2013/07/23. doi: 10.1016/j.chom.2013.06.007
S1931-3128(13)00223-0 [pii]. PubMed PMID: 23870311; PubMed Central PMCID: PMC3752295.
89. Diaz-Ochoa VE, Jellbauer S, Klaus S, Raffatellu M. Transition metal ions at the crossroads of mucosal immunity and microbial pathogenesis. Front Cell Infect Microbiol. 2014;4:2. Epub 2014/01/31. doi: 10.3389/fcimb.2014.00002. PubMed PMID: 24478990; PubMed Central PMCID: PMC3900919.
90. Podschun R, Ullmann U. *Klebsiella spp*. as nosocomial pathogens: epidemiology, taxonomy, typing methods, and pathogenicity factors. Clin Microbiol Rev. 1998;11(4):589-603. Epub 1998/10/10. PubMed PMID: 9767057; PubMed Central PMCID: PMC88898.
91. Warszawska JM, Gawish R, Sharif O, Sigel S, Doninger B, Lakovits K, et al. Lipocalin 2 deactivates macrophages and worsens pneumococcal pneumonia outcomes. J Clin Invest. 2013;123(8):3363-72. doi: 10.1172/JCI67911. PubMed PMID: 23863624; PubMed Central PMCID: PMC3726165.
92. Wright MS, Perez F, Brinkac L, Jacobs MR, Kaye K, Cober E, et al. Population structure of KPC-producing *Klebsiella pneumoniae* isolates from midwestern U.S. hospitals. Antimicrob Agents Chemother. 2014;58(8):4961-5. Epub 2014/06/11. doi: 10.1128/AAC.00125-14
AAC.00125-14 [pii]. PubMed PMID: 24913165; PubMed Central PMCID: PMC4136011.

93. Hsieh PF, Lin TL, Lee CZ, Tsai SF, Wang JT. Serum-induced iron-acquisition systems and TonB contribute to virulence in *Klebsiella pneumoniae* causing primary pyogenic liver abscess. The Journal of infectious diseases. 2008;197(12):1717-27. doi: 10.1086/588383. PubMed PMID: 18433330.
94. Russo TA, Olson R, Macdonald U, Metzger D, Maltese LM, Drake EJ, et al. Aerobactin mediates virulence and accounts for increased siderophore production under iron-limiting conditions by hypervirulent (hypermucoviscous) *Klebsiella pneumoniae.* Infect Immun. 2014;82(6):2356-67. doi: 10.1128/IAI.01667-13. PubMed PMID: 24664504; PubMed Central PMCID: PMC4019165.
95. Siu LK, Fung CP, Chang FY, Lee N, Yeh KM, Koh TH, et al. Molecular typing and virulence analysis of serotype K1 *Klebsiella pneumoniae* strains isolated from liver abscess patients and stool samples from noninfectious subjects in Hong Kong, Singapore, and Taiwan. J Clin Microbiol. 2011;49(11):3761-5. Epub 2011/09/09. doi: 10.1128/JCM.00977-11
JCM.00977-11 [pii]. PubMed PMID: 21900521; PubMed Central PMCID: PMC3209116.
96. Bachman MA, Lenio S, Schmidt L, Oyler JE, Weiser JN. Interaction of lipocalin 2, transferrin, and siderophores determines the replicative niche of *Klebsiella pneumoniae* during pneumonia. MBio. 2012;3(6). Epub 2012/11/22. doi: 10.1128/mBio.00224-11
e00224-11 [pii]
mBio.00224-11 [pii]. PubMed PMID: 23169997; PubMed Central PMCID: PMC3509427.
97. Garcia EC, Brumbaugh AR, Mobley HL. Redundancy and specificity of *Escherichia coli* iron acquisition systems during urinary tract infection. Infect Immun. 2011;79(3):1225-35. Epub 2011/01/12. doi: 10.1128/IAI.01222-10
IAI.01222-10 [pii]. PubMed PMID: 21220482; PubMed Central PMCID: PMC3067483.
98. Brumbaugh AR, Smith SN, Mobley HL. Immunization with the yersiniabactin receptor, FyuA, protects against pyelonephritis in a murine model of urinary tract infection. Infect Immun. 2013;81(9):3309-16. Epub 2013/06/27. doi: 10.1128/IAI.00470-13
IAI.00470-13 [pii]. PubMed PMID: 23798537; PubMed Central PMCID: PMC3754202.
99. Vigil PD, Stapleton AE, Johnson JR, Hooton TM, Hodges AP, He Y, et al. Presence of putative repeat-in-toxin gene tosA in *Escherichia coli* predicts successful colonization of the urinary tract. MBio. 2011;2(3):e00066-11. Epub 2011/05/05. doi: 10.1128/mBio.00066-11
e00066-11 [pii]
mBio.00066-11 [pii]. PubMed PMID: 21540363; PubMed Central PMCID: PMC3088117.
100. Bearden SW, Perry RD. The Yfe system of *Yersinia pestis* transports iron and manganese and is required for full virulence of plague. Mol Microbiol. 1999;32(2):403-14. Epub 1999/05/07. doi: mmi1360 [pii]. PubMed PMID: 10231495.

101. Fetherston JD, Kirillina O, Bobrov AG, Paulley JT, Perry RD. The yersiniabactin transport system is critical for the pathogenesis of bubonic and pneumonic plague. Infect Immun. 2010;78(5):2045-52. Epub 2010/02/18. doi: 10.1128/IAI.01236-09
IAI.01236-09 [pii]. PubMed PMID: 20160020; PubMed Central PMCID: PMC2863531.
102. Palazon A, Goldrath AW, Nizet V, Johnson RS. HIF transcription factors, inflammation, and immunity. Immunity. 2014;41(4):518-28. doi: 10.1016/j.immuni.2014.09.008. PubMed PMID: 25367569; PubMed Central PMCID: PMCPMC4346319.
103. Pugh CW, Ratcliffe PJ. Regulation of angiogenesis by hypoxia: role of the HIF system. Nat Med. 2003;9(6):677-84. doi: 10.1038/nm0603-677. PubMed PMID: 12778166.
104. Forsythe JA, Jiang BH, Iyer NV, Agani F, Leung SW, Koos RD, et al. Activation of vascular endothelial growth factor gene transcription by hypoxia-inducible factor 1. Mol Cell Biol. 1996;16(9):4604-13. Epub 1996/09/01. PubMed PMID: 8756616; PubMed Central PMCID: PMC231459.
105. Cramer T, Yamanishi Y, Clausen BE, Forster I, Pawlinski R, Mackman N, et al. HIF-1alpha is essential for myeloid cell-mediated inflammation. Cell. 2003;112(5):645-57. Epub 2003/03/12. doi: S0092867403001545 [pii]. PubMed PMID: 12628185.
106. Hartmann H, Eltzschig HK, Wurz H, Hantke K, Rakin A, Yazdi AS, et al. Hypoxia-independent activation of HIF-1 by *Enterobacteriaceae* and their siderophores. Gastroenterology. 2008;134(3):756-67. Epub 2008/03/08. doi: 10.1053/j.gastro.2007.12.008
S0016-5085(07)02169-5 [pii]. PubMed PMID: 18325389.
107. Kirienko NV, Kirienko DR, Larkins-Ford J, Wahlby C, Ruvkun G, Ausubel FM. *Pseudomonas aeruginosa* disrupts *Caenorhabditis elegans* iron homeostasis, causing a hypoxic response and death. Cell Host Microbe. 2013;13(4):406-16. Epub 2013/04/23. doi: 10.1016/j.chom.2013.03.003
S1931-3128(13)00113-3 [pii]. PubMed PMID: 23601103; PubMed Central PMCID: PMC3641844.
108. Zinkernagel AS, Peyssonnaux C, Johnson RS, Nizet V. Pharmacologic augmentation of hypoxia-inducible factor-1alpha with mimosine boosts the bactericidal capacity of phagocytes. The Journal of infectious diseases. 2008;197(2):214-7. doi: 10.1086/524843. PubMed PMID: 18173364.
109. Raymond KN, Dertz EA, Kim SS. Enterobactin: an archetype for microbial iron transport. Proc Natl Acad Sci U S A. 2003;100(7):3584-8. doi: 10.1073/pnas.0630018100. PubMed PMID: 12655062; PubMed Central PMCID: PMCPMC152965.
110. Berger T, Togawa A, Duncan GS, Elia AJ, You-Ten A, Wakeham A, et al. Lipocalin 2-deficient mice exhibit increased sensitivity to *Escherichia coli* infection but not to ischemia-reperfusion injury. Proc Natl Acad Sci U S A. 2006;103(6):1834-9. doi: 10.1073/pnas.0510847103. PubMed PMID: 16446425; PubMed Central PMCID: PMCPMC1413671.

111. Li J, Kartha S, Iasvovskaia S, Tan A, Bhat RK, Manaligod JM, et al. Regulation of human airway epithelial cell IL-8 expression by MAP kinases. Am J Physiol Lung Cell Mol Physiol. 2002;283(4):L690-9. doi: 10.1152/ajplung.00060.2002. PubMed PMID: 12225945.
112. Ivan M, Kondo K, Yang H, Kim W, Valiando J, Ohh M, et al. HIFalpha targeted for VHL-mediated destruction by proline hydroxylation: implications for O2 sensing. Science. 2001;292(5516):464-8. doi: 10.1126/science.1059817. PubMed PMID: 11292862.
113. Tacchini L, Bianchi L, Bernelli-Zazzera A, Cairo G. Transferrin receptor induction by hypoxia. HIF-1-mediated transcriptional activation and cell-specific post-transcriptional regulation. J Biol Chem. 1999;274(34):24142-6. PubMed PMID: 10446187.
114. Tannahill GM, Curtis AM, Adamik J, Palsson-McDermott EM, McGettrick AF, Goel G, et al. Succinate is an inflammatory signal that induces IL-1beta through HIF-1alpha. Nature. 2013;496(7444):238-42. doi: 10.1038/nature11986. PubMed PMID: 23535595; PubMed Central PMCID: PMCPMC4031686.
115. Guglani L, Gopal R, Rangel-Moreno J, Junecko BF, Lin Y, Berger T, et al. Lipocalin 2 regulates inflammation during pulmonary mycobacterial infections. PLoS One. 2012;7(11):e50052. doi: 10.1371/journal.pone.0050052. PubMed PMID: 23185529; PubMed Central PMCID: PMCPMC3502292.
116. Zhao H, Konishi A, Fujita Y, Yagi M, Ohata K, Aoshi T, et al. Lipocalin 2 bolsters innate and adaptive immune responses to blood-stage malaria infection by reinforcing host iron metabolism. Cell Host Microbe. 2012;12(5):705-16. doi: 10.1016/j.chom.2012.10.010. PubMed PMID: 23159059.
117. Barrett T, Wilhite SE, Ledoux P, Evangelista C, Kim IF, Tomashevsky M, et al. NCBI GEO: archive for functional genomics data sets--update. Nucleic Acids Res. 2013;41(Database issue):D991-5. doi: 10.1093/nar/gks1193. PubMed PMID: 23193258; PubMed Central PMCID: PMCPMC3531084.
118. del Peso L, Castellanos MC, Temes E, Martin-Puig S, Cuevas Y, Olmos G, et al. The von Hippel Lindau/hypoxia-inducible factor (HIF) pathway regulates the transcription of the HIF-proline hydroxylase genes in response to low oxygen. J Biol Chem. 2003;278(49):48690-5. doi: 10.1074/jbc.M308862200. PubMed PMID: 14506252.
119. Thomas F, Serratrice G, Beguin C, Aman ES, Pierre JL, Fontecave M, et al. Calcein as a fluorescent probe for ferric iron. Application to iron nutrition in plant cells. J Biol Chem. 1999;274(19):13375-83. PubMed PMID: 10224100.
120. Schwyn B, Neilands JB. Universal chemical assay for the detection and determination of siderophores. Anal Biochem. 1987;160(1):47-56. PubMed PMID: 2952030.
121. Jeong HJ, Hong SH, Park RK, Shin T, An NH, Kim HM. Hypoxia-induced IL-6 production is associated with activation of MAP kinase, HIF-1, and NF-kappaB on HEI-OC1 cells. Hear Res. 2005;207(1-2):59-67. doi: 10.1016/j.heares.2005.04.003. PubMed PMID: 15913932.
122. Eltzschig HK, Carmeliet P. Hypoxia and inflammation. N Engl J Med. 2011;364(7):656-65. doi: 10.1056/NEJMra0910283. PubMed PMID: 21323543; PubMed Central PMCID: PMCPMC3930928.

123. Elvidge GP, Glenny L, Appelhoff RJ, Ratcliffe PJ, Ragoussis J, Gleadle JM. Concordant regulation of gene expression by hypoxia and 2-oxoglutarate-dependent dioxygenase inhibition: the role of HIF-1alpha, HIF-2alpha, and other pathways. J Biol Chem. 2006;281(22):15215-26. doi: 10.1074/jbc.M511408200. PubMed PMID: 16565084.
124. Zhang J, Wu Y, Zhang Y, Leroith D, Bernlohr DA, Chen X. The role of lipocalin 2 in the regulation of inflammation in adipocytes and macrophages. Mol Endocrinol. 2008;22(6):1416-26. doi: 10.1210/me.2007-0420. PubMed PMID: 18292240; PubMed Central PMCID: PMCPMC2422824.
125. Lee S, Kim JH, Kim JH, Seo JW, Han HS, Lee WH, et al. Lipocalin-2 Is a chemokine inducer in the central nervous system: role of chemokine ligand 10 (CXCL10) in lipocalin-2-induced cell migration. J Biol Chem. 2011;286(51):43855-70. doi: 10.1074/jbc.M111.299248. PubMed PMID: 22030398; PubMed Central PMCID: PMCPMC3243551.
126. Sickinger S, Maier H, Konig S, Vallant N, Kofler M, Schumpp P, et al. Lipocalin-2 as mediator of chemokine expression and granulocyte infiltration during ischemia and reperfusion. Transpl Int. 2013;26(7):761-9. doi: 10.1111/tri.12116. PubMed PMID: 23701109.
127. Wrighting DM, Andrews NC. Interleukin-6 induces hepcidin expression through STAT3. Blood. 2006;108(9):3204-9. doi: 10.1182/blood-2006-06-027631. PubMed PMID: 16835372; PubMed Central PMCID: PMCPMC1895528.
128. Nemeth E, Ganz T. Regulation of iron metabolism by hepcidin. Annu Rev Nutr. 2006;26:323-42. doi: 10.1146/annurev.nutr.26.061505.111303. PubMed PMID: 16848710.
129. Chen K, McAleer JP, Lin Y, Paterson DL, Zheng M, Alcorn JF, et al. Th17 cells mediate clade-specific, serotype-independent mucosal immunity. Immunity. 2011;35(6):997-1009. doi: 10.1016/j.immuni.2011.10.018. PubMed PMID: 22195749; PubMed Central PMCID: PMCPMC3406408.
130. Murakami M, Hirano T. The pathological and physiological roles of IL-6 amplifier activation. Int J Biol Sci. 2012;8(9):1267-80. doi: 10.7150/ijbs.4828. PubMed PMID: 23136555; PubMed Central PMCID: PMCPMC3491450.
131. Miossec P, Korn T, Kuchroo VK. Interleukin-17 and type 17 helper T cells. N Engl J Med. 2009;361(9):888-98. doi: 10.1056/NEJMra0707449. PubMed PMID: 19710487.
132. Li Q, Laumonnier Y, Syrovets T, Simmet T. Recruitment of CCR6-expressing Th17 cells by CCL20 secreted from plasmin-stimulated macrophages. Acta Biochim Biophys Sin (Shanghai). 2013;45(7):593-600. doi: 10.1093/abbs/gmt049. PubMed PMID: 23681234.
133. Lee HJ, Choi SC, Choi EY, Lee MH, Seo GS, Kim EC, et al. Iron chelator induces MIP-alpha/CCL20 in human intestinal epithelial cells: implication for triggering mucosal adaptive immunity. Exp Mol Med. 2005;37(4):297-310. doi: 10.1038/emm.2005.40. PubMed PMID: 16155407.
134. Fu D, Richardson DR. Iron chelation and regulation of the cell cycle: 2 mechanisms of posttranscriptional regulation of the universal cyclin-dependent kinase inhibitor p21CIP1/WAF1 by iron depletion. Blood. 2007;110(2):752-61. doi: 10.1182/blood-2007-03-076737. PubMed PMID: 17429006.

135. Nurtjahja-Tjendraputra E, Fu D, Phang JM, Richardson DR. Iron chelation regulates cyclin D1 expression via the proteasome: a link to iron deficiency-mediated growth suppression. Blood. 2007;109(9):4045-54. doi: 10.1182/blood-2006-10-047753. PubMed PMID: 17197429.
136. Chepelev NL, Willmore WG. Regulation of iron pathways in response to hypoxia. Free Radic Biol Med. 2011;50(6):645-66. doi: 10.1016/j.freeradbiomed.2010.12.023. PubMed PMID: 21185934.
137. Asikainen TM, Ahmad A, Schneider BK, Ho WB, Arend M, Brenner M, et al. Stimulation of HIF-1alpha, HIF-2alpha, and VEGF by prolyl 4-hydroxylase inhibition in human lung endothelial and epithelial cells. Free Radic Biol Med. 2005;38(8):1002-13. doi: 10.1016/j.freeradbiomed.2004.12.004. PubMed PMID: 15780758.
138. Schmittgen TD, Livak KJ. Analyzing real-time PCR data by the comparative C(T) method. Nat Protoc. 2008;3(6):1101-8. PubMed PMID: 18546601.
139. Yang J, Goetz D, Li JY, Wang W, Mori K, Setlik D, et al. An iron delivery pathway mediated by a lipocalin. Mol Cell. 2002;10(5):1045-56. PubMed PMID: 12453413.
140. Irizarry RA, Hobbs B, Collin F, Beazer-Barclay YD, Antonellis KJ, Scherf U, et al. Exploration, normalization, and summaries of high density oligonucleotide array probe level data. Biostatistics. 2003;4(2):249-64. doi: 10.1093/biostatistics/4.2.249. PubMed PMID: 12925520.
141. Liberzon A, Subramanian A, Pinchback R, Thorvaldsdottir H, Tamayo P, Mesirov JP. Molecular signatures database (MSigDB) 3.0. Bioinformatics. 2011;27(12):1739-40. doi: 10.1093/bioinformatics/btr260. PubMed PMID: 21546393; PubMed Central PMCID: PMCPMC3106198.
142. Sunters A, Armstrong VJ, Zaman G, Kypta RM, Kawano Y, Lanyon LE, et al. Mechano-transduction in osteoblastic cells involves strain-regulated estrogen receptor alpha-mediated control of insulin-like growth factor (IGF) I receptor sensitivity to Ambient IGF, leading to phosphatidylinositol 3-kinase/AKT-dependent Wnt/LRP5 receptor-independent activation of beta-catenin signaling. J Biol Chem. 2010;285(12):8743-58. doi: 10.1074/jbc.M109.027086. PubMed PMID: 20042609; PubMed Central PMCID: PMCPMC2838297.
143. Magill SS, Edwards JR, Bamberg W, Beldavs ZG, Dumyati G, Kainer MA, et al. Multistate point-prevalence survey of health care-associated infections. N Engl J Med. 2014;370(13):1198-208. doi: 10.1056/NEJMoa1306801. PubMed PMID: 24670166; PubMed Central PMCID: PMCPMC4648343.
144. Snitkin ES, Zelazny AM, Thomas PJ, Stock F, Group NCSP, Henderson DK, et al. Tracking a hospital outbreak of carbapenem-resistant *Klebsiella pneumoniae* with whole-genome sequencing. Sci Transl Med. 2012;4(148):148ra16. doi: 10.1126/scitranslmed.3004129. PubMed PMID: 22914622; PubMed Central PMCID: PMCPMC3521604.
145. Munoz-Price LS, Poirel L, Bonomo RA, Schwaber MJ, Daikos GL, Cormican M, et al. Clinical epidemiology of the global expansion of *Klebsiella pneumoniae* carbapenemases. Lancet Infect Dis. 2013;13(9):785-96. doi:

10.1016/S1473-3099(13)70190-7. PubMed PMID: 23969216; PubMed Central PMCID: PMCPMC4673667.
146. Borer A, Saidel-Odes L, Riesenberg K, Eskira S, Peled N, Nativ R, et al. Attributable mortality rate for carbapenem-resistant *Klebsiella pneumoniae* bacteremia. Infect Control Hosp Epidemiol. 2009;30(10):972-6. doi: 10.1086/605922. PubMed PMID: 19712030.
147. Tumbarello M, Viale P, Viscoli C, Trecarichi EM, Tumietto F, Marchese A, et al. Predictors of mortality in bloodstream infections caused by *Klebsiella pneumoniae* carbapenemase-producing *K. pneumoniae*: importance of combination therapy. Clin Infect Dis. 2012;55(7):943-50. doi: 10.1093/cid/cis588. PubMed PMID: 22752516.
148. Lawlor MS, O'Connor C, Miller VL. Yersiniabactin is a virulence factor for *Klebsiella pneumoniae* during pulmonary infection. Infect Immun. 2007;75(3):1463-72. Epub 2007/01/16. doi: IAI.00372-06 [pii]
10.1128/IAI.00372-06. PubMed PMID: 17220312; PubMed Central PMCID: PMC1828572.
149. Bachman MA, Breen P, Deornellas V, Mu Q, Zhao L, Wu W, et al. Genome-Wide Identification of *Klebsiella pneumoniae* Fitness Genes during Lung Infection. MBio. 2015;6(3):e00775. Epub 2015/06/11. doi: 10.1128/mBio.00775-15
e00775-15 [pii]
mBio.00775-15 [pii]. PubMed PMID: 26060277; PubMed Central PMCID: PMC4462621.
150. Holden VI, Bachman MA. Diverging roles of bacterial siderophores during infection. Metallomics. 2015;7(6):986-95. Epub 2015/03/10. doi: 10.1039/c4mt00333k. PubMed PMID: 25745886.
151. Noinaj N, Guillier M, Barnard TJ, Buchanan SK. TonB-dependent transporters: regulation, structure, and function. Annual review of microbiology. 2010;64:43-60. doi: 10.1146/annurev.micro.112408.134247. PubMed PMID: 20420522; PubMed Central PMCID: PMCPMC3108441.
152. Holden VI, Lenio S, Kuick R, Ramakrishnan SK, Shah YM, Bachman MA. Bacterial siderophores that evade or overwhelm lipocalin 2 induce hypoxia inducible factor 1alpha and proinflammatory cytokine secretion in cultured respiratory epithelial cells. Infect Immun. 2014;82(9):3826-36. Epub 2014/07/02. doi: 10.1128/IAI.01849-14
IAI.01849-14 [pii]. PubMed PMID: 24980968; PubMed Central PMCID: PMC4187820.
153. Lu H, Forbes RA, Verma A. Hypoxia-inducible factor 1 activation by aerobic glycolysis implicates the Warburg effect in carcinogenesis. J Biol Chem. 2002;277(26):23111-5. doi: 10.1074/jbc.M202487200. PubMed PMID: 11943784.
154. Huang LE, Gu J, Schau M, Bunn HF. Regulation of hypoxia-inducible factor 1alpha is mediated by an O2-dependent degradation domain via the ubiquitin-proteasome pathway. Proc Natl Acad Sci U S A. 1998;95(14):7987-92. PubMed PMID: 9653127; PubMed Central PMCID: PMCPMC20916.
155. Wang GL, Jiang BH, Rue EA, Semenza GL. Hypoxia-inducible factor 1 is a basic-helix-loop-helix-PAS heterodimer regulated by cellular O2 tension. Proc

Natl Acad Sci U S A. 1995;92(12):5510-4. PubMed PMID: 7539918; PubMed Central PMCID: PMCPMC41725.
156. Peyssonnaux C, Zinkernagel AS, Schuepbach RA, Rankin E, Vaulont S, Haase VH, et al. Regulation of iron homeostasis by the hypoxia-inducible transcription factors (HIFs). J Clin Invest. 2007;117(7):1926-32. doi: 10.1172/JCI31370. PubMed PMID: 17557118; PubMed Central PMCID: PMCPMC1884690.
157. Lin AE, Beasley FC, Olson J, Keller N, Shalwitz RA, Hannan TJ, et al. Role of Hypoxia Inducible Factor-1alpha (HIF-1alpha) in Innate Defense against Uropathogenic *Escherichia coli* Infection. PLoS Pathog. 2015;11(4):e1004818. doi: 10.1371/journal.ppat.1004818. PubMed PMID: 25927232; PubMed Central PMCID: PMCPMC4415805.
158. Skare JT, Ahmer BM, Seachord CL, Darveau RP, Postle K. Energy transduction between membranes. TonB, a cytoplasmic membrane protein, can be chemically cross-linked in vivo to the outer membrane receptor FepA. J Biol Chem. 1993;268(22):16302-8. Epub 1993/08/05. PubMed PMID: 8344918.
159. Podschun R, Ullmann U. Klebsiella capsular type K7 in relation to toxicity, susceptibility to phagocytosis and resistance to serum. J Med Microbiol. 1992;36(4):250-4. doi: 10.1099/00222615-36-4-250. PubMed PMID: 1560447.
160. Safran M, Kim WY, O'Connell F, Flippin L, Gunzler V, Horner JW, et al. Mouse model for noninvasive imaging of HIF prolyl hydroxylase activity: assessment of an oral agent that stimulates erythropoietin production. Proc Natl Acad Sci U S A. 2006;103(1):105-10. Epub 2005/12/24. doi: 0509459103 [pii]
10.1073/pnas.0509459103. PubMed PMID: 16373502; PubMed Central PMCID: PMC1324998.
161. Xue X, Ramakrishnan S, Anderson E, Taylor M, Zimmermann EM, Spence JR, et al. Endothelial PAS domain protein 1 activates the inflammatory response in the intestinal epithelium to promote colitis in mice. Gastroenterology. 2013;145(4):831-41. doi: 10.1053/j.gastro.2013.07.010. PubMed PMID: 23860500; PubMed Central PMCID: PMCPMC3799890.
162. Li F, Sonveaux P, Rabbani ZN, Liu S, Yan B, Huang Q, et al. Regulation of HIF-1alpha stability through S-nitrosylation. Mol Cell. 2007;26(1):63-74. doi: 10.1016/j.molcel.2007.02.024. PubMed PMID: 17434127; PubMed Central PMCID: PMCPMC2905600.
163. Zampell JC, Yan A, Avraham T, Daluvoy S, Weitman ES, Mehrara BJ. HIF-1alpha coordinates lymphangiogenesis during wound healing and in response to inflammation. FASEB J. 2012;26(3):1027-39. doi: 10.1096/fj.11-195321. PubMed PMID: 22067482; PubMed Central PMCID: PMCPMC3470728.
164. Arnold RS, Thom KA, Sharma S, Phillips M, Kristie Johnson J, Morgan DJ. Emergence of *Klebsiella pneumoniae* carbapenemase-producing bacteria. South Med J. 2011;104(1):40-5. doi: 10.1097/SMJ.0b013e3181fd7d5a. PubMed PMID: 21119555; PubMed Central PMCID: PMCPMC3075864.
165. Caza M, Lepine F, Milot S, Dozois CM. Specific roles of the iroBCDEN genes in virulence of an avian pathogenic *Escherichia coli* O78 strain and in production of salmochelins. Infect Immun. 2008;76(8):3539-49. Epub 2008/06/11. doi: 10.1128/IAI.00455-08

IAI.00455-08 [pii]. PubMed PMID: 18541653; PubMed Central PMCID: PMC2493193.
166. Singh V, Yeoh BS, Xiao X, Kumar M, Bachman M, Borregaard N, et al. Interplay between enterobactin, myeloperoxidase and lipocalin 2 regulates *E. coli* survival in the inflamed gut. Nat Commun. 2015;6:7113. doi: 10.1038/ncomms8113. PubMed PMID: 25964185.
167. Yano K, Liaw PC, Mullington JM, Shih SC, Okada H, Bodyak N, et al. Vascular endothelial growth factor is an important determinant of sepsis morbidity and mortality. J Exp Med. 2006;203(6):1447-58. doi: 10.1084/jem.20060375. PubMed PMID: 16702604; PubMed Central PMCID: PMCPMC2118329.
168. Weis SM, Cheresh DA. Pathophysiological consequences of VEGF-induced vascular permeability. Nature. 2005;437(7058):497-504. doi: 10.1038/nature03987. PubMed PMID: 16177780.
169. Shah YM, Ito S, Morimura K, Chen C, Yim SH, Haase VH, et al. Hypoxia-inducible factor augments experimental colitis through an MIF-dependent inflammatory signaling cascade. Gastroenterology. 2008;134(7):2036-48, 48 e1-3. doi: 10.1053/j.gastro.2008.03.009. PubMed PMID: 18439915; PubMed Central PMCID: PMCPMC2533811.
170. Sahly H, Podschun R, Oelschlaeger TA, Greiwe M, Parolis H, Hasty D, et al. Capsule impedes adhesion to and invasion of epithelial cells by *Klebsiella pneumoniae*. Infect Immun. 2000;68(12):6744-9. PubMed PMID: 11083790; PubMed Central PMCID: PMCPMC97775.
171. Suresh MV, Ramakrishnan S, Thomas B, Machado-Aranda D, Bi Y, Talarico N, et al. Activation of Hypoxia-Inducible Factor 1α in Type 2 Alveolar Epithelial Cell Is a Major Driver of Acute Inflammation Following Lung Contusion. Critical Care Medicine
. 2014;42(10):11. doi: 10.1097/CCM.0000000000000488.
172. Yan SF, Tritto I, Pinsky D, Liao H, Huang J, Fuller G, et al. Induction of interleukin 6 (IL-6) by hypoxia in vascular cells. Central role of the binding site for nuclear factor-IL-6. J Biol Chem. 1995;270(19):11463-71. PubMed PMID: 7744784.
173. Peyssonnaux C, Datta V, Cramer T, Doedens A, Theodorakis EA, Gallo RL, et al. HIF-1alpha expression regulates the bactericidal capacity of phagocytes. J Clin Invest. 2005;115(7):1806-15. doi: 10.1172/JCI23865. PubMed PMID: 16007254; PubMed Central PMCID: PMCPMC1159132.
174. Imtiyaz HZ, Williams EP, Hickey MM, Patel SA, Durham AC, Yuan LJ, et al. Hypoxia-inducible factor 2alpha regulates macrophage function in mouse models of acute and tumor inflammation. J Clin Invest. 2010;120(8):2699-714. doi: 10.1172/JCI39506. PubMed PMID: 20644254; PubMed Central PMCID: PMCPMC2912179.
175. Proper SP, Saini Y, Greenwood KK, Bramble LA, Downing NJ, Harkema JR, et al. Loss of hypoxia-inducible factor 2 alpha in the lung alveolar epithelium of mice leads to enhanced eosinophilic inflammation in cobalt-induced lung injury. Toxicol Sci. 2014;137(2):447-57. doi: 10.1093/toxsci/kft253. PubMed PMID: 24218148; PubMed Central PMCID: PMCPMC3908723.

176. Endler A, Chen L, Li Q, Uchida K, Hashimoto T, Lu L, et al. Int6/eIF3e silenced HIF2alpha stabilization enhances migration and tube formation of HUVECs via IL-6 and IL-8 signaling. Cytokine. 2013;62(1):115-22. doi: 10.1016/j.cyto.2013.01.021. PubMed PMID: 23478175.
177. Sutherland RE, Olsen JS, McKinstry A, Villalta SA, Wolters PJ. Mast cell IL-6 improves survival from *Klebsiella pneumonia* and sepsis by enhancing neutrophil killing. J Immunol. 2008;181(8):5598-605. PubMed PMID: 18832718; PubMed Central PMCID: PMCPMC2610024.
178. Cai S, Batra S, Lira SA, Kolls JK, Jeyaseelan S. CXCL1 regulates pulmonary host defense to *Klebsiella* Infection via CXCL2, CXCL5, NF-kappaB, and MAPKs. J Immunol. 2010;185(10):6214-25. doi: 10.4049/jimmunol.0903843. PubMed PMID: 20937845; PubMed Central PMCID: PMCPMC2974054.
179. Greenberger MJ, Strieter RM, Kunkel SL, Danforth JM, Laichalk LL, McGillicuddy DC, et al. Neutralization of macrophage inflammatory protein-2 attenuates neutrophil recruitment and bacterial clearance in murine *Klebsiella pneumonia*. The Journal of infectious diseases. 1996;173(1):159-65. PubMed PMID: 8537653.
180. Nemeth E, Tuttle MS, Powelson J, Vaughn MB, Donovan A, Ward DM, et al. Hepcidin regulates cellular iron efflux by binding to ferroportin and inducing its internalization. Science. 2004;306(5704):2090-3. doi: 10.1126/science.1104742. PubMed PMID: 15514116.
181. Tanabe O, Akira S, Kamiya T, Wong GG, Hirano T, Kishimoto T. Genomic structure of the murine IL-6 gene. High degree conservation of potential regulatory sequences between mouse and human. J Immunol. 1988;141(11):3875-81. PubMed PMID: 3263439.
182. Zlotnik A, Yoshie O. Chemokines: a new classification system and their role in immunity. Immunity. 2000;12(2):121-7. PubMed PMID: 10714678.
183. Gargalovic PS, Gharavi NM, Clark MJ, Pagnon J, Yang WP, He A, et al. The unfolded protein response is an important regulator of inflammatory genes in endothelial cells. Arterioscler Thromb Vasc Biol. 2006;26(11):2490-6. doi: 10.1161/01.ATV.0000242903.41158.a1. PubMed PMID: 16931790.
184. Toosi S, Orlow SJ, Manga P. Vitiligo-inducing phenols activate the unfolded protein response in melanocytes resulting in upregulation of IL6 and IL8. J Invest Dermatol. 2012;132(11):2601-9. doi: 10.1038/jid.2012.181. PubMed PMID: 22696056; PubMed Central PMCID: PMCPMC3443495.
185. Ron D, Walter P. Signal integration in the endoplasmic reticulum unfolded protein response. Nat Rev Mol Cell Biol. 2007;8(7):519-29. doi: 10.1038/nrm2199. PubMed PMID: 17565364.
186. Libermann TA, Baltimore D. Activation of interleukin-6 gene expression through the NF-kappa B transcription factor. Mol Cell Biol. 1990;10(5):2327-34. PubMed PMID: 2183031; PubMed Central PMCID: PMCPMC360580.
187. Ohmori Y, Fukumoto S, Hamilton TA. Two structurally distinct kappa B sequence motifs cooperatively control LPS-induced KC gene transcription in mouse macrophages. J Immunol. 1995;155(7):3593-600. PubMed PMID: 7561058.

188. Widmer U, Manogue KR, Cerami A, Sherry B. Genomic cloning and promoter analysis of macrophage inflammatory protein (MIP)-2, MIP-1 alpha, and MIP-1 beta, members of the chemokine superfamily of proinflammatory cytokines. J Immunol. 1993;150(11):4996-5012. PubMed PMID: 8496601.
189. Pereira ER, Frudd K, Awad W, Hendershot LM. Endoplasmic reticulum (ER) stress and hypoxia response pathways interact to potentiate hypoxia-inducible factor 1 (HIF-1) transcriptional activity on targets like vascular endothelial growth factor (VEGF). J Biol Chem. 2014;289(6):3352-64. doi: 10.1074/jbc.M113.507194. PubMed PMID: 24347168; PubMed Central PMCID: PMCPMC3916539.
190. Kjeldsen L, Cowland JB, Borregaard N. Human neutrophil gelatinase-associated lipocalin and homologous proteins in rat and mouse. Biochim Biophys Acta. 2000;1482(1-2):272-83. PubMed PMID: 11058768.
191. Hua KF, Yang FL, Chiu HW, Chou JC, Dong WC, Lin CN, et al. Capsular Polysaccharide Is Involved in NLRP3 Inflammasome Activation by *Klebsiella pneumoniae* Serotype K1. Infect Immun. 2015;83(9):3396-409. doi: 10.1128/IAI.00125-15. PubMed PMID: 26077758; PubMed Central PMCID: PMCPMC4534678.
192. Regueiro V, Moranta D, Campos MA, Margareto J, Garmendia J, Bengoechea JA. *Klebsiella pneumoniae* increases the levels of Toll-like receptors 2 and 4 in human airway epithelial cells. Infect Immun. 2009;77(2):714-24. doi: 10.1128/IAI.00852-08. PubMed PMID: 19015258; PubMed Central PMCID: PMCPMC2632040.
193. Schutyser E, Struyf S, Van Damme J. The CC chemokine CCL20 and its receptor CCR6. Cytokine Growth Factor Rev. 2003;14(5):409-26. PubMed PMID: 12948524.
194. Saini Y, Harkema JR, LaPres JJ. HIF1alpha is essential for normal intrauterine differentiation of alveolar epithelium and surfactant production in the newborn lung of mice. J Biol Chem. 2008;283(48):33650-7. Epub 2008/09/20. doi: 10.1074/jbc.M805927200
M805927200 [pii]. PubMed PMID: 18801745; PubMed Central PMCID: PMC2586263.
195. Saini Y, Kim KY, Lewandowski R, Bramble LA, Harkema JR, Lapres JJ. Role of hypoxia-inducible factor 1{alpha} in modulating cobalt-induced lung inflammation. Am J Physiol Lung Cell Mol Physiol. 2010;298(2):L139-47. Epub 2009/11/17. doi: 10.1152/ajplung.00252.2009
00252.2009 [pii]. PubMed PMID: 19915160; PubMed Central PMCID: PMC2822559.
196. Broberg CA, Wu W, Cavalcoli JD, Miller VL, Bachman MA. Complete Genome Sequence of *Klebsiella pneumoniae* Strain ATCC 43816 KPPR1, a Rifampin-Resistant Mutant Commonly Used in Animal, Genetic, and Molecular Biology Studies. Genome Announc. 2014;2(5). Epub 2014/10/08. doi: 10.1128/genomeA.00924-14
e00924-14 [pii]
2/5/e00924-14 [pii]. PubMed PMID: 25291761; PubMed Central PMCID: PMC4175196.

197. Miller VL, Mekalanos JJ. A novel suicide vector and its use in construction of insertion mutations: osmoregulation of outer membrane proteins and virulence determinants in Vibrio cholerae requires toxR. J Bacteriol. 1988;170(6):2575-83. Epub 1988/06/01. PubMed PMID: 2836362; PubMed Central PMCID: PMC211174.
198. CDC. Antibiotic Resistance Threats in the United States, 2013. In: Services DoHaH, editor. Atlanta, GA2014.
199. Bratu S, Landman D, Haag R, Recco R, Eramo A, Alam M, et al. Rapid spread of carbapenem-resistant *Klebsiella pneumoniae* in New York City: a new threat to our antibiotic armamentarium. Arch Intern Med. 2005;165(12):1430-5. doi: 10.1001/archinte.165.12.1430. PubMed PMID: 15983294.
200. Patel G, Huprikar S, Factor SH, Jenkins SG, Calfee DP. Outcomes of carbapenem-resistant *Klebsiella pneumoniae* infection and the impact of antimicrobial and adjunctive therapies. Infect Control Hosp Epidemiol. 2008;29(12):1099-106. doi: 10.1086/592412. PubMed PMID: 18973455.
201. van Duin D, Perez F, Rudin SD, Cober E, Hanrahan J, Ziegler J, et al. Surveillance of carbapenem-resistant *Klebsiella pneumoniae*: tracking molecular epidemiology and outcomes through a regional network. Antimicrob Agents Chemother. 2014;58(7):4035-41. doi: 10.1128/AAC.02636-14. PubMed PMID: 24798270; PubMed Central PMCID: PMCPMC4068524.
202. Alexander DB, Zuberer DA. Use of chrome azurol S reagents to evaluate siderophore production by rhizosphere bacteria. Biology and Fertility of Soils. 1991;12(1):39-45.
203. Stojiljkovic I, Hantke K. Hemin uptake system of *Yersinia enterocolitica*: similarities with other TonB-dependent systems in gram-negative bacteria. EMBO J. 1992;11(12):4359-67. PubMed PMID: 1425573; PubMed Central PMCID: PMCPMC557009.
204. Ouyang Z, Isaacson R. Identification and characterization of a novel ABC iron transport system, fit, in *Escherichia coli*. Infect Immun. 2006;74(12):6949-56. doi: 10.1128/IAI.00866-06. PubMed PMID: 16982838; PubMed Central PMCID: PMCPMC1698097.
205. Ouyang Z, Isaacson R. Identification of a Novel Regulator for the *Escherichia coli* fit Iron Transport System. Open Microbiol J. 2008;2:94-9. doi: 10.2174/1874285800802010094. PubMed PMID: 19088918; PubMed Central PMCID: PMCPMC2593036.
206. Nikaido H, Rosenberg EY. Cir and Fiu proteins in the outer membrane of *Escherichia coli* catalyze transport of monomeric catechols: study with beta-lactam antibiotics containing catechol and analogous groups. J Bacteriol. 1990;172(3):1361-7. PubMed PMID: 2407721; PubMed Central PMCID: PMCPMC208606.
207. Curtis NA, Eisenstadt RL, East SJ, Cornford RJ, Walker LA, White AJ. Iron-regulated outer membrane proteins of *Escherichia coli* K-12 and mechanism of action of catechol-substituted cephalosporins. Antimicrob Agents Chemother. 1988;32(12):1879-86. PubMed PMID: 3072926; PubMed Central PMCID: PMCPMC176037.

208. Groicher KH, Firek BA, Fujimoto DF, Bayles KW. The *Staphylococcus aureus* lrgAB operon modulates murein hydrolase activity and penicillin tolerance. J Bacteriol. 2000;182(7):1794-801. PubMed PMID: 10714982; PubMed Central PMCID: PMCPMC101860.
209. Fouts DE, Brinkac L, Beck E, Inman J, Sutton G. PanOCT: automated clustering of orthologs using conserved gene neighborhood for pan-genomic analysis of bacterial strains and closely related species. Nucleic Acids Res. 2012;40(22):e172. doi: 10.1093/nar/gks757. PubMed PMID: 22904089; PubMed Central PMCID: PMCPMC3526259.
210. Arnow LE. Colorimetric determination of the components of 3,4-dihydroxyphenylalanine tyrosine mixtures. Journal of Biological Chemistry. 1937;118(2):531-7. PubMed PMID: WOS:000187603100024.
211. Chen L, Yang J, Yu J, Yao Z, Sun L, Shen Y, et al. VFDB: a reference database for bacterial virulence factors. Nucleic Acids Res. 2005;33(Database issue):D325-8. doi: 10.1093/nar/gki008. PubMed PMID: 15608208; PubMed Central PMCID: PMCPMC539962.
212. Struve C, Bojer M, Krogfelt KA. Characterization of *Klebsiella pneumoniae* type 1 fimbriae by detection of phase variation during colonization and infection and impact on virulence. Infect Immun. 2008;76(9):4055-65. doi: 10.1128/IAI.00494-08. PubMed PMID: 18559432; PubMed Central PMCID: PMCPMC2519443.
213. Bottomley SS, Wolfe LC, Bridges KR. Iron metabolism in K562 erythroleukemic cells. J Biol Chem. 1985;260(11):6811-5. PubMed PMID: 2987233.
214. Bomford A, Isaac J, Roberts S, Edwards A, Young S, Williams R. The effect of desferrioxamine on transferrin receptors, the cell cycle and growth rates of human leukaemic cells. Biochem J. 1986;236(1):243-9. PubMed PMID: 3790074; PubMed Central PMCID: PMCPMC1146812.
215. Zanninelli G, Glickstein H, Breuer W, Milgram P, Brissot P, Hider RC, et al. Chelation and mobilization of cellular iron by different classes of chelators. Mol Pharmacol. 1997;51(5):842-52. PubMed PMID: 9145923.
216. Richardson D, Ponka P, Baker E. The effect of the iron(III) chelator, desferrioxamine, on iron and transferrin uptake by the human malignant melanoma cell. Cancer Res. 1994;54(3):685-9. PubMed PMID: 8306330.
217. Brock JH, Pickering MG, McDowall MC, Deacon AG. Role of antibody and enterobactin in controlling growth of *Escherichia coli* in human milk and acquisition of lactoferrin- and transferrin-bound iron by *Escherichia coli*. Infect Immun. 1983;40(2):453-9. PubMed PMID: 6220972; PubMed Central PMCID: PMCPMC264876.
218. Mori K, Lee HT, Rapoport D, Drexler IR, Foster K, Yang J, et al. Endocytic delivery of lipocalin-siderophore-iron complex rescues the kidney from ischemia-reperfusion injury. J Clin Invest. 2005;115(3):610-21. doi: 10.1172/JCI23056. PubMed PMID: 15711640; PubMed Central PMCID: PMCPMC548316.
219. Devireddy LR, Gazin C, Zhu X, Green MR. A cell-surface receptor for lipocalin 24p3 selectively mediates apoptosis and iron uptake. Cell.

2005;123(7):1293-305. doi: 10.1016/j.cell.2005.10.027. PubMed PMID: 16377569.
220. Abergel RJ, Clifton MC, Pizarro JC, Warner JA, Shuh DK, Strong RK, et al. The siderocalin/enterobactin interaction: a link between mammalian immunity and bacterial iron transport. J Am Chem Soc. 2008;130(34):11524-34. doi: 10.1021/ja803524w. PubMed PMID: 18680288; PubMed Central PMCID: PMCPMC3188318.
221. Brickman TJ, McIntosh MA. Overexpression and purification of ferric enterobactin esterase from *Escherichia coli.* Demonstration of enzymatic hydrolysis of enterobactin and its iron complex. J Biol Chem. 1992;267(17):12350-5. PubMed PMID: 1534808.
222. CDC. *Klebsiella pneumoniae* in Healthcare Settings. In: Prevention CfDCa, editor. Atlanta, GA2012.
223. Scholz RL, Greenberg EP. Sociality in *Escherichia coli*: Enterochelin Is a Private Good at Low Cell Density and Can Be Shared at High Cell Density. J Bacteriol. 2015;197(13):2122-8. doi: 10.1128/JB.02596-14. PubMed PMID: 25733620; PubMed Central PMCID: PMCPMC4455259.
224. Holt KE, Wertheim H, Zadoks RN, Baker S, Whitehouse CA, Dance D, et al. Genomic analysis of diversity, population structure, virulence, and antimicrobial resistance in *Klebsiella pneumoniae*, an urgent threat to public health. Proc Natl Acad Sci U S A. 2015;112(27):E3574-81. doi: 10.1073/pnas.1501049112. PubMed PMID: 26100894; PubMed Central PMCID: PMCPMC4500264.
225. Standiford TJ, Wilkowski JM, Sisson TH, Hattori N, Mehrad B, Bucknell KA, et al. Intrapulmonary tumor necrosis factor gene therapy increases bacterial clearance and survival in murine gram-negative pneumonia. Hum Gene Ther. 1999;10(6):899-909. doi: 10.1089/10430349950018300. PubMed PMID: 10223724.
226. Sivick KE, Mobley HL. An "omics" approach to uropathogenic *Escherichia coli* vaccinology. Trends Microbiol. 2009;17(10):431-2. doi: 10.1016/j.tim.2009.07.003. PubMed PMID: 19758805; PubMed Central PMCID: PMCPMC2770165.
227. Tanaka T, Kishimoto T. The biology and medical implications of interleukin-6. Cancer Immunol Res. 2014;2(4):288-94. doi: 10.1158/2326-6066.CIR-14-0022. PubMed PMID: 24764575.
228. Budzikiewicz H. Siderophore-antibiotic conjugates used as trojan horses against *Pseudomonas aeruginosa*. Curr Top Med Chem. 2001;1(1):73-82. PubMed PMID: 11895295.
229. Moreau-Marquis S, Coutermarsh B, Stanton BA. Combination of hypothiocyanite and lactoferrin (ALX-109) enhances the ability of tobramycin and aztreonam to eliminate *Pseudomonas aeruginosa* biofilms growing on cystic fibrosis airway epithelial cells. J Antimicrob Chemother. 2015;70(1):160-6. doi: 10.1093/jac/dku357. PubMed PMID: 25213272; PubMed Central PMCID: PMCPMC4267504.
230. Moreau-Marquis S, O'Toole GA, Stanton BA. Tobramycin and FDA-approved iron chelators eliminate *Pseudomonas aeruginosa* biofilms on cystic

fibrosis cells. Am J Respir Cell Mol Biol. 2009;41(3):305-13. doi: 10.1165/rcmb.2008-0299OC. PubMed PMID: 19168700; PubMed Central PMCID: PMCPMC2742750.